SPATILA MODELING OF GEO-HAZARD SUCEPTIABLITY TO ASSESS ITS IMPACT ON THE MAJOR INFRASTRUCTURE: THE CASE OF MIDDLE AWASH BASIN, ETHIOPIA

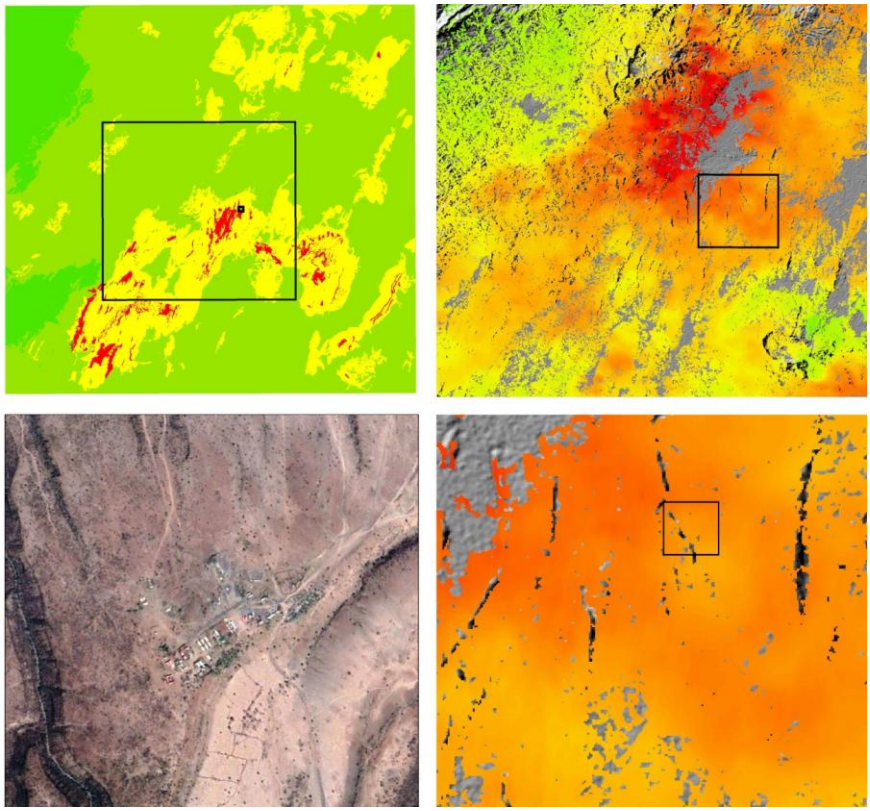

Tewabe Melkamu

A Thesis Submitted to

School of Earth Sciences

Presented in Partial Fulfillment of the requirements for the Degree of Master of Science in (Remote sensing and Geo-informatics)

Addis Ababa University
አዲስ፡አበባ፡ዩኒቨርሲቲ
SEEK WISDOM, ELEVATE YOUR INTELLECT AND SERVE HUMANITY !

ADDIS ABABA UNIVERSITY

Addis Ababa, Ethiopia

June ,2019

Spatila modeling of Geo-hazard suceptiablity to assess its impact on the major infrastructure: The case of Middle awash Basin, Ethiopia

Tewabe Melkamu

A Thesis Submitted to

School of Earth Sciences

Presented in Partial Fulfillment of the requirements for the Degree of Master of Science in (Remote sensing and Geo-informatics)

ADDIS ABABA UNIVERSITY

Addis Ababa, Ethiopia

June ,2019

DECLARATION

I hereby declare that the study entitled: "*Spatila modeling of Geo-hazard suceptiablity to assess its impact on the major infrastructure: the case of middle awash basin, Ethiopia*" is being submited by me in the Partial Fulfillment of the requirements for the Degree of Master of Science in (**Remote sensing and Geo-informatics**). The matter embodies in this study has not been submitted to any other Universities or instituations for the award of degree.The thies work is my orginal work and it has not been presented earlier in this manner. All sources of materials used for the thesis have been duly acknowledged.

Tewabe Melkamu Fentahun

Signature _____ Date_____

School of Earth Science

June, 2019

SIGNATURE PAGE

Addis Ababa University

Graduate Studies

This is to certify that the thesis prepared by **TEWABE MELKAMU**, entitled: "*Spatila modeling of Geo-hazard suceptiablity to assess its impact on the major infrastructure: the case of middle awash basin, Ethiopia*" and submitted in partial fulfillment of the requirements for the Dgree of Masters of Science in Remote sensing and Geo-informatics complies with the regulations of the University and meets the accepted standards with respect to the originality and quality.

Signed By The Examining Committee:

Advisor: Dr. Tesfaye Korme Signature _____ Date _____

Examiner: Dr. Tarun Kumar Raghuvanshi Signature _____Date_____

Examiner: Dr. K.V.Suryabhagavan Signature_____ Date _____

Chairperson: Dr. Tarun Kumar Raghuvanshi Signature _____Date_____

Chair of School or Graduate Program Coordinator

ACKNOWLEDGMENTS

Thanks to the 'Almighty God' for all thing which happenes to be happended through my life!

First of all I would like to express my deep sense of gratitude to my advisor **Dr. Tesfaye Korme.** I don't believe as my word is enough strong to adress my thankfulness to him. His golden word, advices, helpful discussions, comments and valuable suggestions were direct input of my work and the knowledge I held. His simple speech is my pure motivation to conduct my research work. His personality and profession, is my always wish and dream!

I am grateful to Debre Birhan University for sponsoring me to pursue my post graduate study at Addis Ababa University. This is a great opportunity to thank Addis Ababa University School of Earth Science staff members directly or indirectly for their support during my study pareiod.

I would like to express my sincere thanks to European Space Agency (ESA) for their free SAR Data. They give free data access, software access and unbelievable limitless guidance. Generally they help me to learn and conduct my research work. I also like to acknowledge United geological survey, SOTER and Geological Survey of Ethiopia for providing the necessary data and information to carry out this research.

Finally, I would like to express my special thanks to my instructor ,family and friends they were close to me in all aspect of my life. All names could not be mentioned separately because of their independent encouragement and cooperation. My friends, Melkamu Abdurrahman, Fikadu, Mintesnot, Seid, Gezahegn and many others, thanks! I passed enjoyable and memorable time. Thanks!

Tewabe,Melkamu

LIST OF FIGURES

LIST OF TABLES

LIST OF APPENDIX

AHP	Analytical Hierarchy Process
A.A	Addis Ababa
E.D	Epicentral Distance
AUC	Area Under The Curve
CNES	National Centre For Space Studies
DEM	Digital Elevation Model
DInSAR	Differential Synthetic Aperture Radar Interferometry
EM-DAT	Emergency Management Database
EMA	Ethiopian Metrological Agency
ENVI	Environment for Visualizing Images
EOS	Earth Observation System
ERDAS	Earth Resource Development Assessment System
ESA	European Space Agency
GIS	Geographic Information System
GSDRC	Governance, Social Development, And Humanitarian Conflict
GSE	Geological Survey of Ethiopia
InSAR	Interfrometric Synthetic Aperture Radar
LULC	Land use land cover
MERV	Main Ethiopian Rift Valley
OLI	Operational Land Imagery
PGA	Peak Ground Acceleration
RADAR	RAdio Detection And Ranging
ROC	Receiver Operating Characteristics
SAR	Synthetic Aperture Radar
SNAP	Sentinel Application Platform
SOTER	Soil and Terrain Digital Database
USDA	United States Department of Agriculture
USGS	United State Geological Survey
WFB	Wonji Fault Belt
WGS	World Geodetic System

ABSTRACT

Spatila modeling of Geo-hazard suceptiablity to assess its impact on the major infrastructure: The case of Middle Awash Basin, Ethiopia.

Tewabe Melkamu Fentahun, MSc. Thesis
Addis Ababa University, June 2019

Geo-hazards, including earthquakes, ground fissuring, volcanic eruptions, and landslides, are crucial problems in Ethiopia causing heavy limitation on urbanization and infrastructural projects and, more in general, for the socioeconomic development of the country. Relatively speaking, the Main Ethiopia Rift Valley region is more susceptible to thus natural disasters. The production of susceptibility maps /hazard zonation mapping/ is the first step in managing a sustainable risk mitigation program in any geo-hazard -prone area. These study focused on Geo-hazard susceptibility mapping using Remote sensing and GIS technology, to assess the vulnerability of existing infrastructures at the middle Awash basin, Main Ethiopian Rift Valley. An attempt was made to map three geo-hazard susceptibilities namely; landslide, seismic, volcanism and associated of the three geo-hazards using Analytical Hierarchy Process method. For these purpose, eight spatial data layers were generated and evaluated. Thus are land use landcover, Faults, and lineaments; active volcanic vent, slope, topography, soil texture and lithology. The Data were combined based on their significance, to produce a susceptibility map of each hazard type. The result of the susceptibility mapping done for each hazard has been classified into four classes and their spatial area coverage also calculated.

To validate the geo-hazard susceptibility generated by Analytical Hierarchy Process technique, differential interferogram (DInSAR) method were applied. The method was done by using a two year six months temporal baseline master and slave image co-registration. The two results (i.e AHP model and SAR result) were correlated using linear regression and Receiver Operating Characteristics curve analysis. From this; the result revealed that the performance of the model was acceptable. The hazard zones could practically be used to assess the vulnerability of existing infrastructure in the study area. Finally using the three combined hazard risk map the vulnerability of infrastructures and other property was assessed through spatial overlay in their location.

Keywords: Analytical Hierarchy Process, Differential Synthetic Aperture Radar Interferometry,Geo-hazard, susceptibility

CHAPTE- I INTRODUCTION

1.1 Background of the study

Natural hazards are intense events within our global system, which brings forth major changes in the environment over a short period of time (Olalekan et al., 2014). The outcome of which leads to injury or death of living organisms, smash up of expensive properties such as a communication system, physical infrastructure, and loss of natural wealth like agricultural land, environment, forests, etc. (Van et al., 2000). They have a profound impact on the socioeconomic system of a Nation. In developed societies, hazards can cause great damage to property with associated high costs. This is not to say that developing countries do not suffer heavy economic losses due to a natural disaster.

Due to the active crustal mobility causing the on going rifting between the Arabian and African plates, Ethiopia as a country and particularly the Rift region is vulnerable to different Geo-hazard type (Fubelli et al., 2015; Faure 1975; Bekele Abebe et al., 2007). For instance, seismically induced landslides reported by (Gouin, 1979), among which the huge slope failure,has occured which destroyed the town of Ankober in 1842 and the fast-moving landslides that killed two people in Dese town during the 1977 earthquake can be mentioned. Concerning volcanic hazard at least 5-10 of the 65 Holocene volcanoes recognized in the country have been classified as “high risk “by the Global Facility for Disaster Risk Reduction (Sparks et al.,2012). However, there is no more research conducted particularly to model hazard-prone areas and their effect, especially using remote sensing and GIS technology.

Remote-sensing techniques and GIS tools are frequently used in applications for disaster management in pre, during and post-disaster activities. Pre-disaster applications are associated with early warning mitigation and preparedness efforts. Mitigation refers to activities that reduce the vulnerability of societies to the impacts of a disaster, while preparedness refers to activities that facilitate preparation for responding to a disaster when it occurs (Mansourian et al., 2007). Due to the recent development and planning of new road networks, dams, reservoirs, and the establishment of new urban settlements in a previously uninhabited area, natural hazards will pose great disaster on such activity(Bekele Abebe et al., 2010).

1.2 Statement of the Problem

Geo-hazards, including earthquakes, ground fissuring, volcanic eruptions, and landslides, are crucial problems in Ethiopia (Bekele bebe et al., 2010; Fubelli et al., 2015), causing heavy limitation on urbanization and infrastructural projects and, more in general, for the socioeconomic development of the country.

Relatively speaking, the Main Ethiopia Rift Valley region is more susceptible to seismic prone hazards: including earthquakes, volcanic eruptions, landslide and other related natural disasters (Bekele Abebe et al., 2010). Kinde Simachew, (2002) explains that Gouin estimates 15,000 tremors occurred in Ethiopia and the Horn of Africa in the 20th century, while another study by (Fikadu Kebede, 1996) identified a total of 16 recorded earthquakes of magnitude 6 and higher in Ethiopia rift in the same period. According to the Emergency management database (**EM-DAT database)** from 1900 to 2013 in Ethiopia, there were a total of three volcanic eruptions, killing 69 people, and affecting 11,000 people. Volcanoes that have been active since with 1900 could pose greater risks as a result of a higher hazard ranking, including Alutu, Fentale, Kone and Tullu Moje (Brown et al., 2015). As several studies revealed, in addition to Highland part of the country the rift valley of Ethiopia; especially the rift margin is more susceptible to landslide activity. Settlements and infrastructures, located at the base or at the edge of high fault escarpments in seismic prone areas are exposed to risk (Fubelli et al., 2015).

Since the study area is one of the part of the Main Ethiopian Rift valley (MERV), thus hazards have happened and expected to happen in the future. Uncontrolled Reservoir problem at Kessem dam, ground fissural cracks on roads in many places, Continuous Lake level change of Beseka, recent and fresh volcanic rock and edifices around mount Fentale, well-recognized faults and fault scarps and others can be indicative of Geohazards in this area (Biggs et al., 2011;Brown et al., 2015).

In this research study, different data are collected from the disaster-prone area and provide the most vulnerable places to natural hazards such as landslide, earthquake, and volcanism, and finally gives overlay of this hazards using GIS overlay analysis.

1.3 Objectives

1.3.1 Main objectives

The main objective of this study is to assess Geo-hazard susceptible environments and vulnerability of existing infrastructures through quantitative analysis of data collected from disaster-prone areas using geospatial technology, in the MERV.

1.3.2 Specific Objectives

- ✓ To assesses and prepare Landslide, seismic and volcanic hazard susceptibilities maps using AHP technique
- ✓ To asses area's susceptible to the three associated Geo-hazards
- ✓ Validate the hazard susceptibilities maps using DInSAR method

1.4 Significance of the Study

The significance of this study is to mitigate natural hazards facing on infrastructure projects such as road networks, dams, reservoirs, settlements and other properties in the Rift region. The proposed study provide the most vulnerable places to natural hazards particularly to landslide, earthquake, and volcanism. The study show the application of geospatial technology in natural hazard mitigation, both at pre and post risk management planning process.

❖ Generally, this study have the following significances:

- Enables to identify hazard-prone areas in the study area
- Deomonstrate significance of geospatial technology in geohazaard studies.
- Provide relevant information that will contribute to the environmental management planners and disaster management activity.
- It will serve as an input for further studies

1.5 The Scope of the Study

In Ethiopia, Most of the Natural hazards related to the geological phenomena have little attention in terms of vulnerability of infrastructural property and human life. Given the fact of current and future geohazard susceptibility problems, there is a need for decision making and planning to maintain at least some strategy for disaster management.

Remote sensing and GIS techniques can help to get up-to-date information to asses and monitor changes related to geohazard aspect with low cost. Therefore, this research will give

insight to future researchers for geohazard study using the science of remote sensing and GIS. In addition, this study will give a spot place to perform for future geohazard monitoring.

1.6 Limitation of the study

One of the limitations of the study was lack of precise secondary data. For inctance their was a lack of historical earthquake epicenter data. In addation expert based evaluation of parameters could made the work to be more subjective, However it was validatied using DInSAR method. An additional challenge was occurred to process huge radar image processing which could propagate errors in the result. Nevertheless, this study provides valuable information and insight that can be of great importance for the relevant information regarding to Geohazard risk assessment and the study was not mach affected by the limitations.

1.7 Thesis Chapters organization

This thesis is composed of five Chapters. The First Chapter is about introduction to the subject and presents the statement of the problem, research objectives and scope of the study. Chapter Two gives an overview of remote sensing and GIS technology in geohazard studies, and It introduces the previous studies' in the rift valley of Ethiopia as well the study area. Chapter Three presents the methods and materials applied and used to perform the study. It gives a detail description of the study area, the datasets that were used and the overall explanation ,applied to conduct the research. Chapter Four explains the results and discussion, which mainly introduces the results of and findings primarily leading to map geohazard susceptibility of the study area. Finally, Chapter Five gives the conclusion and recommendations of the study.

CHAPTE- II LITERATURE REVIEW

Preamble

A natural hazard has been defined by Varnes ,(1984) as the probability of occurrence within a specified period of time and within a given area of a potentially damaging phenomenon. Our world is frequently exposed to geo-hazards, including earthquakes, landslides, volcanic eruptions, and others, As a consequence of these events, humanity is experiencing increasing loss of life and property. The occurrence of any of these events today has the potential to trigger global disasters in a globally interconnected and interdependent society. Our dependency on the availability of services such as power, communication, the internet and transportation, and the dependency of other services such as food, water, sewage, and health on these services would amplify the impact of extreme hazards compared to their effects in earlier times.

2.1 Geo-hazard and the Ethiopian rift valley

In Ethiopia, 90 % of the seismic related geo-hazard has occurred to the East African rift system (Haile Melaku, 2004). The East African Rift System is a 50km to 60km wide zone of volcanoes and faults that extend north to south in Eastern Africa for more than 3000km (1864 miles), from Ethiopia in the north to the Zambezi in the south. It cuts through Ethiopia in a NE-SW direction (Acocella et al., 2002; Atalye Ayele and Kuthanek, 2007). Landslide, earthquake and volcanic eruption are associated geo-hazards that will pose a threat in this region(Atalye Ayele,2017; Biggs et al., 2011;Brown et al., 2015)

2.1.1 Landslides

A landslide is defined as the movement of a mass of rock, debris, or earth down a slope. Landslides are a type of "mass wasting," which denotes any down-slope movement of soil and rock under the direct influence of gravity (https://en.wikipedia.org/wiki/Landslide).

Landslides hazard and its associated slope deformation in different regions of the Ethiopian rift margins and its associated highlands have been studied by many researchers. (e.g Bekele Abebe et al., 2010; Asfawosen Asrat et al., 1997; Lulseged Ayalew, 1999; Lulseged Ayalew and Yamagishi, 2002; Tenalem Ayenew and Barbierie, 2005; kifle Woldearegay et al., 2011) .

Landslide hazard is one of the crucial environmental problems for the development of Ethiopia, representing a limiting factor for urbanization and infrastructural projects and, generally, for all the activities performed on and at the foot of slopes (Bekele Abebe et al.,

2010). The damage produced by landslides in Ethiopia is relevant: from 1993 to 1998 alone, more than 200 houses were destroyed, more than 500 km of roads were interrupted and about 300 people were killed (Lulseged Ayalew, 1999).

The widespread distribution of landslides in Ethiopia is mainly related to the occurrence of several predisposing factors such as rugged morphology, high relief energy, and the nature of the outcropping rocks. The triggering factors are essentially connected with the rainfall regime and with seismicity, particularly along the rift margin (Bekele bebe et al., 2010).

In the last years, detailed geomorphological–geotechnical studies on landslide susceptibility/hazard of selected areas in Ethiopia have been published (Berhanu Temesgen et al.,2001; Tenalem Ayenew and Barbieri 2005; Fubelli et al., 2008; Barbieri,2012; Zvelebil et al., 2010). A preliminary assessment of landslide risk in the Dese urban area has been recently published by (Fubelli et al., 2013).

2.1.2 Seismicity

An earthquake is the shaking of the surface of the Earth, resulting from the sudden release of energy in the Earth's lithosphere that creates seismic waves. Earthquakes can range in size from those that are so weak that they cannot be felt to those violent enough to toss people around and destroy whole cities (https://en.wikipedia.org/wiki/Earthquake).

Sesmic hazard assessment in Ethiopia was initially recognized by the scientific community in the early 1960s after the catastrophic earthquakes of Kara Kore- Mejete (1961) and later in Serdo(1969). The first seismic hazard maps were prepared by Gouin, (1976) using a probabilistic approach**.**

According to Asrat Worku, (2011) the country is divided into five zones approximately equal seismic risks depending on the known distribution of earthquakes.

These zones are no damaging zone (0 zones), less damaging zones (zone 1 and 2) and zones of major damaging (zone 3 and 4). From the seismic hazard map of Ethiopia, the study area of this work falls at zone 4 as shown in (Fig 2.1). This map is based on the amplitude of the ground acceleration to be expected during 100 years return period.

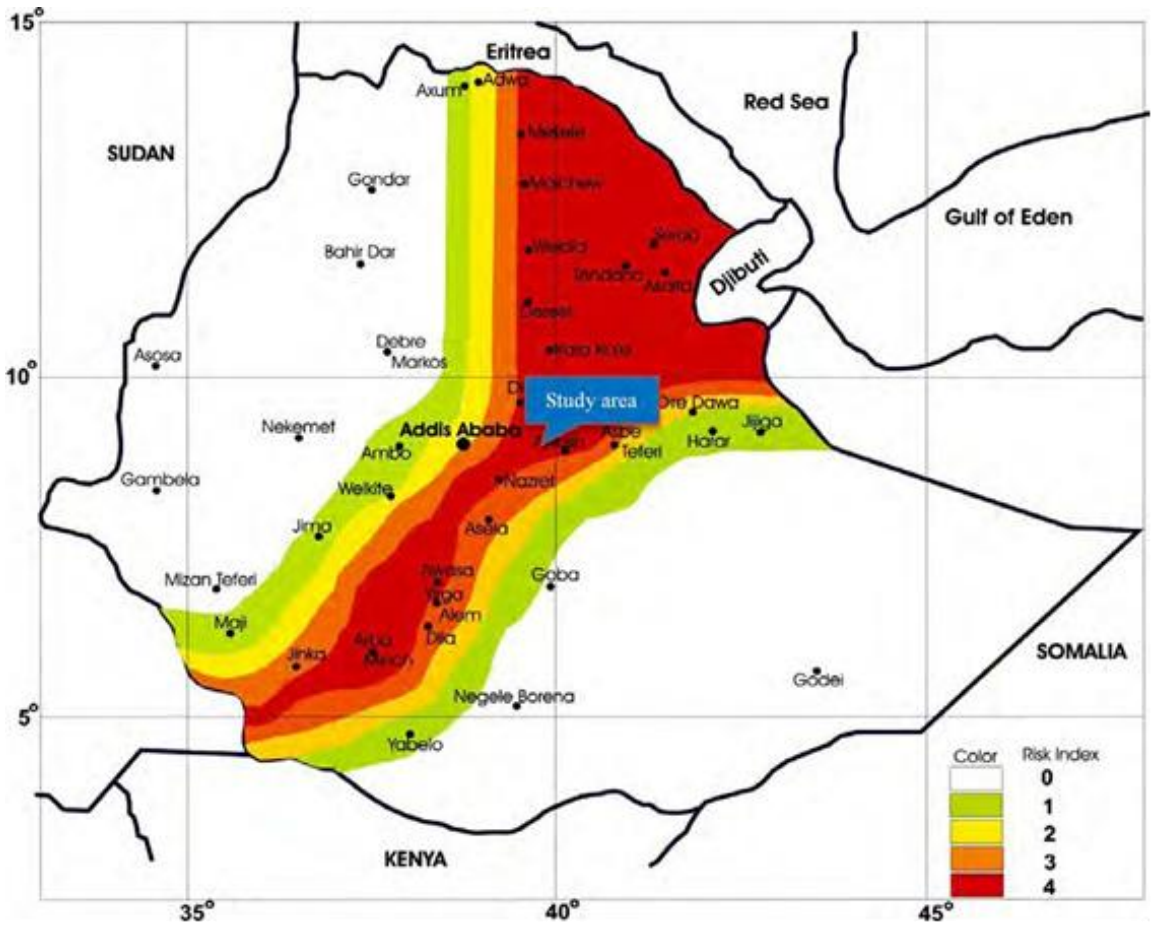

Fig 2. 1: Seismic hazard map of Ethiopia for the 100-year return period as per Ethiopian Building Code Standards (EBCS) (Asrat Worku, 2011

Another study Atalay Ayele (2017), states that most of the Earthquakes in Ethiopia are related to the rift system. (Table 2.1) shows some of the earthquakes occurred associated with the rift system from 1900 to 2010 Archive from a different source.

Table 2. 1: Some Examples of earthquakes in the Ethiopia rift system Archive from different sources

No	Year of occurrence	Place	Magnitude	E.D from A.A	Author/source/
1	1906	Langano Earthquake	6.8	100	GSDRC
2	1961	Kara Kore Earthquake	6.7	150	‘’
3	1969	Sardo/ Central Afar/	6.3		‘’
4	1983	Wondo Genet earthquake	-	300	‘’
5	1985	Langano Earthquake	6.2	110	‘’
6	1987	Rift Valley Earthquake	6.2	200	‘’
7	1989	Dobi graben Earthquake	6.3	200	‘’
8	1993	Nazret Earthquake	6	<100	‘’
9	2005	10.67N;40.30E	4.8	-	https://www.emsccsem.org
10	2006	10.91N;40.58E	4.7	-	‘’
11	2007	10.34N;40.26E	4.4	-	‘’
12	2008	10.93N;39.86E	4.6	-	‘’
13	2009	10.24N;40.90E	4.5	-	‘’
14	2010	7.54N;37.81E	5.2	-	‘’
15	2011	92 km NW Alemaya	3.2	-	‘’
16	2012	11km SW Borena	4.3	489km	‘’
17	2013	145km E Desse	4.1	349km	‘’
18	2014	29km SE Aseita	4.6	162km	‘’
16	2015	11km NW Metehara	4.4	121km	‘’
17	2016	32 km W Awasa	4.4	234km	‘’
18	2017	36km S Ziway	5.3	155km	‘’

2.1.2 Volcanism and volcanic hazard

According to Mohr (1962), for the last centuries, several volcanic eruptions have been recorded in the MER and the Afar Triangle. Another study (Fubelli et al., 2015) volcanic activity is associated with the rifting. In Ethiopia, 59 Holocene volcanoes are currently known (Bekele Abebe et al., 2007; Siebert et al., 2010). They form two distinct lines of volcanoes which can be seen within the East African Rift. The first line is the Main Ethiopian Rift, a NE-trending line that bisects the middle of the country. The second line is oriented NNW, nearer the border with Eritrea, and consists of a series of smaller en-echelon lines of volcanoes in the area of the Afar Depression.

As in other countries in the East African Rift, a significant number of these volcanoes are mafic with basaltic volcanic fields (cinder cones and fissures), shields and monogenetic cones with a predominantly effusive eruption style (Bekele bebe et al., 2007); there is less evidence

of explosive volcanism (Brown et al., 2015). However, seven of Ethiopia's volcanoes are currently known to have produced felsic pyroclastic flow deposits, including some large volume ignimbrites (Brown et al., 2015). The limited records of explosive volcanism in Ethiopia, whether due to poor preservation of the record or absence of eruptions of this nature, should not be used to indicate a low probability of such an eruption in the future (Lenhardt and Oppenheimer, 2014).

The population exposure to volcanic hazards in Ethiopia is high; there are 1.5 million people (1.6% of the population) living within 10 km of a Holocene volcano, over 11 million (12.3%) within 30 km, and over 42 million (46.5%) within 100 km (Brown et al.,2015). Based on the calculated population exposure index, the following systems have high exposure in Ethiopia: the Bishoftu Volcanic Field, Sodore, the Butajiri Silti Field, Corbetti Caldera, the Bilate River Field and Hobicha Caldera (Fig 2. 2). However, volcanoes that have been active since with 1900 with a lower population exposure could pose greater risks as a result of a higher hazard ranking, including Alutu, Fentale, Kone and Tullu Moje.

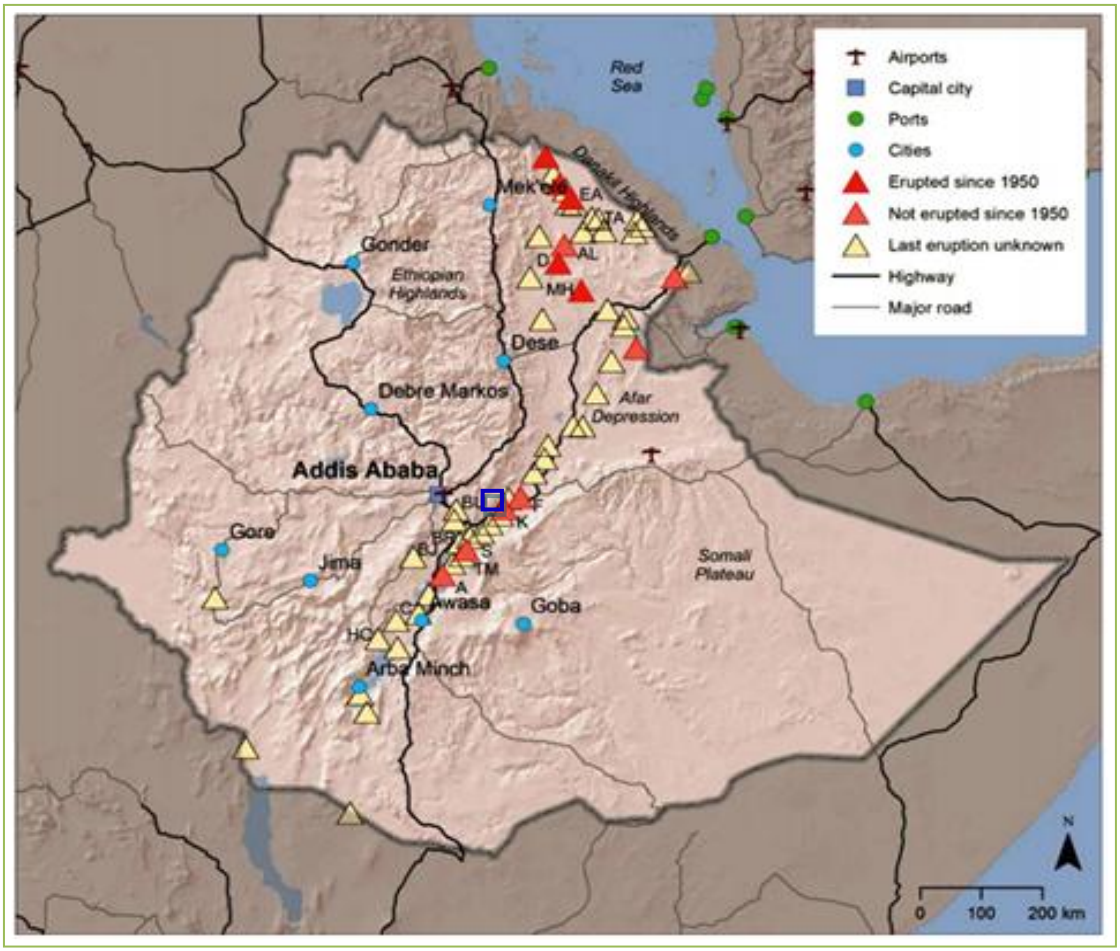

Fig 2. 2: Location of active volcanoes in Ethiopia. (Source: Brown et al. 2015). The study area is highlighted in a blue rectangle.

2.2 Role of Remote sensing and GIS in Geo- hazard studies

In the current scenario owing to the increasing efficient quality of the sensor technology and increase in the number of operational satellites that are launched by many space research organizations and firms around the world, the field of remote sensing or earth observation has made a remarkable development and achievement in all fields of life. Earth Observation System (EOS) otherwise known as Remote Sensing (RE) and GIS assist professionals of Geo-hazard studies and disaster management in a very effective manner and provides more precise data's (Krishnamoorthi, 2016). With this technology, it is easy to obtain homogeneous data covering the entire world over a short period of time.

Diverged Array of spectral bands in visible (VIS), near infrared (NIR), short wave infrared (SWIR), thermal infrared (TIR) and synthetic aperture radar (SAR) provide sufficient spectral coverage for observing natural hazards and also aids in computer enhancement of the acquired data. Each sensor provides distinctive information about different properties of surface objects or the shallow layers of the earth. For instant to measure surface temperature thermal sensors are employed, microwave sensors used to detect dielectric properties (Krishnamoorthi, 2016).

2.2.1 Optical remote sensing

The field of optical remote sensing has a wide-ranging number of applications. It is also possible to consider optical remote sensing from a variety of scales. Environmental remote sensing typically refers to detailed field-based measurements (e.g. field spectrometry); airborne imagery; and satellite imagery. Specifically, the type of data acquired in optical remote sensing makes use of the visible, near-infrared (NIR), and shortwave infrared (SWIR) parts of the electromagnetic radiation (EMR) spectrum. A sensor is termed 'panchromatic' if it acquires data in a single region or waveband of the spectrum. A 'multispectral' sensor will acquire several (up to ten) broad spectral bands, while a 'hyperspectral' sensor will acquire many more narrow bands. The increasing availability of high-quality optical satellite images enables, in principle, the continuous monitoring of Earth's surface changes (Leprince, et al.,2008).

2.2.2 Synthetic Aperture Radar (SAR)

Radar (SAR) systems, peculiar radar sensors capable of providing high-resolution microwave images. Due to the larger wavelength compared to visible and infrared radiation, microwaves (wavelength between 1 cm and 1 m) exhibit the important property of penetrating clouds,

fog,and possible ash or powder coverage (for example, in case of an erupting volcano or a collapsed building). This important property provides an imaging capability in any weather condition or environment, although some atmospheric disturbances can affect both the amplitude and, more importantly, the phase of SAR images.

Ground deformations are estimated using the Differential Synthetic Aperture Radar Interferometry(DInSAR) technique, which is based on the exploitation of microwave image pairs (France schetti and Lanari1,999); this technique is particularly powerful for its capability to generate actually dense deformation maps of large areas, with centimeter to millimeter accuracy (Gabriel et al., 1989; Massonnet and Feigl,1998; Burgmann et al., 2000). The investigation of deformation phenomena affecting the Earth surface is a key element for the analysis of natural events such as earthquakes (Okada,1985; Chinnery, 1961), volcano unrest phases (Mogi,1958) and landslides (Farrell ,1972).

More specifically, the DInSAR technique exploits the phase difference (interferogram) between SAR image pairs acquired at different times (whose separation is referred to as temporal baseline) but with the same illumination geometry and from sufficiently close flight tracks (whose separation is referred to as spatial baseline) (Franceschetti and Lanari,1999). To separate the deformation contribution from the topographic one, the DInSAR technique analyses the so-called differential interferograms, which are generated by compensating interferograms with their topography-related phase component, usually computed by means of an external Digital Elevation Model (DEM) (Gabriel et al.,1989; Massonnet and Feigl ,1998; Franceschetti and Lanari,1999; Burgmann et al. ,2000).

2.2.3 Geographical information system (GIS)

Different types of GIS definitions exist in different areas and disciplines. But all GIS definitions recognize the use of spatial data. Many alternative definitions of GIS have been suggested, but a simple definition is that a GIS is a computer-based system for the capture, storage, retrieval, analysis and display of spatial data (Skidmore, 2002).

"A geographic information system (GIS) is a computer-based tool for mapping and analyzing things that exist and events that happen on earth. GIS technology integrates common database operations such as query and statistical analysis with the unique visualization and geographic analysis benefits offered by maps. "http://www.gis.com/content/what-gis.

GIS technology now a day's has a potential to delineate and predicts disaster places which are vulnerable and most probable to occur (Bahuguna et al, 2013). Therefore by understanding and knowing the areas where the disaster happens, it is easy for more effective

and efficient methods to mitigate further risks. The extent of damage is dependent on the density of the population, physical infrastructure and means accessible for mitigation purposes such as evacuation site, flood control dams, etc (Krishnamoorthi, 2016).

GIS synthesize information from a vast number of different data resources and helps in assessing disaster impact, plan response and relief strategies. Remote sensing and Geographic Information system play a vital role to evolve suitable and sustainable strategies for assessing, managing and mitigating the disasters and also provides an occupational framework to identify and fill the gaps (Krishnamoorthi, 2016).

Remotely sensed data helps rapidly in identifying hardest-hit areas, manipulates population density in disaster-prone areas, monitors rehabilitation or reconstruction after major havoc. During a crisis, it facilitates a plan for timely evacuation and recovery operations. Remote sensing is the only way to overview the disaster events happening on the earth's crust. (Krishnamoorthi, 2016)

Integrated work of Remote sensing and GIS plays a vital role in many aspects of disaster management, ranging from risk modeling and vulnerability analysis to early warning.

CHAPTE- III MATERIAL AND METHODS

3.1 Description of the study area

3.1.1 Location

The study area is a part of the main Ethiopian rift valley (MERV) and is located in the middle catchment of the Awash River basin. Geographically it lies between UTM Zone 37, 545000 - 633000 Easting and 968000 - 107000 Northing (Fig 3.1) and has an altitude that range from 703 to 3549 m above mean sea level. It has an average distance of 126km east of the country capital city, Addis Ababa and its administrative location are at the boundary of Oromia, Amhara, and Afar regional states. The area covers an approximate of 7176 km ^{2}.

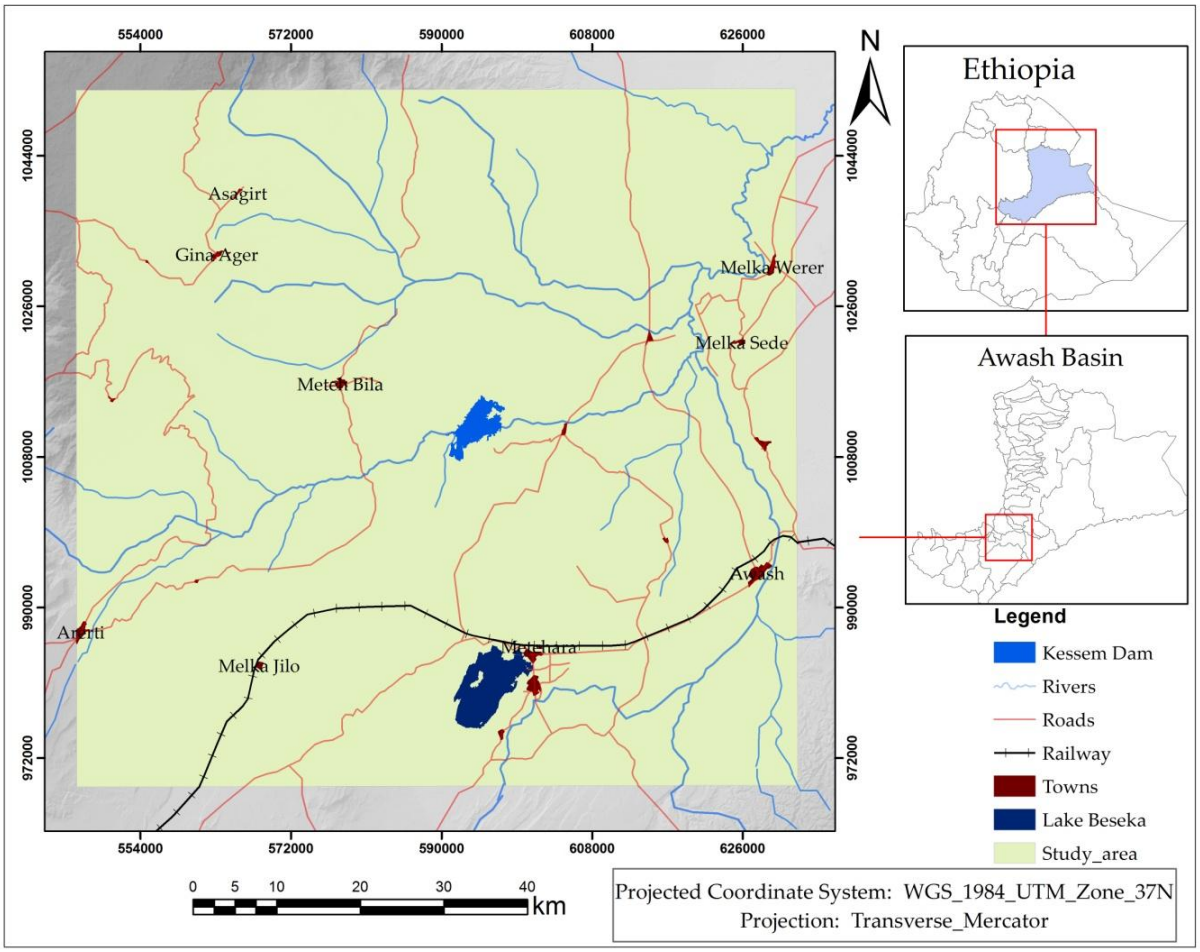

Fig 3. 1: Location of the study area

3.1.2 Topography and Drainage

3.1.2.1 Topography

The study area has variable altitude, ranging from very low land (703m), very flat areas (950 m) to undulating plains (1100 m), hills (1500 m) to mountains (1900 m), and the highest elevation reaches up to (3549m) above mean sea level (Fig 3.2). The area covers the rift floor, the western rift margin and at some extent the western plateau. The study area also contains, the well known volcanic mountains called Kone, Fentale, and Dofan; which is believed to be created by the recent volcano that occurred in the region at the end of the Eighteenth Century(Brown et al.,2015). The west rift margin of the study area clearly shows sloppy fault scarps that are the main characteristics of the Ethiopian rift valley.

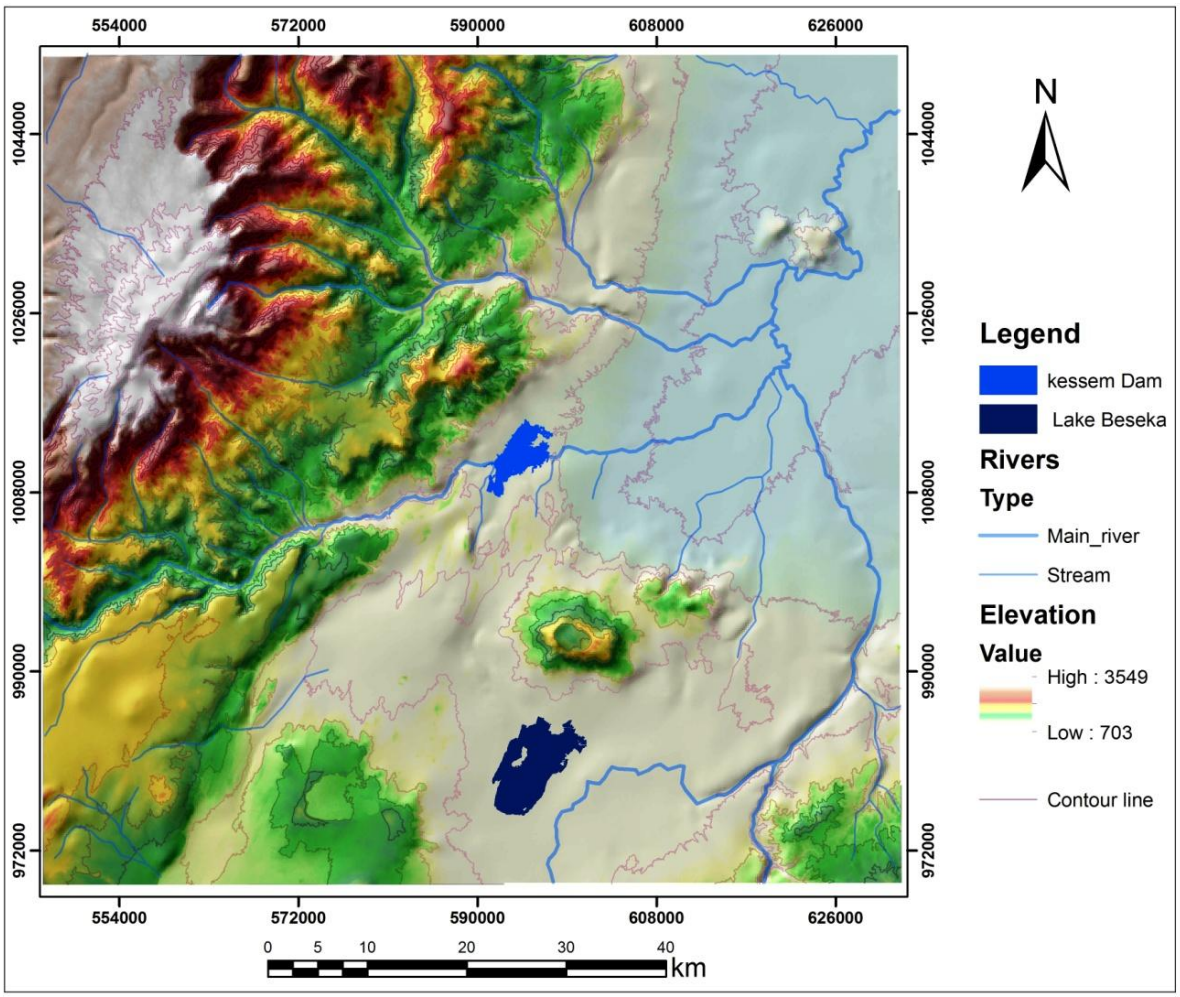

Fig 3. 2: Phisography of the study area

3.1.2.2 Drainage pattern

There are many rivers and streams which cross the study area. These streams and rivers start from the NW, W and SSW part of the study area and they draine to-wards NE and finally to the Awash River. Kessem, Kebena, Dufanta, and Awash are the major rivers, which can be mentioned at the first rank. Especially Awsh River is the most known river found in the Northern rift valley Basin. This river is also governed by the rift structure, (Tenalem Ayenew, 2004). It flows parallel to the trending direction of the rift structure. The reason could be, they can't cross the rift fault (Tenalem Ayenew, 2004). Rivers drained from North and South East direction forms drainage pattern, whereas rivers coming from S and NNE direction are almost parallel to each other (Fig 3.3).

,

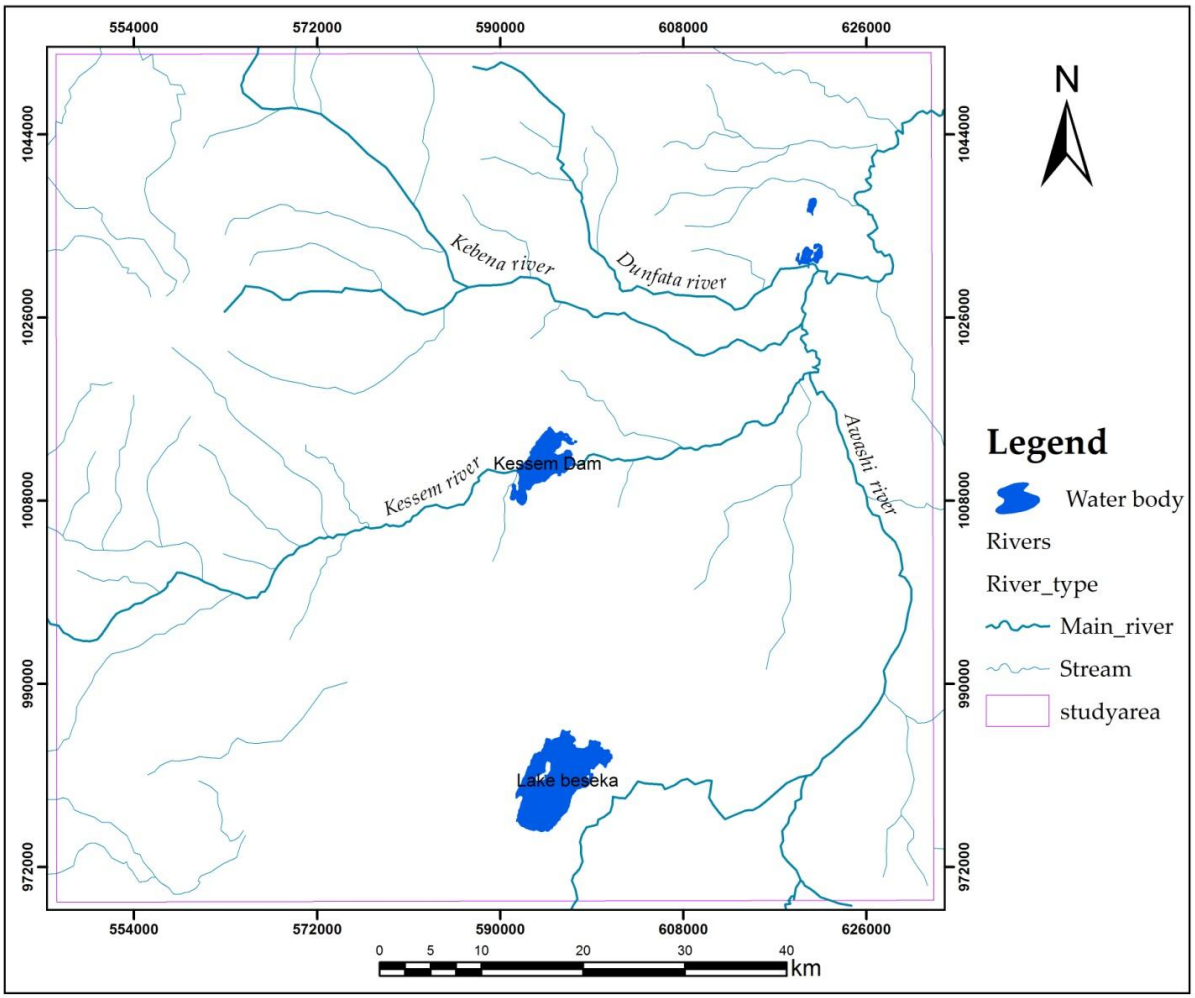

Fig 3. 3 : The Drainage pattern

3.1.3 Climate

3.1.3.1 Rainfall Distribution

The study area has the characteristics of a semi-arid climate with a bimodal and erratic rainfall distribution pattern (Madani et al.,2015). The main rainy season occurs from July to September and accounts for about 70% of the total rainfall of the area. The minor rain season, which accounts for about 30% of the total rainfall, occurs occasionally from February/March to April. The mean monthly rainfall from (2005-2017) is presented in (Fige.4). The minimum, mean and maximum annual precipitations during this period are 308.7 mm, 522.7mm and 863.5mm respectively. (Fige.4).

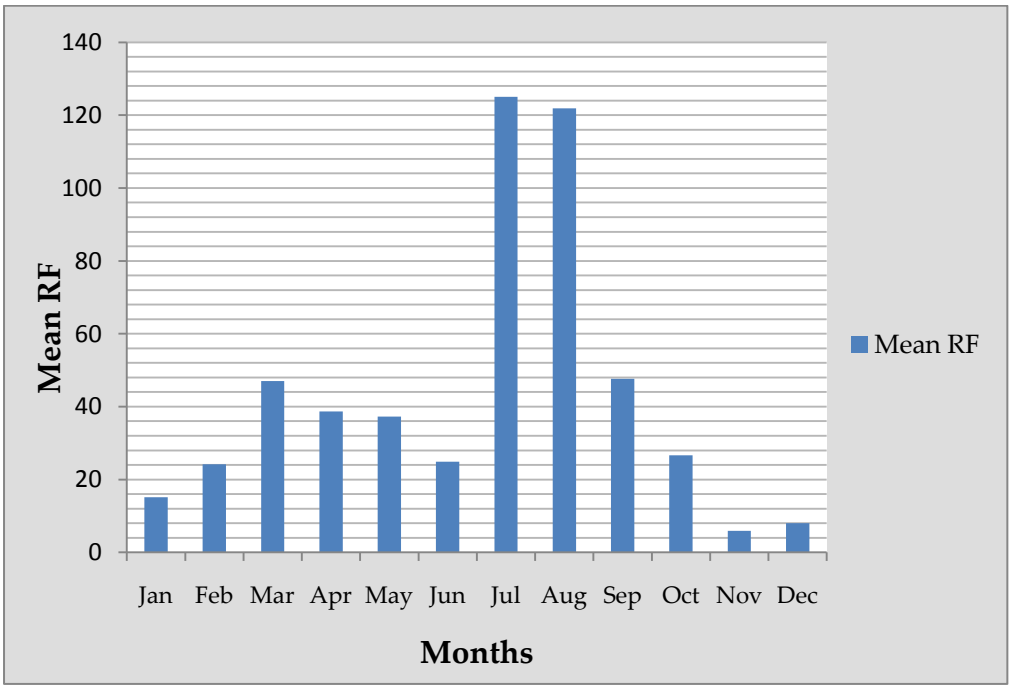

Fig 3. 4: Mean Monthly Rainfall from 1970-2015 (source: Dershaye Belay,2017)

3.1.3.2 Temperature

The minimum and maximum mean monthly temperature values in the study area is 21.8°C in December and 28.9°C in June respectively (Fig 3.5). The mean annual temperature of the study area is 30.47°C. The minimum and maximum monthly temperatures in the area were recorded in 2007and 2016 respectively.

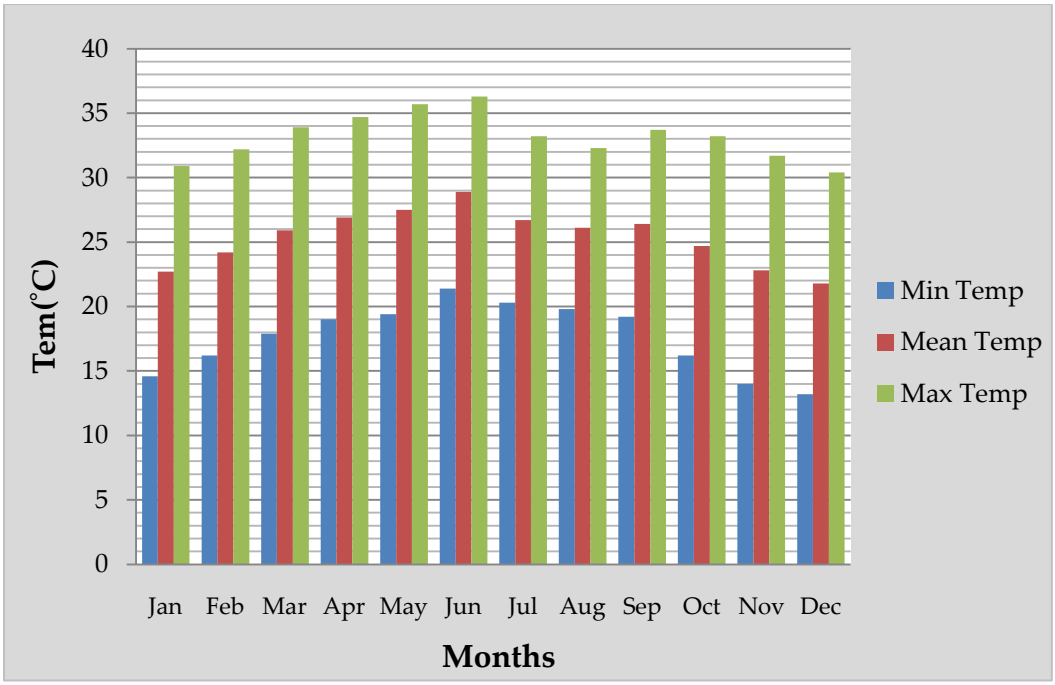

Fig 3. 5: Mean monthly temperature from 1970-2015 (source : Dershaye Belay,2017)

3.1.4 Geology and Rift Structure

3.1.4.1 Geology

Most of the outcrops exposed along the rift are dominated by Tertiary volcanic rocks except for a few locations where the crystalline basement is uncomformably overlain by Mesozoic sedimentary and /or Tertiary volcanic rocks (Giday WoldeGabriel et al., 1990). A thick succession of ignimbrites, unwelded tuffs, ash flows, rhyolites and trachytes collectively known as the Nazareth Group constitute the larger part of the rift floor and also outcrop in the escarpments and on the adjacent plateau margins (Habtamu Eshetu et al., 2012). Lacustrine sediments in the rift proper comprise clay, silt, tuff, travertine, and diatomite with intercalation of pumice (Habtamu Eshetu et al., 2012).

Basically, the rock units in the study area are basalt, trachyte, Ignimbrite and alluvial and ash flows of the two groups: Nazreth Group (oldest) and Wonji Group (youngest) of the Fentale and post –Fentale volcanic. These lithology units are generalized from a geological map of Debere Birhan and Nazrite sheet NC 37-11 and NC 37-11 respectively(Daniel Meshesha et al., 2010). Descriptive of all lithology units are shown in Table 3.1 and(Fig 3.6).

Ta**ble 3. 1**: Classification of lithologies and their stratigraphy

Age		Lithographic units	Symbol	Lithologies
		Superficial Deposits	**Qa**	Alluvium with minor ignimbrite (Qal)
			Qel	Eluvium (Qel)
Cenozoic	Quaternary	Volcanic rocks	**Qwt**	Young basaltic scoria(Qwt)
			Qwo	Recent basaltic flow(Qwo)
			Qwi	Young ignimbrite of fentale(Qwi)
			Qdb	Dofan basalt (Qdb) vesicular basalt, aphanitic basalt, olivine-phyric basalt, and recent scoria cones
			Qft	Fantale Trachyte (Qft)
			Qfig	Fentale-Alay Dege ignimbrite (Qfig) ignimbrite, tuffs, ash flows, agglomerate, and minor obsidians
	Tertiary	Volcanic rocks	**Ttb**	Tarmaber-Megezez basalt (Ttb) plagioclase phyric and olivine-plagioclase phyric basalts with minor olivine-phyric, pyroxene phyric, plagioclase-pyroxene-olivine phyric and aphanitic basalts.
			Tdig	Sela Diagay-Debre Birhane_Goro ignimbrite: ignimbrite, tuff, rhyolite, basalt, tuffaceous sediment, ash, and agglomerate
			Tt	Trachyte (Tt)
			Tkb	Kesem basalt (Tkb) aphanitic basalt intercalated with plagioclase phyric basalts and thin beds of ignimbrite

(Source: Daniel Meshesha et al., 2010)

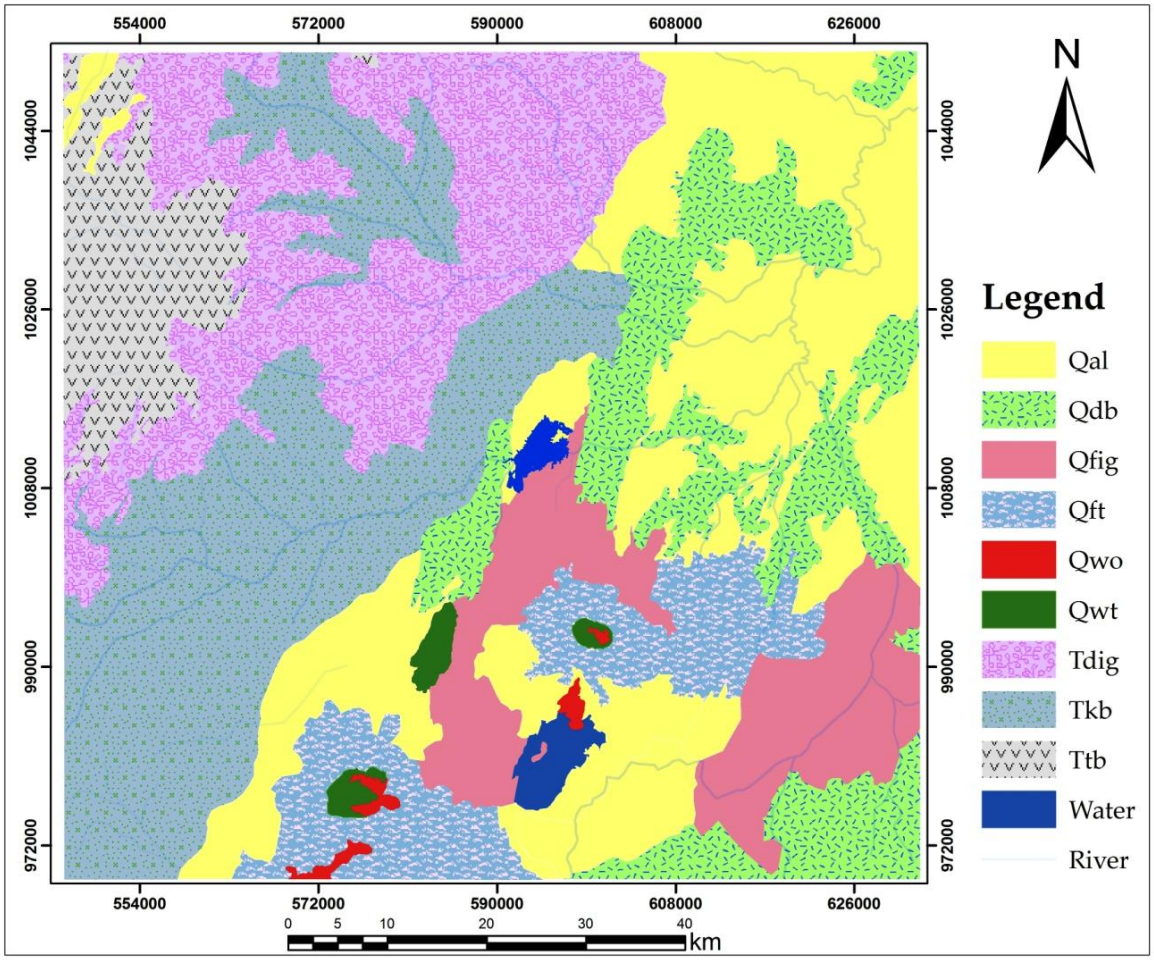

Fig 3. 6 : Geological map of the study area, symbols are explained in (sorurce:GSE)

3.1.4.2 Rift structures

The present MER is made up of northern, central and southern sectors (Giday WoldeGabriel et al., 1990). There is a difference of ~15˚ in the trend of the northern and southern sectors nevertheless, the overall mean direction of the MER remains NE-SW (N40˚E) (Acocella et. al., 2002). The youngest part of the MER is the axial zone, which coincides with the so-called Wonji Fault Belt (WFB), mainly formed during the Quaternary (Mohr1987; Boccaletti et. al., 1998, 1999). Despite the overall NE-SW trend of the MER, the WFB is characterized by active NNE-SSW-trending extension fractures and normal faults. These are often set in a dextral en-echelon arrangement and associated with volcanic activity (Acocella et. al., 2002). The slightly different trend of the Quaternary WFB with regard to the MER margin suggests a change in the extension direction during Quaternary (Bonini et al., 1997; Boccaletti et al., 1998). (Fig 3.7) shows a clear confirmation of the previous literature works including the dextral en-echelon arrangement faults and fractures located at the axial zone (WFB) and also the general trend direction such structures indicated using a rose diagram.

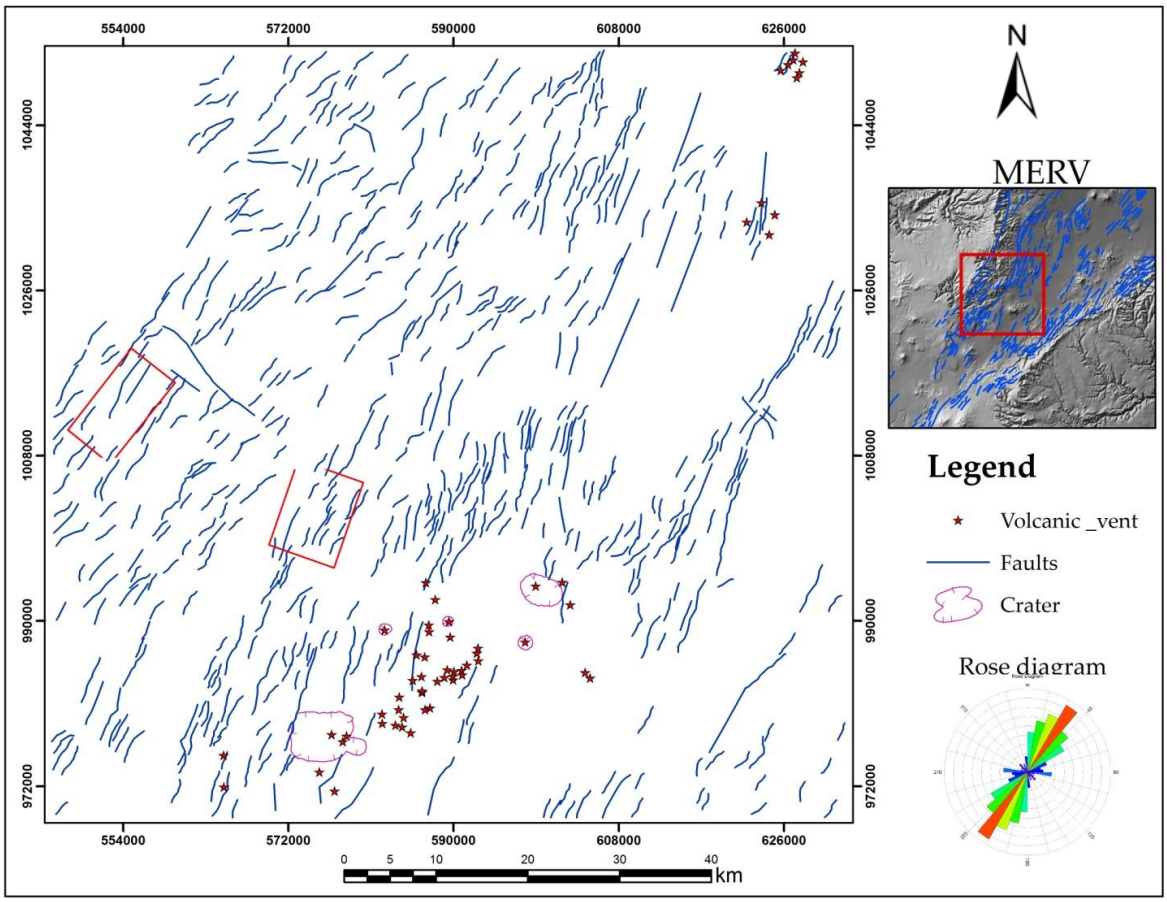

Fig 3. 7: Structural map of the study area (Generated : using satellite image)

3.1.4.3 Active Volcanic vents and mountains

The study area is also characterizes by its well-known volcanic centers called Kone, Fentale and Dofan; which are located along the rift axial zone. Thus volcanic vents are studied by several researchers and their eruption histories are believed to be at the end of the Eighteenth Century (Brown et al., 2015).

(Fig3.8) depicts,these volcanic vents and mountains, zooming by their elevation and their spatial location. These volcanic edifices situated along a southwest to northeast direction following the rift axial zone orientation. They are also the main source of fresh volcanic rocks observed in the study area and, they could be the most possible threats for volcanic hazard (Brown et al., 2015).

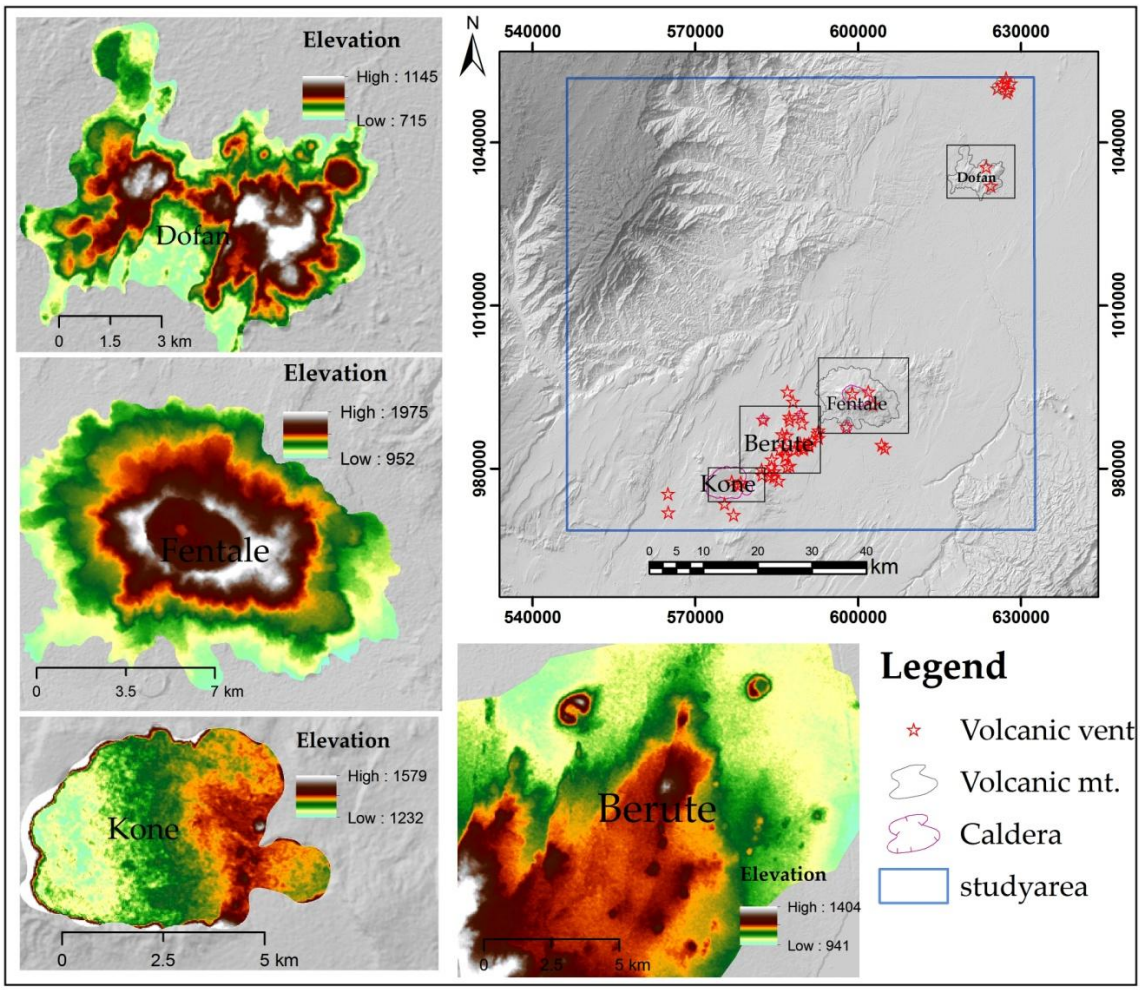

Fig 3. 8: Active volcanic vent and mountains in the study area zoom by their elevation (Generated using ASTER DEM)

3.2 Materials and sources

3.2.1 Satellite image archives

Landsat imagery of 2018 (OLI) with Path 168 and row 054 and 30m, ASTER DEM acquired from one source of free satellite imagery (USGS). The images were used to extract different thematic data layers such as LULC, fault, lineaments and active volcanic vent, while the DEM was used to generate drainage networks, slope, and elevation of the study area.

Table 3. 2: Satellite data description

Data of acquisition	Sensor	Spatial resolution	Data type	Format	Source
2018	Landsat 8(OLI)	30m	LULC	Raster	USGS
			Structures		
			Active volcanic		

			vents		
2017	ASTER (DEM)	30m	Slope	Raster	USGS
			Drainage		
			Topography		

3.2.2 Ancillary data source

To accomplish this work in addition to a satellite data source other secondary data were Used. These data were collected from the Geological Survey of Ethiopia (GSE) and from Global and National Soil and Terrain Digital Database (SOTER). The data collected from GSE were lithology, and SOTER data were soil.

Table 3. 3: Description of Ancillary data source

Data type	Format	Source
Lithology	Jpg image	GSE
Soil	Raster	SOTER

Table 3. 4: Software used to process the data

NO	Software name	Version	Mainly used for
1	Arc GIS	10.5	Data analysis and map preparation
2	ERDAS	2014	Image processing
3	ENVI	5.4	Image processing
4	Geomtica	2018	Fault and lineament extraction
5	SNAP	6.0	Radar image processing
6	SAGA GIS	2.3.2	Soil texture analysis
7	IDRISI selva	17.0	Image processing and statistical data analysis
8	Rock work	17	Rose diagram preparation

3.3 Methods and data processing

Preparation of different thematic data layer was the main activity to build spatial modeling of Geo-hazard susceptibility. The entire data layers created were retrieved for the model input. These layers were LULC, fault, lineament, active volcanic vent, slope, elevation, soil and lithology. (Fig 3.9) shows the general methodological flow chart.

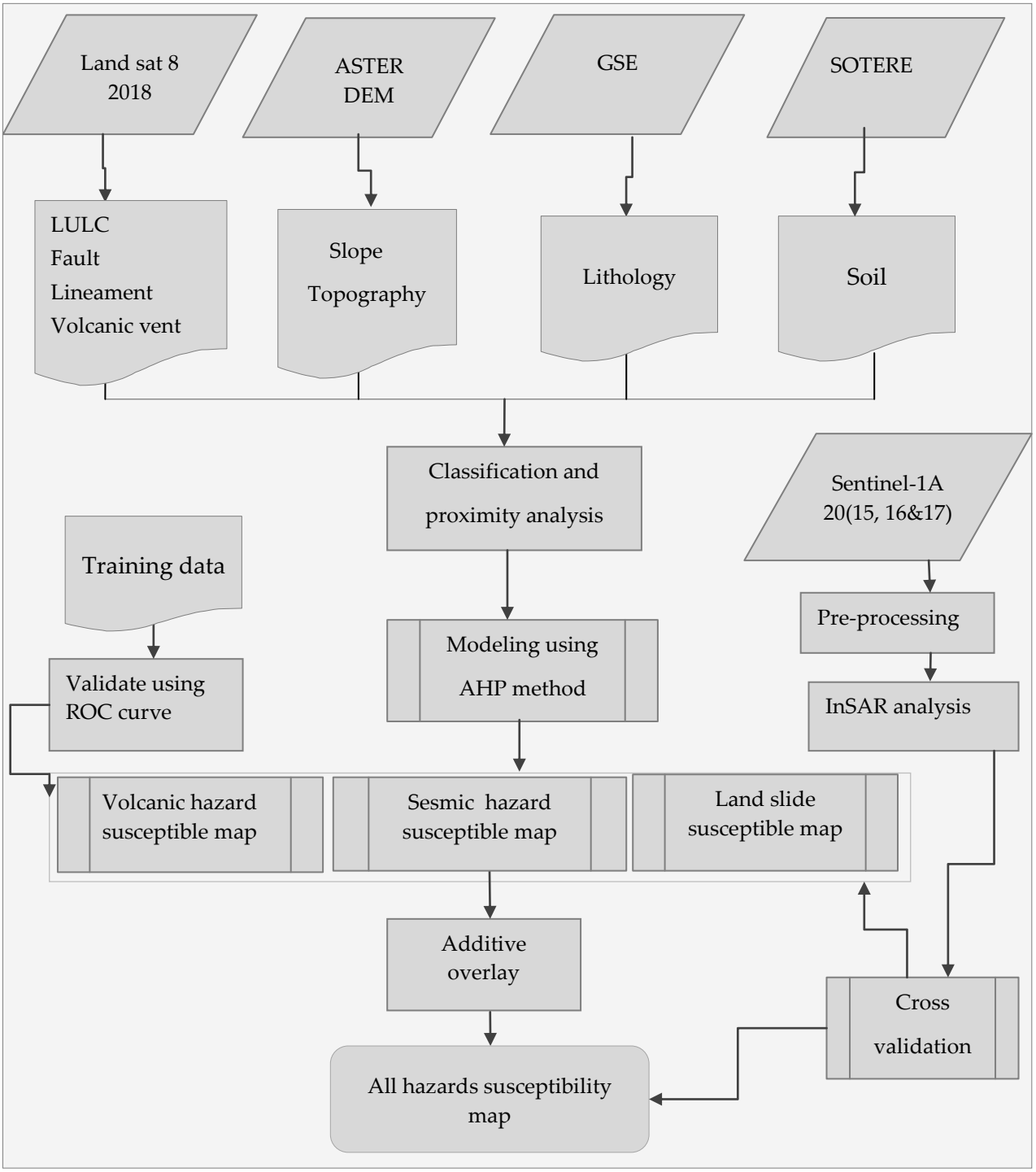

Fig 3. 9: Procedural workflow chart

3.3 .1 Processing of Land sat image

The digital image processing is largely concerned with four basic operations: image restoration, image enhancement, image classification, and image transformation (Lillesand et al., 2004). The image restoration is concerned with the correction and calibration of images in order to achieve a faithful representation of the earth surface as possible. Image enhancement is predominantly concerned with the modification of images to optimize their appearance to the visual system. To get a better-enhanced image, different image enhancement techniques are available with different digital image processing software(Lillesand et al., 2004). One of the image enhancement works done in Landsat image in this work was the spectral enhancement technique called principal component analysis.

3.3.1.1 Pans sharpening

"Pan Sharpening" is shorthand for "Panchromatic sharpening". It means using a panchromatic (single band) image to "sharpen" a multispectral image (an image that contains more than one spectral band). In this sense, to "sharpen" means to increase the spatial resolution of a multispectral image. A multispectral image contains a higher degree of spectral resolution than a panchromatic image, while often a panchromatic image will have a higher spatial resolution than a multispectral image. A pan-sharpened image represents a sensor fusion between the multispectral and panchromatic images which gives the best of both image types, high spectral resolution, and high spatial resolution(Lillesand et al., 2004).
In this work 15m spatial resolution of Landsat 8 (OLI) panchromatic band were used to sharpen the multispectral image for the principal component analysis.

3.3.1.2 Principal component analysis

Principal Components Analysis (Karhunen-Loeve or Hotelling transform) is a mathematical technique which transforms the original image data, typically highly correlated, to a new set of uncorrelated variables called principal components. These new components are linear combinations of the original image bands and are derived in decreasing order of importance so that, for example, the first principal component accounts for as much as possible of the variation in the original data(Lillesand et al., 2004).
Thus, useful information for the identification of the units that exist within the image can be compressed properly into two or three components. Let us leave the mathematical background of the transformation; however, the general conceptual aspect of data

transformation in PCA analysis is shown in (Fig 3.10).

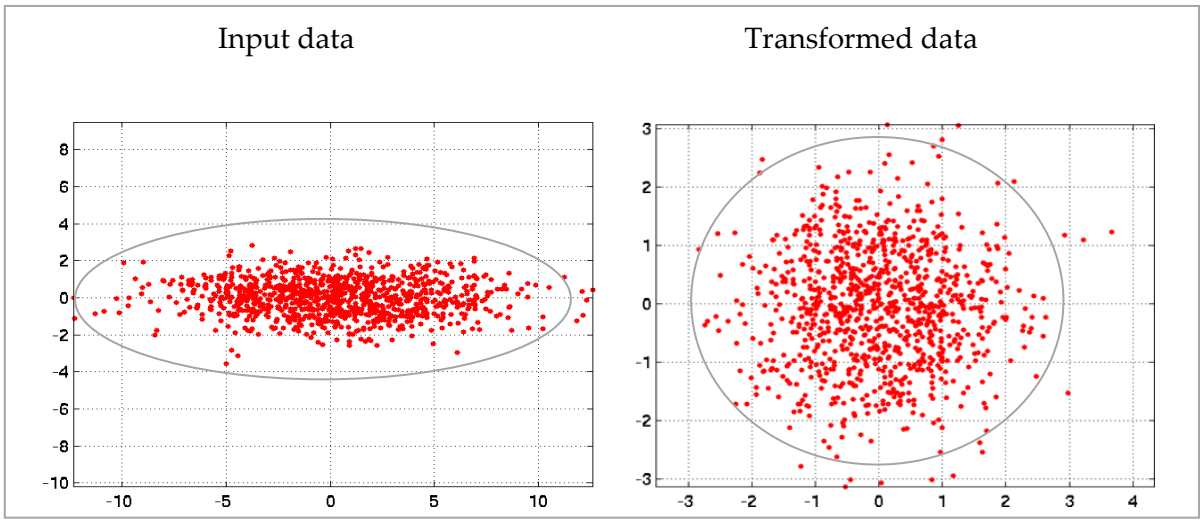

Fig 3. 10: Conceptual framework of data transformation in PCA analysis (Source of Figure: Mark et al., 2004)

Jensen , (1996) claims that, generally, the first component of the PCA consists of both near and middle-infrared information (eg. Bands 4, 5 and 7). Similarly Nama, (2004) argues that the geological information such as faults, lineaments and other subtle features can be easily identified using PCA of the Landsat image, which removes redundant information from visible and NIR multi-spectral data.

In this study, the principal components (PCs) were performed using Landsat 8 pans sharped image with band (1-7) input channels. Table 3.5 shows the general image statistics of the principal components (PCs) which were done. The eigenvalues indicate the decreasing variance in successive principal components. The first principal component contains 88.3% of the total variance. From the total band, the three components contain 98.2 % of the total variance within the whole volume of the data .

Table 3. 5: The General statistical report of Landsat 8 images PCA analysis

Cor. Matrix	B1	B2	B3	B4	B5	B6	B7
B1	1	0.982544	0.942496	0.868576	0.784756	0.753586	0.741950
B2	0.982544	1	0.982933	0.930184	0.801826	0.778778	0.764969
B3	0.942496	0.982933	1	0.976416	0.840815	0.829857	0.816699
B4	0.868576	0.930184	0.976416	1	0.864232	0.883468	0.863224
B5	0.784756	0.801826	0.840815	0.864232	1	0.915598	0.830028
B6	0.753586	0.778778	0.829857	0.883468	0.915598	1	0.967668
B7	0.741950	0.764969	0.816699	0.863224	0.830028	0.967668	1

Components	PCA 1	PCA 2	PCA 3	PCA 4	PCA 5	PCA 6	PCA 7
% Var.	**88.302915**	7.471360	2.420551	1.526663	0.195121	0.057462	0.025935
Eigenval.	6.181204	0.522995	0.169439	0.106866	0.013658	0.004022	0.001815
Eigenvec.1	0.371837	-0.451048	-0.015550	-0.595072	0.076881	-0.459095	-0.295401
Eigenvec.2	0.382227	-0.424304	0.050864	-0.079669	0.103256	0.388934	0.709227
Eigenvec.3	0.391245	-0.274475	0.077927	0.321133	-0.224238	0.511200	-0.592270
Eigenvec.4	0.390930	-0.053523	0.122717	0.682043	0.126764	-0.576939	0.123040
Eigenvec.5	0.368866	0.280975	-0.828809	-0.021454	-0.299792	-0.025716	0.084081
Eigenvec.6	0.374301	0.487580	0.047704	-0.125123	0.736575	0.201488	-0.145231
Eigenvec.7	0.365482	0.470786	0.535573	-0.234771	-0.533533	-0.050196	0.125105

Loading	PCA 1	PCA 2	PCA 3	PCA 4	PCA 5	PCA 6	PCA 7
B1	**0.924462**	-0.326191	-0.006401	-0.194532	0.008985	-0.029117	-0.012587
B2	**0.950294**	-0.306850	0.02037	-0.026044	0.012067	0.024667	0.030219
B3	**0.972715**	-0.198496	0.032077	0.104980	-0.026207	0.032421	-0.025236
B4	**0.971932**	-0.038707	0.050514	0.222963	0.014815	-0.036591	0.005243
B5	**0.917075**	0.203197	-0.341162	-0.007013	-0.035036	-0.001631	0.003583
B6	**0.930589**	0.352610	0.019636	-0.040903	0.086083	0.012779	-0.006188
B7	**0.908661**	0.340465	0.220458	-0.076747	-0.062354	-0.003184	0.005331

Faults, lineaments and active volcanic centers were easily extracted using PCA 1 band which contains 88.3% information in the image after Principal Component Analysis (PCA). (Fig 3.11) shows PCA 1 band which contain majority of information in the image and PCA7 are noises in the image which were removed.

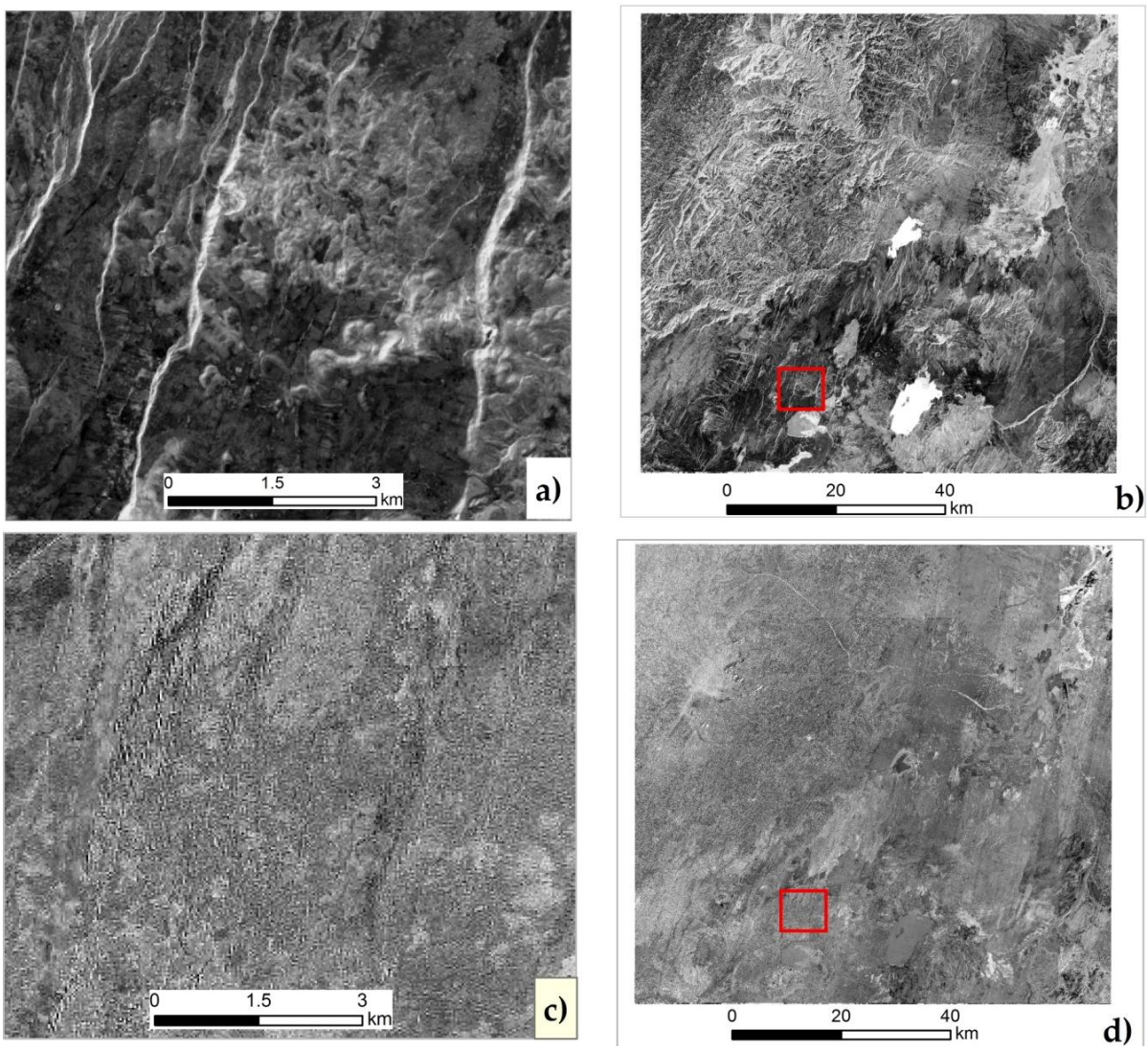

Fig 3. 11: PCA analysis result: a) PCA1 image, b) zooming view subset from PCA1 image, c) PCA7 image, and d) zooming view subset from PCA7 image

3.3.2 Feature extraction

3.3.2 .1 Fault and lineament extraction

Faults and Lineaments (structures) are defined as mapable linear surface features, which differ distinctly from the patterns of adjacent features and presumably reflect subsurface phenomena (O'Leary et al., 1976). The subsurface effect is valid if the origin of the linear features is controlled by geological structures such as faults and fractures. Not faults, but lineaments could result from morphological effects (stream channels or drainage divides) or human effects (roads, field boundaries) can also exist in the region(Koike et al.,1995).

Faults and lineaments were generated using an integrated manual and automatic feature extraction technique. Automated extraction was performed by using the Algorithm of

Automated Lineament Extraction in Geomatica 2018 software. LINE module of Geomatica extracts linear features from an image and records the polylines in vector segments. The image used to extract the features was PCA1 band from pan sharped Landsat 8 image. This method takes an advantage to perform operations in a short time and to extract lineaments which are not recognized by the human eyes over the manual extraction technique(Koçal, 2004).

In the manual extraction method, these features were extracted from satellite image by using visual interpretation. They usually appear as straight lines or "edges" on the images, which in all cases is contributed by the tonal differences within the surface material. The knowledge and the experience of the user is the key point in the identification of features in the image (Wang et al., 1990). Even though some general features like straight valleys, continuous scarps, Straight rock boundaries, Systematic offset of rivers, sudden tonal variations, alignment of vegetation were used to identify these features

Several methods have been used to improve the quality and efficiency of extracted faults and lineament data. Especially to detect faults data, 30m ASTER DEM, Hill shed generated from the DEM, intensity band of SAR image, slope, secondary scan map, and Google earth were used. Their length and preferred orientation are also shown using a rose diagram. They have a great correlation with the regional work done by many researchers (Acocella et. al., 2002, Bonini et al., 1997; Boccaletti et al., 1998).

Fig 3.12, depicts the final map of both faults and lineaments generated from the image. The blue box highlights on both images show the difference in orientation of structures at the axial zone and rift margin. Along the axial zone, structures are tilted towards North whereas at the margin they are almost NE-SW.

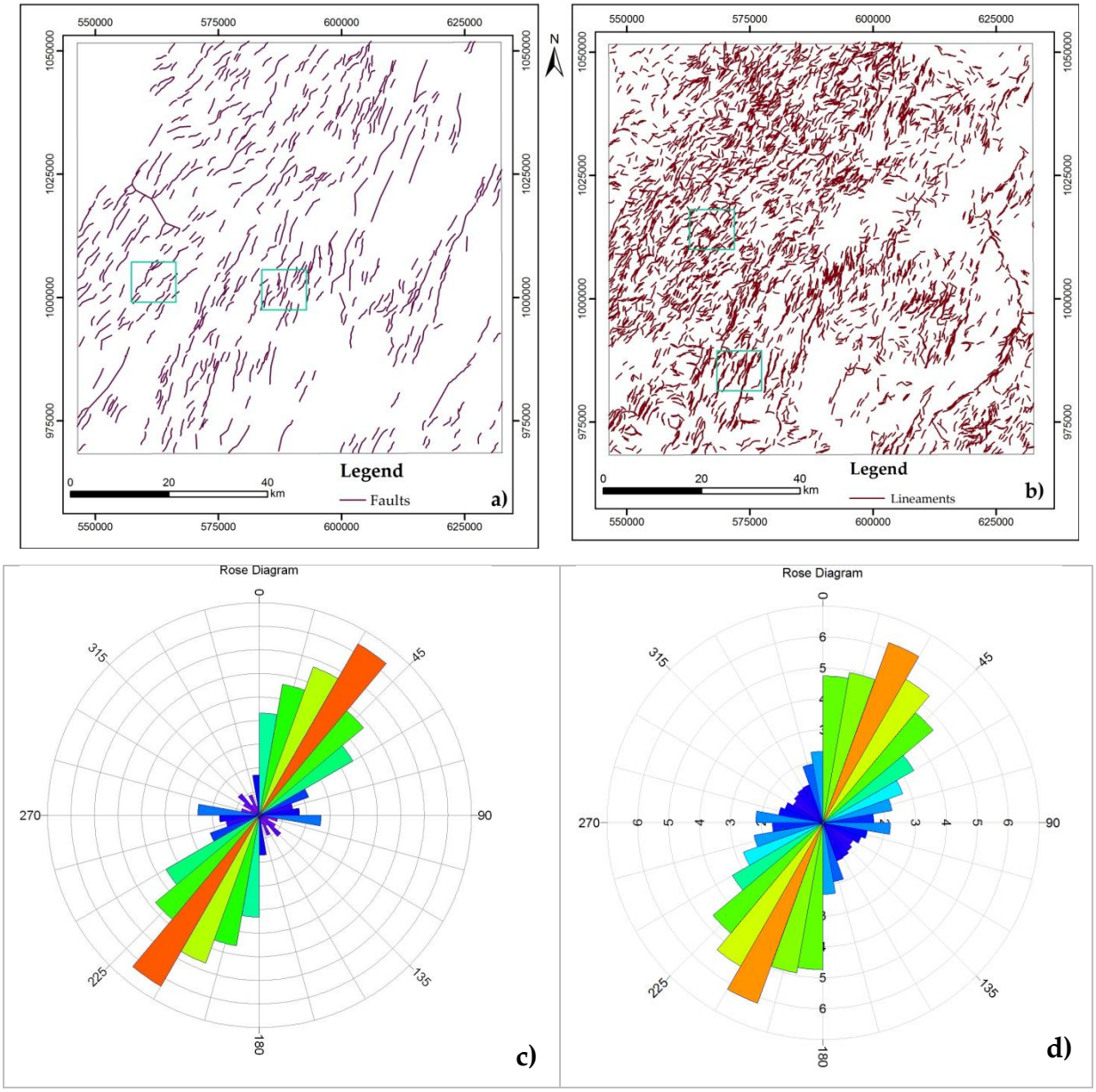

Fig 3. 12: Structural map: a) Fault , b) Lineament,c) rose diagram for faults and d) rose diagram for lineaments

3.3.3 Data Generation from Digital Elevation Model (DEM)

Digital elevation model (DEM) is defined as the representation of continuous elevation values over a topographic surface by a regular array of z-values, referenced to a common vertical datum. DEMs are typically used to represent the bare-earth terrain, void of vegetation and manmade features https://learn.arcgis.com/. With the invention of Geographical Information Systems (GIS), the role of digital terrain model (DTM) or digital elevation model (DEM) has become very important and effective tools in analytical Geo-hazard studies (Abolghasem et al., 2016).

Spatial data used in GIS analysis come from a wide variety of sources, in a number of different formats, resolutions, scales, and projections. One of the data sources for GIS is Digital Elevation. Digital elevation models are essential for a number of topographic and hydrological analysis including slope and aspect computation, Shaded topographic relief or hill-shading generation, stream generation, watershed delineation, etc. In this study, a combination of various forms of Digital elevation data has been used to identify and model geo-hazard prone areas. The most important data that were extracted from DEM includes slope, drainage, hill shed and the elevation.

3.3.4 Manual digitizing

The geological map from geological survey of Ethiopia with a scale of 1:5000 was used to generate lithologic units which found in the study area. The (jpg) map first geo-referenced, then after using the user-defined database the rock units become converted to shapefile. Their topology was also build by using the editor tool in Arc GIS.

3.4 Method of data analysis

3.4.1 Classification and weighting of thematic maps

Classification of thematic data layers has been conducted using expert-based manual classification and natural breaks in Arc GIS software. Five number of classes are chosen, to take consideration of the logical AHP classes (i.e every low, low, medium, high and very high). The class also assigned a value based on their contribution to generating a susceptibility map of the proposed geo-hazard type.

A natural break classification

Natural breaks classes are based on natural groupings inherent in the data. Class breaks are identified that best group similar values and that maximize the differences between classes. The features are divided into classes whose boundaries are set where there are relatively big differences in the data values https://learn.arcgis.com/.

3.4.1.1 Land use land cover (LULC)

Land cover /land-use map of 2018 was produced by supervised classification using maximum likelihood classifier. Seven land-cover/land-use classes were intended to be mapped for the study area. These classes include Agricultural land, bare land, built up area Forest, shrubland, sugar plantation and water body (Fig.3.14)

Table 3. 6: Land Use/Land Cover Classes descriptions

ID	Land use land cover class	Description
1	Agricultural land	Including crop fields, pasture, and open grasslands
2	Bare land	Including sandy, rocky and bare soil
3	Built up area	Including urban settlements and Asphalted roads
4	Forest	Specifically natural forests
5	Shrubland	Scattered trees and bushland
6	Sugar plantation	Includes, only Economic vegetation
7	Waterbody	Including and lakes artificial dams

The effect of land cover on slope stability has been studied since 1960 (Mehdi et al., 2012). Generally, land use land cover has an effect on the strength of slope materials against sliding and control of water content of slope. For instance (Nielsen, et al., 1979), plant roots reinforce the slope and normally are considered as reinforcements. In studies performed by Komac, 2006), this parameter has been considered as one of the most important factors in preparing landslide susceptibility maps.

For this work the seven LULC classes generalized into five classes and their relative contribution for landslide susceptibility mapping is depicting in (Fig 3.13). These classes are cropland; bare land and built up area forest and plantation; shrubland; and water body. The class of LULC type also reclassify based on their contribution to landslide susceptibility

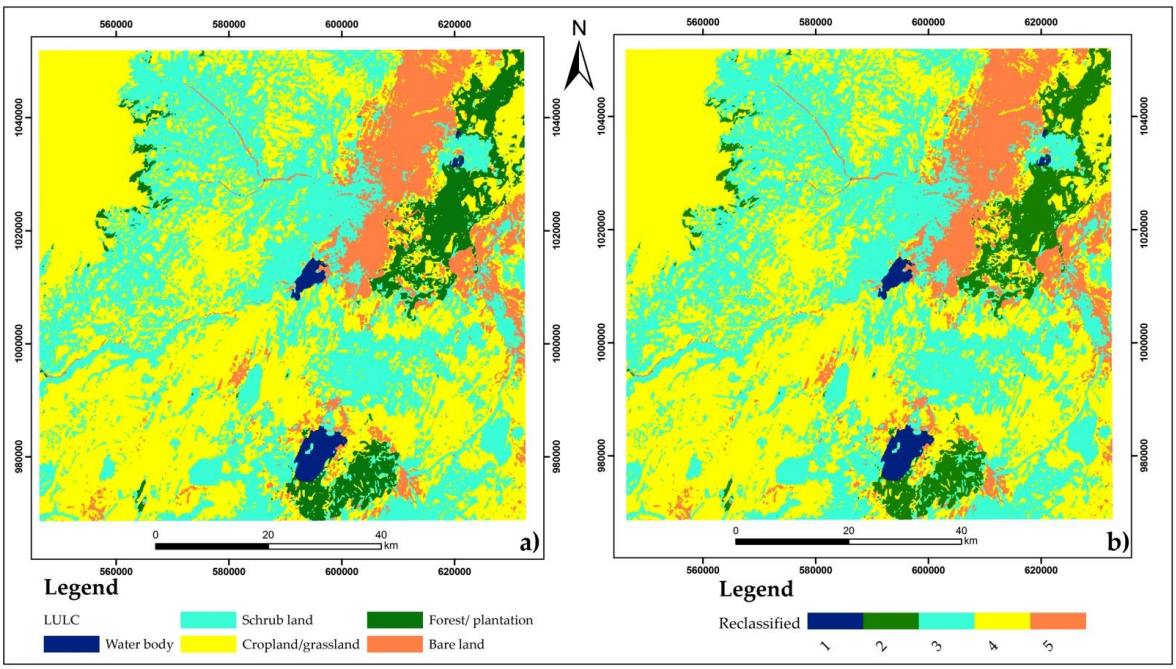

Fig 3. 13: Land use land cover factor map: a) classification and b) Reclassified

3.4.1.2 Fault proximity analysis

A fault is a fracture or zone of fractures between two blocks of rock. Faults allow the blocks to move relative to each other. This movement may occur rapidly, in the form of an earthquake - or may occur slowly, in the form of creep https://www.usgs.gov/faqs/fault. Historical ruptures traces of a fault are an important dataset to interpret future fault ruptures. Thus historical rupture traces have been used in many geo-hazard assessments and susceptibility mapping (Mark et al., 2004). Seismic hazard is significantly related to faults.

The study area of this work is characterized by many active fault traces that can be mapped using satellite images. They are the major one and can be considered as the main source of seismicity in the region. To characterize their possible effect a proximity analysis by Euclidian distance tool has been used. And the reverse effect of the distance from fault lines had been ranked by reclassifying the distance raster into five classes using natural break classification in arc GIS (Fig 3.14)

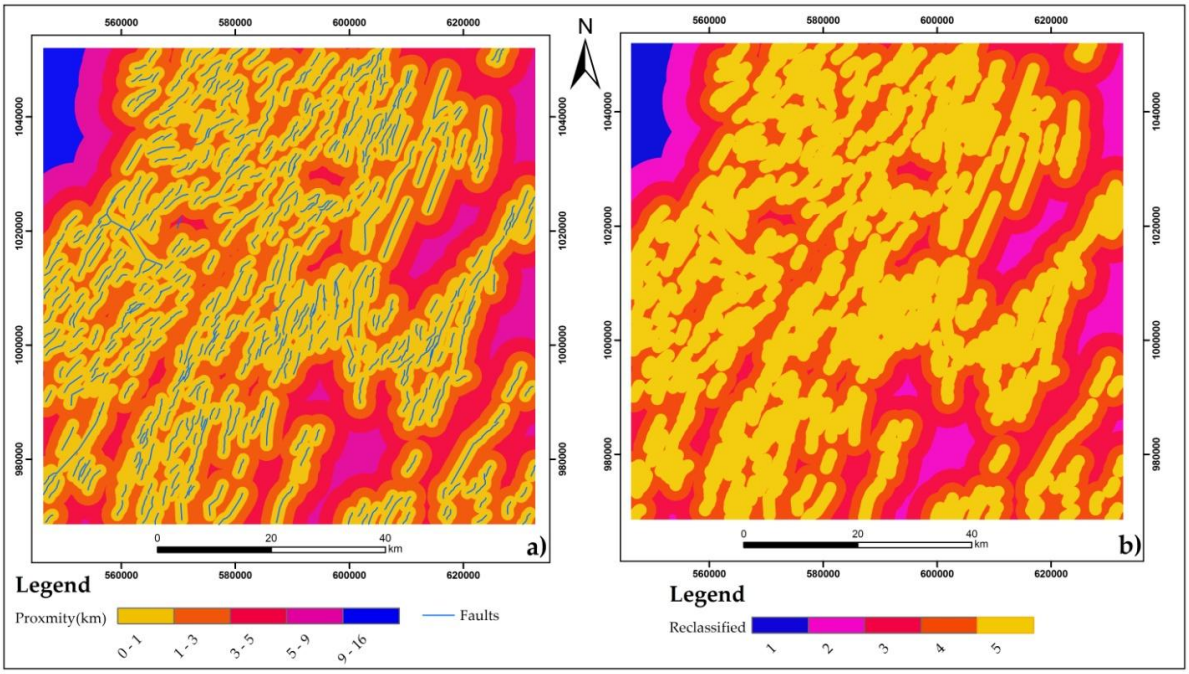

Fig 3. 14: Fault proximity map: a) Classification and b) Reclassified

3.4.1.3 Lineament density

Lineaments are map-able linear features present on the surfaces of the earth, which indicates the zone of weakness and structural discontinuities in a rock. Its source could be faults, foliations, joints, and bedding planes and its shape can be curved, linear and slightly curve. In engenering point of view, such discontinuities are a result of a rupture in rocks or a boundary in rock or soil that indicates a change in the rock mass (Hencher, 1989)

In geo-hazard study knowing the spatial distribution of lineaments and their density is very

crucial because it is directly related to the zone of weak masses in a rock. According to authors like (Saha et al., 2002; Ferdaus and Chow, 2004; Roslee et al., 2006; Ramli et al., 2010) indicated that a high density of fractures and joints in a rock mass, which is related to the lineaments can lower the stability of rock by reducing the overall rock mass strength. Therefore both in the case of landslide and earthquake hazard assessment lineament density are a very important parameters.

The lineament density was generated by extracted lineament shown in (Fig 3.15). The lineament density was also classified using natural breaks function in Arc GIS and reclassified based on their significance to model susceptibility of hazards (Fig 3.16).

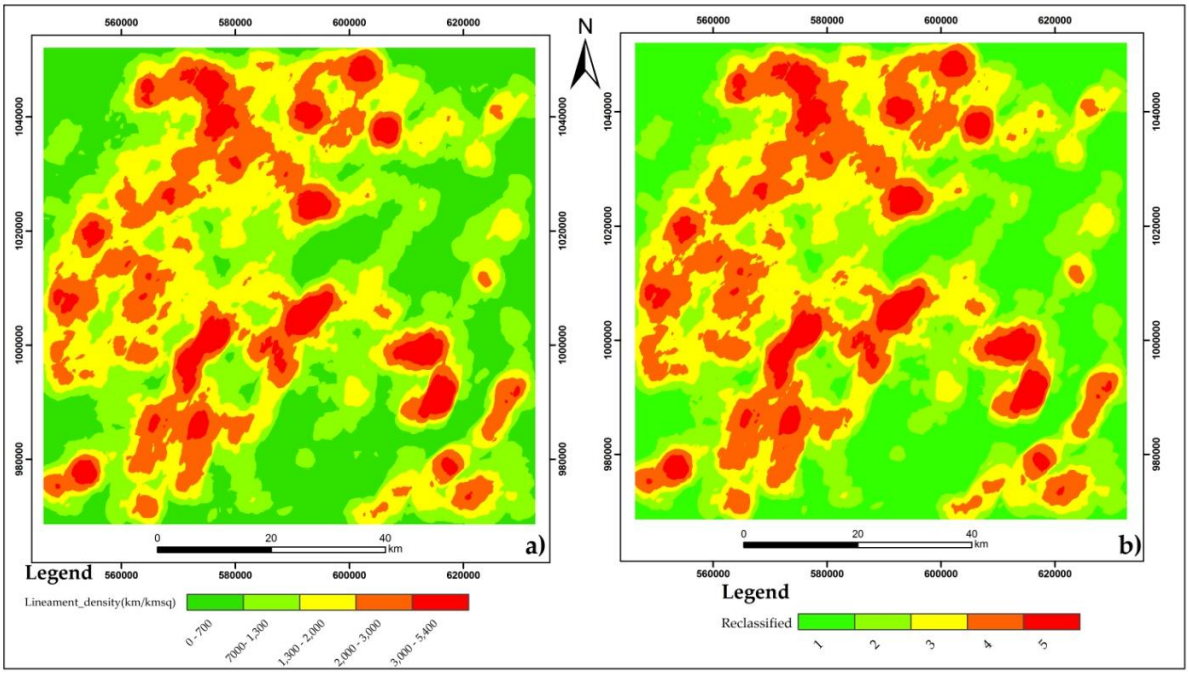

Fig 3. 15: Lineament density map: a) Classification, and b) Reclassified

3.4.1.4 Volcanic vent proximity

Volcanic vents- are openings in the Earth's crust from which lava and pyroclastic flows are ejected. Their forms determine the varied types of eruptions that gave them shape. Volcanic vents originate in the magma chamber - an underground pool of liquefied rock (magma) underneath the surface of the Earth https://owlcation.com/stem/Types-of-Volcanic-Vents.

Determine the position of vents based on knowledge of past eruptions and characterize their spatial interrelations will provide the basis for establishing the probability of vent opening (i.e., volcanic susceptibility) (Felpeto et al., 2007; Martí and Felpeto, 2010; Bartolini et al., 2013).

Existence of the well-known active volcanic centers and spatter cones, made the study area more susceptibility to volcanic hazard(Brown et al., 2015). Kone, Berue, Fentale, and Dofan

are a subset of this area. Including this, all other possible past volcanic vents are extracted using satellite images, and their proximity within a spatial area has been conducted using Euclidian distance function. To produce volcanic hazard susceptiblity map, buffering zone of volcanic vents classified and reclassified using natural break statistics in Arc GIS (Fig 3.16).

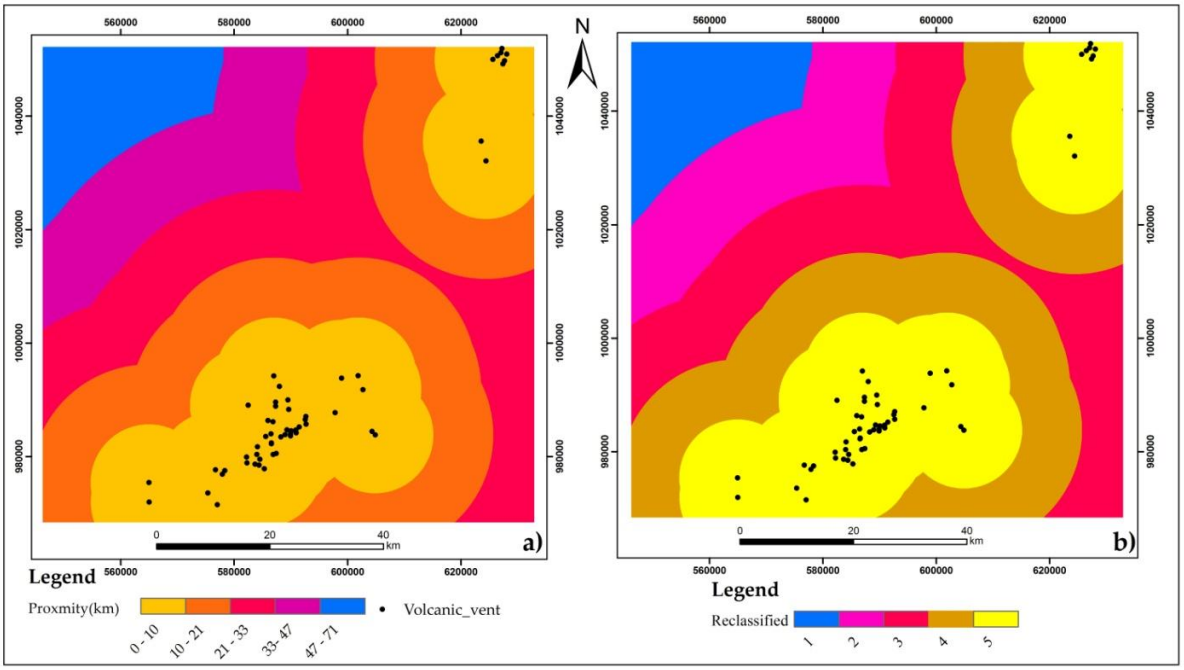

Fig 3. 16: Volcanic vent proximity map: a) Classification and b) Reclassified

3.4.1.5 Slope classification

Slope is one of the most important topographic parameters influencing the occurrence of geo-hazards mainly landslides. In general, if the slope is steeper it will be more susceptible for instabilities as compared to gentle slope. The gravity pull which is the main driving force for instability is directly proportional to the slope gradient (Raghuvanshi et al., 2014; Bisson et al., 2013, 2010). The slope angle directly affects landslide, thus it is used in preparing landslide susceptibility maps (Cevik et al.,2003; Clerici et al.,2002; Ercanoglu et al., 2004; Lee, 2005). Another study by Erden and Karaman,(2012) this parameter has been considered as one of the most important factors in landslide susceptibility assessment. Even today it is the leading parameter when landslide hazard assessment is concidered.

The slope for this study was extracted from the ASTER DEM. Generally speaking, as slope increases, the probability of landslide occurrence also increases, having this logic the slope map classified into five categories (Fig 3.17). Using the class their contribution also ranked.

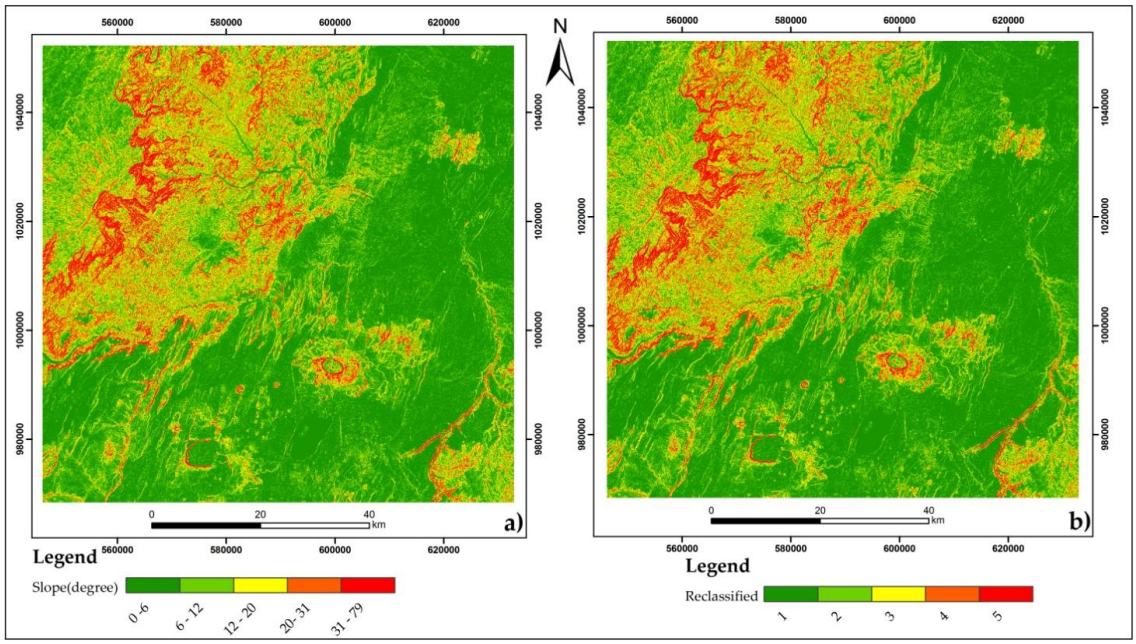

Fig 3. 17: slope map: a) classification, and b) reclassified

3.4.1.6 Topography classification

The topography of an area could refer to the surface shapes and features associated with it. Understanding how material flows over the ground is very important to assess volcanic hazards. Scott et al., 2001 stated that, the proximal volcanic hazard zone is defined as those areas which are subjected to rapidly moving, devastating pyroclastic flows, debris avalanches, and lahars.In this work, ASTER 30 DEM were used to prepare this data layer. The DEM was classified into ranges of elevation using natural break statistics in Arc GIS (Fig 3.18).

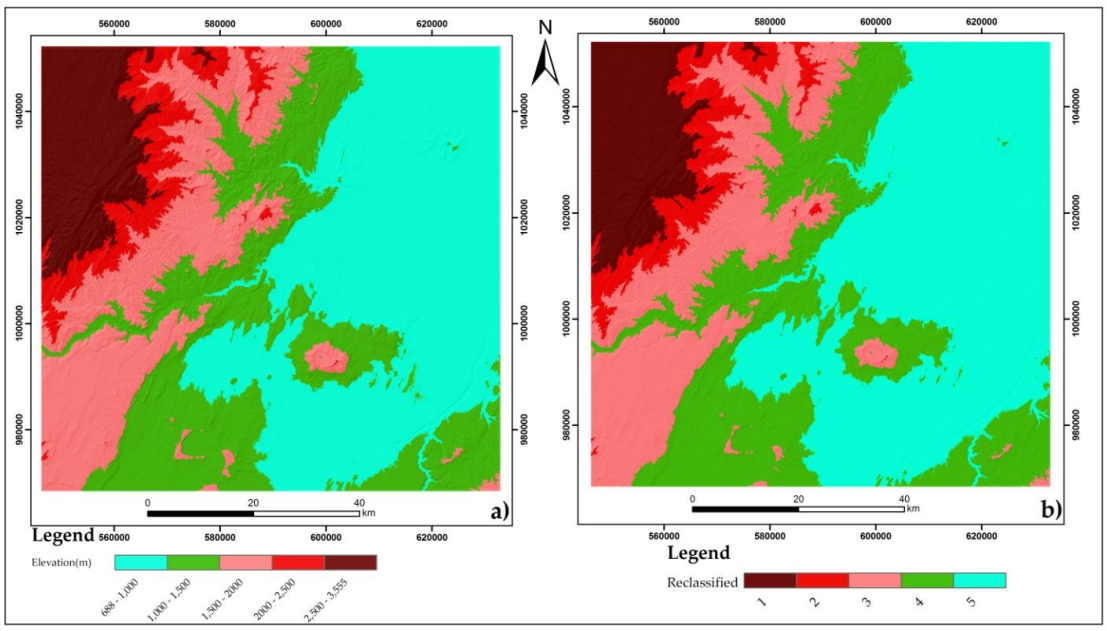

Fig 3. 18: Topographic map: a) Classification and b) Reclassified

3.4.1.7 Soil texture analysis

The texture of soil represents the relative proportion of sand, silt, and clay content. Soils with a high percentage of clay form very stable aggregates resistant to detachment. On the other hand, light soils like sandy or coarse loams are easy to detach, resulting inability to form very stable aggregates (Das and Agarwal ,2002). In general soil with more in sandy texture is more susceptible for both earthquake and landslide hazard. Usually, Soil liquefaction occurs in such soil.

This means when soils lose strength and stiffness in response to an applied stress such as shaking during an earthquake or other sudden change in stress condition.

The soil data layer was generated from the Global and National Soil and Terrain Digital Database (SOTER). The data obtained was 250m grid (GeoTiffs). It is converted to soil texture classification using **SAGA GIS** (2.3.2) free software. The software has a module: soil texture classification, which derives soil texture classes with USDA scheme from sand, silt and clay contents. A total of 12 textural classes were obtained, however, four significant classes are selected (Appendix V). The selected class also rated based on their contribution to the model (Fig 3.19).

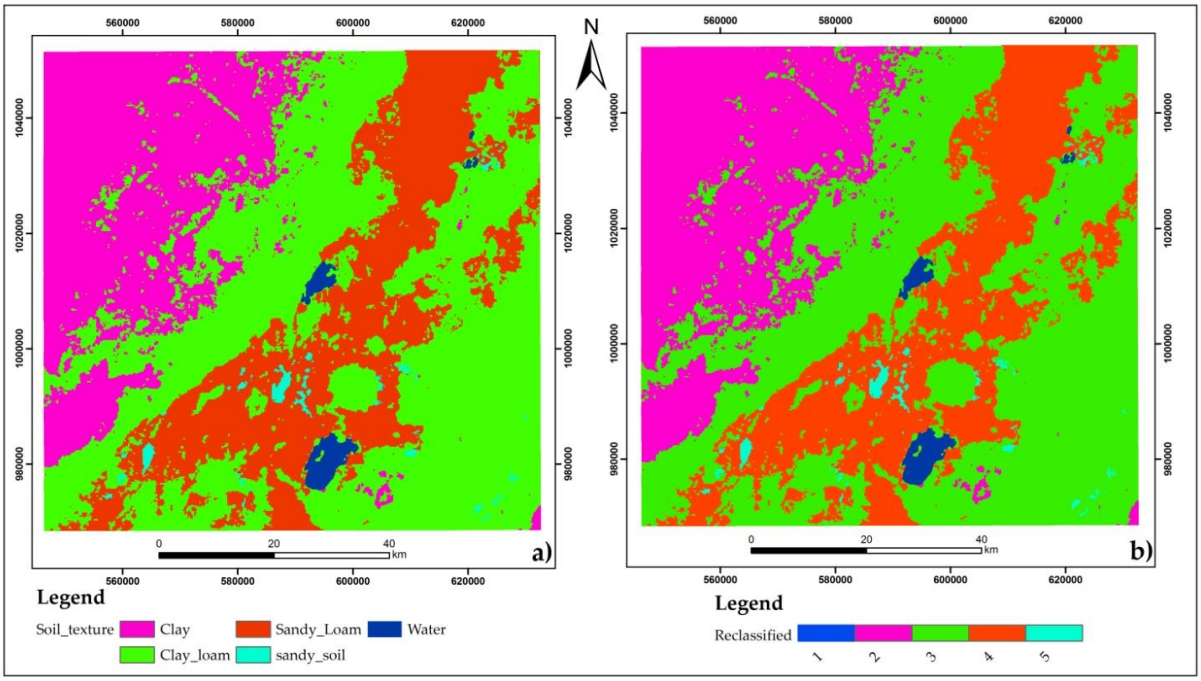

Fig 3. 19: Soil texture map: a) Classification, and b) Reclassified

3.4.1.8 Lithology classification

Lithology is one of the main controlling factors in Geo-hazard susceptibility assessment. It is an immediate formation beneath the surface. It has great contribution to determine whether the hazard becomes more prone or not. Studies by Lluleseged Ayalew et al., 2005; Dai et al.,

2001; Yalcin , 2008) characterize the effect of geology on Geo-hazard assessment.

In the present study, a total of nine Lithological units are generated by digitizing the geological sheets of the study area obtained from Ethiopian geological survey(GSE). These are: Alluvium with minor ignimbrite (Qal); Young basaltic scoria(Qwt); Recent basaltic flow(Qwo); Dofan basalt (Qdb) vesicular basalt, aphanitic basalt, olivine-phyric basalt and recent scoria cones; Tarmaber-Megezez basalt (Ttb) plagioclase phyric and olivine-plagioclase phyric basalts with minor olivine-phyric, pyroxene phyric, plagioclase-pyroxene-olivine phyric and aphanitic basalts; Sela Diagay-Debre Birhane_Goro ignimbrite(Tdig) :ignimbrite, tuff, rhyolite , basalt, tuffaceous sediment, ash and agglomerate; Kesem basalt (Tkb) aphanitic basalt intercalated with plagioclase phyric basalts and thin beds of ignimbrite (Fig 3.6 and Table 3.1).

The main criterion which was adopted for ratings and subcategories of lithology is; the response of the rocks to the processes of weathering and erosion; their density and relative age. This criterion was to generalize the all over rock mass strength. In logic, hard formation s are strong to tackle external effect compared to weak formations. The study area mainly covered by the recent volcanic rocks, they are vulnerable to weathering and may easily contribute to landslides, However, they have a clear difference in density and relative age. This was taken for category and rating of lithology units (Appendix I). Sub categories and rating of lithologic units are depicted in (Fige 3.20) .

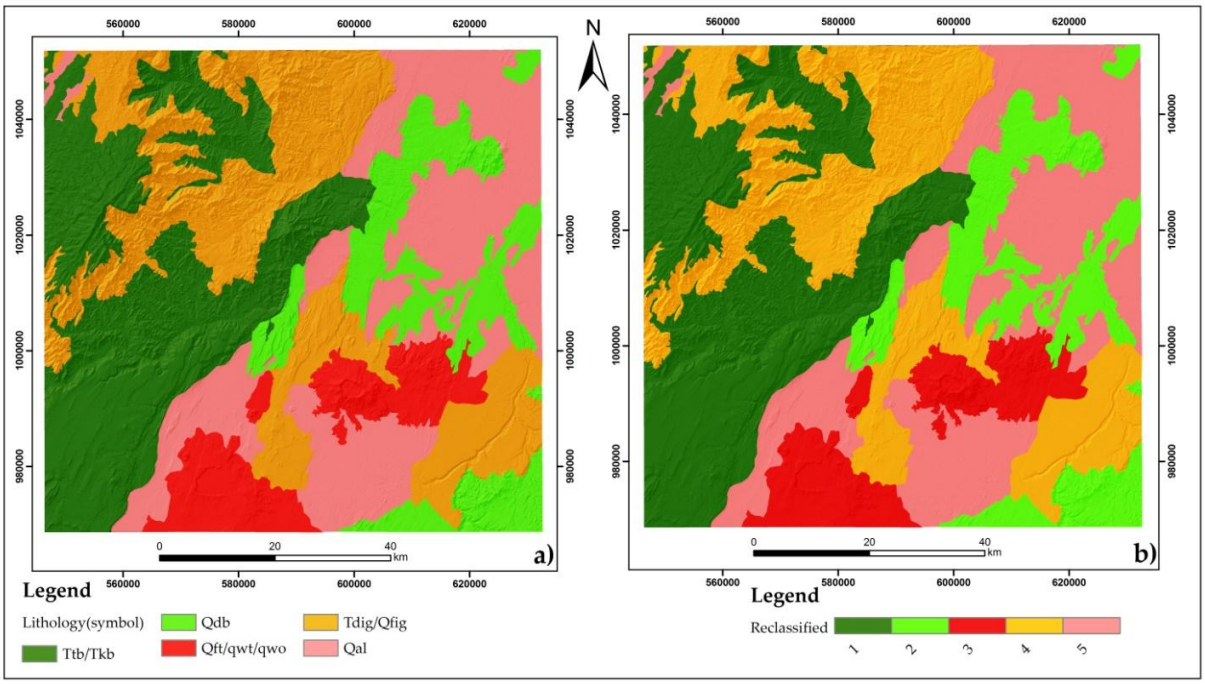

Fig 3. 20: Lithology map : a) Classification, and b) Reclassified

Table 3. 7: General information about classification and reclassification of spatial data layer

Layer	Class	Area (km^2)	Area (%)	Priority value	Class importance
LULC	Waterbody	73.71	1.03	1	Very low
	Forest/plantation/ Shrubland	460.13	6.42	2	Low
		2473.76	34.49	3	Medium
	Agriculture land	3443.47	48.04	4	High
	Bare land	719.03	10.03	5	Very High
Fault proximity (km)	0-1	3705.01	51.42	5	Very high
	1-3	2082.07	28.86	4	High
	3-5	929.29	12.89	3	Medium
	5-9	364.72	5.06	2	Low
	9-16	127.44	1.77	1	Very low
Lineament (km/ km^2)	0-700	1861.83	25.83	1	Very low
	700-1,300	1930.37	26.79	2	Low
	1,300-2,000	1845.41	25.61	3	Medium
	2,000-3,000	1195.61	16.60	4	High
	3,000-7994	372.796	5.18	5	Very high
Volcanic vent proximity(km)	0-10	2061.36	28.36	5	Very high
	10-21	2033.65	27.97	4	High
	21-33	1635.67	22.50	3	Medium
	33-47	942.679	12.97	2	Low
	47-71	596.35	8.20	1	Very low
Slope(degree)	0-6	2721.16	37.92	1	Very low
	6-12	2511.84	35.00	2	Low
	12-20	1027.79	14.74	3	Medium
	20-31	649.84	9.06	4	High
	31-79	265.54	3.70	5	Very high
Elevation(m)	688-1000	3013.71	41.42	5	Very high
	1000-1,500	1783.99	24.52	4	High
	1500-2,000	1364.68	18.76	3	Medium
	2,000-2,500	419.21	5.76	2	Low
	2,500-3555	694.45	9.54	1	Very low
Soil(texture)	Water	73.71	1.02	1	Very low
	Clay	1795.3	25.18	2	low
	Clay Loam	3481.54	48.48	3	Medium
	Sandy loam	1770.25	24.52	4	High
	sandy	58.16	0.80	5	Very high
Lithology (Symbol)	Ttb/Tkb	2012.22	28.03	1	Very low
	Qdb	920.17	12.82	2	Low
	Qft/qwt/qwo	632.86	8.82	3	Medium
	Tdig/Qfig	1908.20	26.58	4	High
	Qal	1706.08	23.76	5	Very high

3.5 Parameter weighting

In order to produce the proposed hazards susceptibility model, AHP method of statistical analysis was adopted. The Analytic Hierarchy Process (AHP) was originally proposed by

Myers and Alpert in 1968, and in 1977 it was developed as a model by Saaty to be used in the solution of decision-making problems. This involves making decisions concerning complex problems by arranging the factors in aij matrix format. It is a semi-qualitative process in which pair wise comparisons of controlling factors help to assign weight values to them varying from 1 to 9 (Saaty 1977,2005,2008; Saaty and Vargas, 2001). The standard scale for making pair-wise comparisons is given in (Table 3.8).

Table 3. 8: Scales for the pair-wise comparisons methods (Saaty 1977,2005,2008)

1/9	**1/7**	**1/5**	**1/3**	**1**	**3**	**5**	**7**	**9**
Extremely	Very strongly	Strongly	Moderately	Equally	Moderately	Strongly	Very strongly	Extremely
Less Important						Very important		
The rest value								
Intermediates		(2,4,6,8)			Preference made halfway			

According to the paired comparison used to establish the matrix, aij is the compared value between i and j, while the diagonal shows the self-comparison of elements that have a value of 1. The lower left values in the matrix are the comparison results of the expert decision makers; while the upper right values are the reciprocals of the upper right values (Eq.1).

$$A = \begin{bmatrix} 1 & a12 & \dots & a1n \\ a21 & 1 & \cdots & a2n \\ \vdots & \vdots & \dots & \vdots \\ an1 & an2 & \cdots & 1 \end{bmatrix} = \begin{bmatrix} 1 & a12 & \dots & a1n \\ 1/a12 & 1 & \cdots & a2n \\ \vdots & \vdots & \dots & \vdots \\ 1/a1n & 1/a2n & \cdots & 1 \end{bmatrix} \quad \text{(Eq.1)}$$

For checking the consistency of the comparison matrix, the consistency ratio (CR) will be calculated using (Eq.2) (Saaty, 2008) considering that the comparison was randomly generated as C.R. approached 1, and that greater consistency appeared as C.R. approached 0. Generally, C.R. ≤ 0.1 is acceptable.

$$C.R = \frac{C.I}{R.I} \quad \text{(Eq.2)}$$

Where: CI is the consistency index calculated using the formula in (Eq. 3), and RI is the random index in the comparison matrix.

$$C.I = \frac{\lambda \max - n}{n-1} \quad \text{(Eq.3)}$$

n is the order of the matrix and λmax is the major value of the matrix.
RI (random index) is the consistency of the randomly generated pair-wise matrix and is dependent on the size of the matrix as given in (Table 3.9).

Table 3. 9: Values of random index R.I. (Saaty, 1977)

Rank	1	2	3	4	*5*	6	7	8	9	10
R.I.	0.00	0.00	0.58	0.90	1.12	1.24	1.32	1.41	1.45	1.49

3.5.1 Pair-wise comparisons of Factors

The pair-wise comparison matrix was made for each geo-hazard type form factors mentioned at (Table3.7). The diagonal elements of the square matrix always 1 because comparing the same factors has the same weight, while the lower left values in the matrix are the comparison results of the expert decision makers and the upper right values are the reciprocals of it.

In this work, three geo-hazard types were taken to assess their risk using this technique. They are landslide, earthquake, and volcanism. For landslide hazard susceptibility assessment six factors evaluated in the comparison matrix such as LULC, fault proximity, lineament density, lithology, soil and slope (Table 3.10). In the case of earthquake hazard fault proximity, lineament density, lithology, soil and slope were compared (Table3.11). For volcanic hazard, structure (fault proximity and lineament density), topography (elevation) and slope used (Table 3.12).

Table 3. 10: Pair-wise comparison of factors used for landslide susceptibility mapping

	LULC	Fault proximity	Lineament density	Lith-ology	Soil	Slope
LULC	1					
Fault proximity	3	1				
Lineament density	3	1	1			
Lithology	3	1/3	1/3	1		
Soil	2	1/3	1/2	1	1	
Slope	3	2	2	3	3	1

Table 3. 11: Pairwise comparison of factors used for seismic hazard susceptibility mapping

	Fault proximity	Lineament density	Lith-ology	Soil	Slope
Fault proximity	1				
Lineament density	1	1			
Lithology	1/2	1	1		
Soil	1/2	1/2	1	1	
Slope	1/3	1/3	1/3	1/3	1

Table 3. 12: Pairwise comparison of factors used for volcanic hazard susceptibility mapping

	Volcanic vent	Fault proximity	Elevation	Slope
Volcanic Vent	1			
Fault proximity	1/3	1		
Elevation	1/3	1/2	1	
slope	1/5	1/5	1	1

3.5.2 Weight and consistency ratio

After the comparison matrix has been developed, consistency or inconsistency of the comparison matrix was checked. The weight of each factor also calculated using IDRISI 17.0 software. The software has a module that enables to calculate weights by providing a series of pair-wise comparisons of the relative importance of factors to the suitability of pixels for the activity being evaluated. The procedure by which the weights are produced follows the logic developed by T. Saaty under the Analytical Hierarchy Process (AHP). weight value of each factor for each geo-hazard-type is shown in (Table 3.13, 3.14, 3.15).

Table 3. 13: Eigenvectors of the pair-wise comparison matrix used for landslide susceptibility mapping

ID	Factor	Weight	Weight %
1	LULC	0.07	7
2	Fault proximity	0.22	22
3	Lineament density	0.20	20
4	Lithology	0.09	9
5	soil	0.11	11
6	slope	0.31	30
Consistency ratio =0.03; Consistency is acceptable.			

Table 3. 14: Eigenvectors of the pair-wise comparison matrix used for sesmic hazard susceptibility mapping

ID	Factor	Weight	Weight %
1	Fault proximity	0.30	30
2	Lineament density	0.26	26
3	Lithology	0.20	20
4	Soil	0.17	17
5	Slope	0.08	8
Consistency ratio =0.02; Consistency is acceptable.			

Table 3. 15: Eigenvectors of the pair-wise comparison matrix used for volcanic hazard susceptibility mapping

ID	Factor	Weight	Weight %
1	Volcanic vent	0.50	51
2	Structure	0.27	27
3	Elevation	0.12	12
4	slope	0.10	9
Consistency ratio = 0.07, Consistency is acceptable.			

3.5.3 Geohazard suceptiblity mapping

To identify and map hazard-prone areas, the eight data sets described in the previous section have been combined according to their significance. Three hazards namely, landslide earthquake and volcanism have been modeled using AHP technique. To map landslide susceptible areas, six major landslide causative factors were used; these are LULC, fault proximity, lineament density, lithology, soi, and slope. In the same approach to map seismic hazard susceptible areas; five parameters such as fault proximity, lineament density, lithology, soil, and slope were taken. For volcanic hazard, structures (fault proximity plus lineament density), topography (elevation) and slope were combined.

Finally, the Landslide Hazard susceptibility Index (LHZI), Seismic Hazard susceptibility Index (SHZI) and volcanic Hazard susceptibility Index (VHZI) value for each considered pixel were computed by summation of each factor's weight multiplied by the class weight of

each referred factors using (Eq.5).

$$\mathbf{HSI} = \sum_{i=1}^{n}(\boldsymbol{WiRi}) \quad \text{(Eq.5)}$$

Where: HSI is the required hazard susceptibility index of the given pixel, *Wi* is a weighting of factor *i*, and *Ri* is the criteria score of factor *i*.

3.7 Model validation method

3.6.1 Interferometric synthetic aperture radar (InSAR) analysis

Synthetic Aperture RADAR Interferometry (InSAR) provides a unique tool for the quantitative measurement of the Earth's surface deformations induced by a variety of natural phenomena (such as volcanic eruptions, landslides and earthquakes) and anthropogenic (e.g., ground-water extraction in highly-urbanized areas, deterioration of buildings and public facilities) processes(e.g Antonio Pepe et al., 2017; Lu et al., 2003; Bürgmann et al., 2002; Simons and Rosen, 2015).

For this work Sentinel -1A SLC product image of 2015, 2016 and 2017 were taken from ESA. The data was used to validate Geo-hazard susceptibility models produced by AHP technique. For this differential Interferometric synthetic aperture radar (DInSAR) and displacement map were generated.

Table 3. 16: SAR data description

	Specification	Name
1	Data set/satellite /	Sentilnel-1A
2	Product type	L1 single look complex(SLC)
3	Beam mode	IW
4	Polarization	VV
5	Frequency	C-Band
6	Flight direction	Ascending

3.6.2 Differential Interferometric synthetic aperture radar (DInSAR)

'Differential interferometry' is the commonly used term for the production of interferograms from which the topographic contribution has been removed. In the Differential Interferometric synthetic aperture radar (DInSAR) generation, a two-year data with six-month interval have been used. When the time interval is short the coherence interferogram fringes increase (Nestor et al., 2016). To resolve the problem of coherence the time interval was reduced to six months.

In this work, a total of 5 SLC products within 2-year baseline were used to generate DInSAR. From these four DInSAR and four displacement maps has been produced using a pair of AB, BC, CD and DE master and slave image respectively (Table3.17). In order to identify deformation spots, an average of yearly displacement map was generated. All over procedure is shown in (Fig 3.21)

Table 3. 17: Specification of SAR data used for DInSAR processing

Pairs	Date of acquisition		Sub-swath	Initial burst	Final burst
	Master	Slave			
AB	09 apr2015	180ct2015	IW1/2	2	7
BC	180ct2015	10mar2016	IW1/2	2	7
CD	10mar2016	18sep2016	IW1/2	2	7
DF	18sep2016	11mar2017	IW1/2	2	7

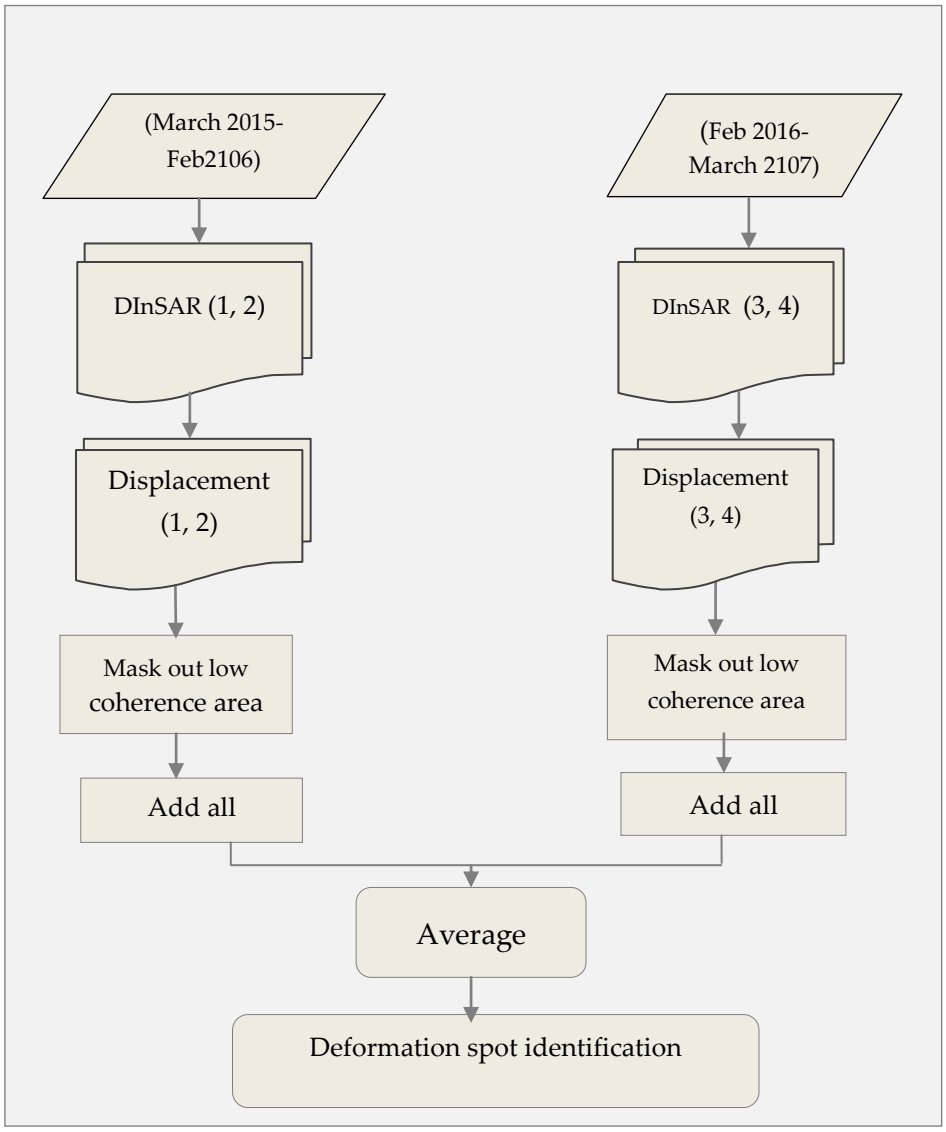

Fig 3. 21: Flowchart for radar image processing

4.5.3 Estimation of Surface Displacements

InSAR Technique for the Estimation of Surface Displacements SAR interferometry nowadays is mostly used for the detection/monitoring of surface changes occurring between passages of the RADAR sensor over the same scene (Antonio and Fabiana, 2017). In such a case, as a slight change across the two SAR acquisition times happens in the imaged scene, an additive term in the interferometric phase associated with the RADAR line of sight (LOS) component of the surface displacement arises. By the inspection of the imaging geometry depicted in (Fig 3.22) we get:

$$\Delta\varphi = \frac{-4\pi}{\lambda} + \frac{b\perp}{r\ sin\ \vartheta} + \frac{4\pi}{\lambda\ dLOS} \qquad \text{(Eq.4)}$$

Where dLOS represents the projection of the occurred deformation with respect to sensor LOS direction. For the sake of convenience, the presence of the flat earth phase contribution was leftout.

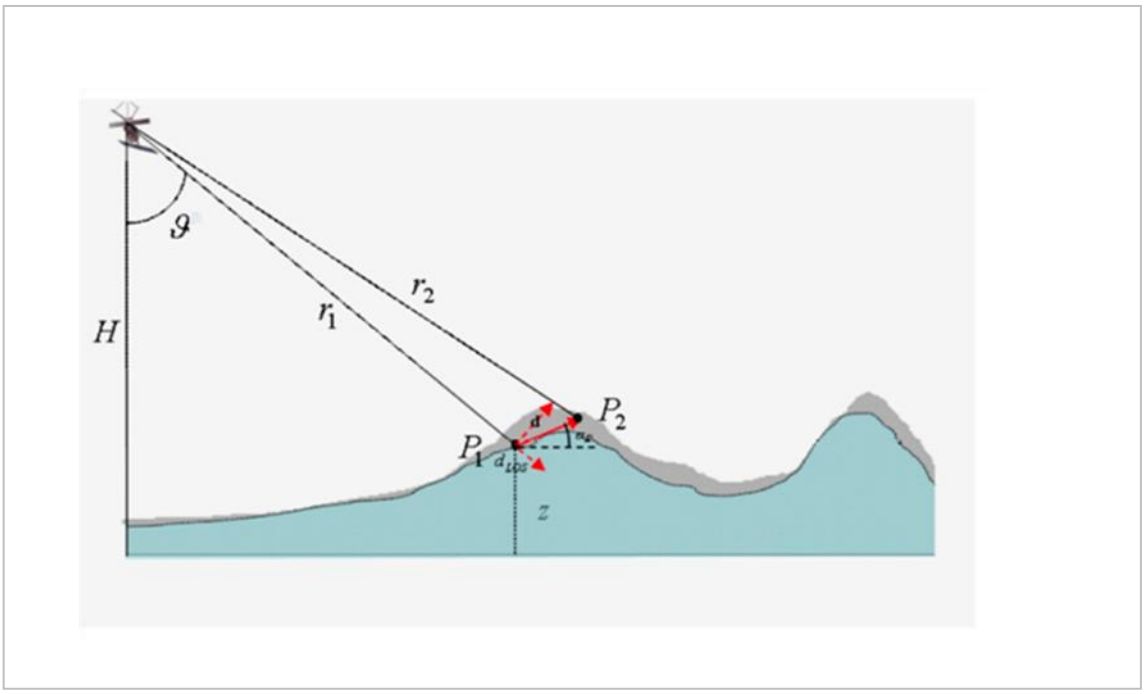

Fig 3. 22: InSAR geometry for the estimation of the displacement of earth's surface. (Source: Antonio and Fabiana, 2017)

CHAPTE- IV RESULTS AND DISCUSSION

4.1 RESULTS

4.1.1 Landslide hazard susceptibility (LHS)

Applying the AHP technique, the Landslide hazard susceptibility map values were computed by using wighted overlay analysis in Arc GIS 10.5. These LHS values were then divided into four classes based on the class of weighted overlay analysis obtained from the computation. These are low, medium, high and very high hazard susceptibility, qualitative class.

The landslide Hazard susceptibility map prepared for the present study (Fig 4.1) revealed that 43%(3034.01km^2) of the study area occupies low, 26% (1870.89km^2) medium,29% (2090.47km^2) High, and the rest 2% (142.82km^2) very high hazard zones.

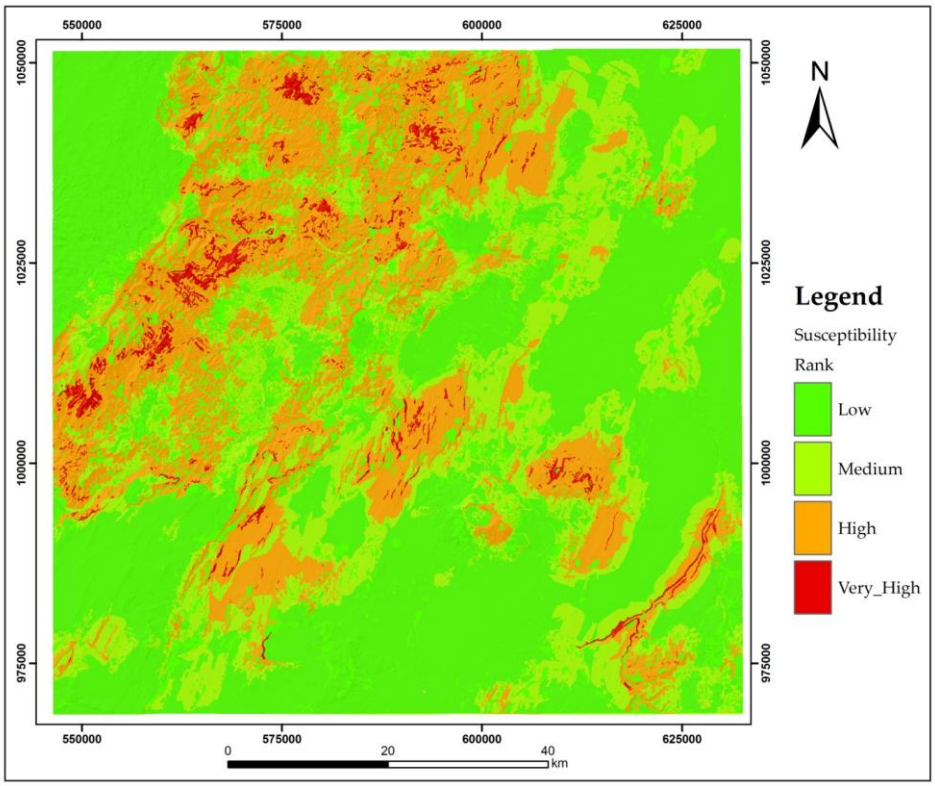

Fig 4. 1: Landslide hazard susceptibility map

The result of the susceptibility map shows the spatial distribution of landslide-prone areas is throughout the whole area. However, the level of susceptibility to landslide concentrates towards the north and North West part of the study area. More than 50% of high and very high landslide susceptibility areas are found around that place.

Table 4. 1: Landslide susceptibility statistics of the study area

ID	Susceptibility rank	Area(km^2)	Area (%)
1	Low	3034.01	43
2	Medium	1870.89	26
3	High	2090.47	29
4	Very high	142.82	2

4.1.2 Seismic hazard susceptibility (SHS)

Applying similar techniques as the previous section, the Seismic hazard susceptibility map values were also computed by using wighted overlay analysis in Arc GIS 10.5. These SHS values were then divided into four classes based on the class of weighted overlay analysis obtained from the computation. The classes are also low, medium, high and very high hazard susceptibility.

The susceptibility map prepared (Fig 4.2) revealed that 8%(561.51km^2) of the study area occupies low hazard, 53% (3801.99km^2) medium,35% (2526.04 km^2) as High, and the rest 2% (142.82km^2) as very high hazard zones.

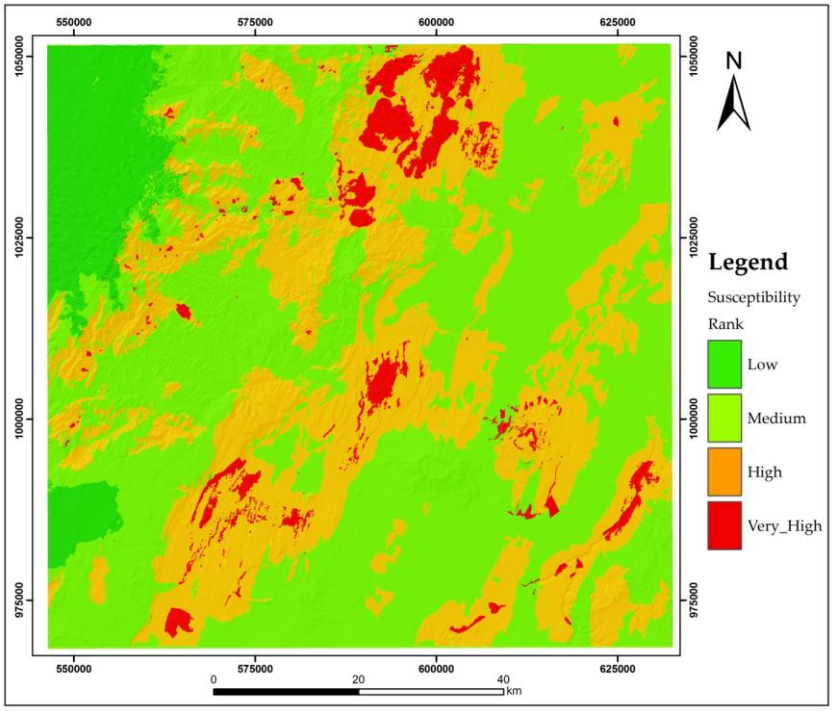

Fig 4. 2: Seismic hazard susceptibility map

The result of the seismic susceptibility map shows that the seismic hazard/earthquake/ is not restricted to the rift axial zone. But, it includes the rift margin. Particularly recognized spots are shown around NNE part of the study area ((Fig 4.2). In addition high to very high hazard susceptible zones also depicted following the major fault structure running from NNE to

SSW direction. Historical earthquake epicenters archive from USGS also overlay on the succeptiablity map and ,thus points are found closer and on the high hazard zone.

Table 4. 2: Seismic hazard susceptibility statistics of the study area

ID	Susceptibility rank	Area(km^2)	Area (%)
1	Low	561.51	8
2	Medium	3801.99	53
3	High	2536.04	35
4	Very high	285.23	4

4.1.3 Volcanic hazard susceptibility (VHS)

By using a similar approach like a landslide and seismic hazard mapping, the volcanic hazard-prone area also modeled by using wighted overlay analysis in Arc GIS 10.5. The derived VHS values were also divided into four classes based on the class of weighted overlay analysis obtained from the computation. Thus classes are low, medium, high and very high hazard susceptibility.

The volcanic Hazard susceptibility map prepared (Fig 4.3), revealed that 33% (2366.52km^2) of the study area falls under low, 34% (2447.60 km^2) medium, 25% (1810.08 km^2) high and the rest 8% (614.69 km^2) very high hazard zones.

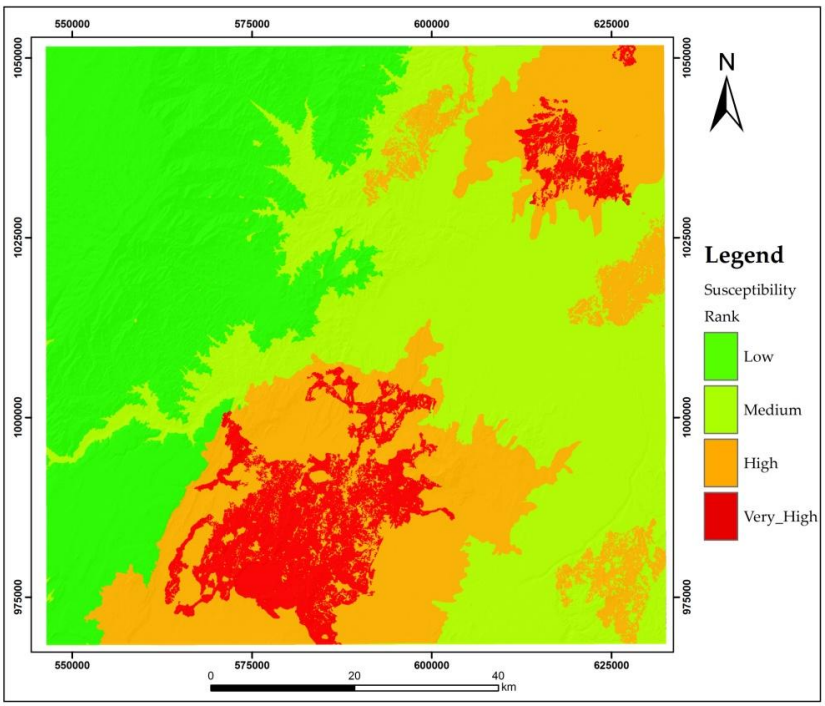

Fig 4. 3: Volcanic hazard susceptibility map

The result of volcanic hazard susceptibility map shows most volcanic hazard zone is found along the rift axial zone, mainly along the existing active volcanic spatter cones. This is due

to the factor influence given for active volcanic vents. The volcanic hazard zones also modified using the topography of the land. The North West high land parts of the study were grouped as low volcanic hazard zone using threshold elevation value of 2500m above means level. In addition, the unwanted pixels were filtered and updated by a zone of great contributor class.

Table 4. 3: Volcanic hazard susceptibility statistics of the study area

ID	Susceptibility rank	Area(km^2)	Area (%)
1	Low	2366.52	33
2	Medium	2447.60	34
3	High	1810.08	25
4	Very high	614.69	8

4.1.4 The three combined Geo-hazard susceptibility map (TCGS)

The three geo-hazard susceptibility result was added using (Eq.6) and the area susceptible to the three hazards were mapped. Like the previous section, the results of the computation were classified into low, medium, high and very high hazard susceptibility class.

$$TCGS = LHS+SHS+VHS \quad \text{(Eq.6)}$$

The prepared map (Fig 4.4) revealed that 10%(705.98 km^2) of the study area occupies low, 65% (4712.69km^2) medium, 23% (1636.31km^2) High, and the rest 2% (150.25km^2) very high hazard zones.

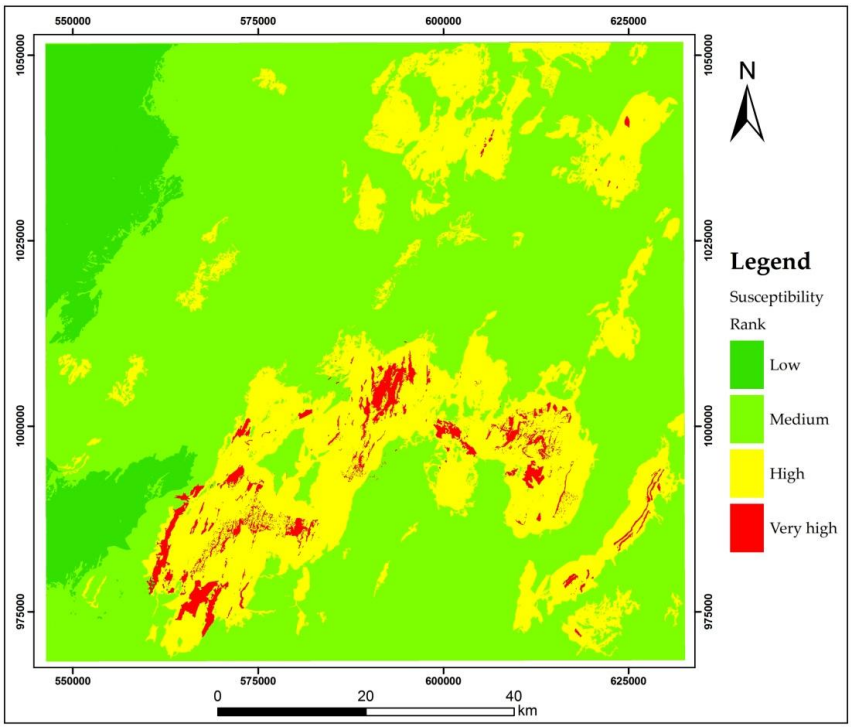

Fig 4. 4: The three combined Geo-hazard susceptibility map

he result of the model shows that main geo-hazard prone area lies along the rift axial zone. It is concentrated west and north of Lake Beseka and south of Kessem dam. In addition, high-rank classes are also shown around the northeast margin of the study area. However, the majority of the study area is mapped as medium geo-hazard prone area. The low combined hazard zones lies in the North West and at the margin of the western plateau.However the plateau are exceptionally prone to landslide hazard.

Table 4. 4: The three associated Geo-hazard susceptibility statistics of the study area

ID	Susceptibility rank	Area(km^2)	Area (%)
1	Low	705.98	10
2	Medium	4712.69	65
3	High	1636.31	23
4	Very high	150.25	2

4.2 Model validation

4.2.1 DInSAR result

Differential Synthetic Aperture Radar Interferometry (DInSAR) represents a well-established remote sensing technique, that allows detecting and monitoring Earth surface deformation phenomena by exploiting the phase difference (interferogram) of SAR data pairs collected at a different time and with slightly different sensor positions(Massonnet et al.,1998; Bürgmann et al.,2000).

In the present study Sentinel- 1A SLC data were analyzed in ESA SNAP platform. Processes like applying precise orbit file, co-registration of master and slave images, interferogram formation and topographic phase removal were conducted to generate differential interferogram. Four DInSAR results were produced with a six-month interval (Fig 4.5).

If the phase shift related to topography is removed from the interferograms, the difference between the resulting products will show surface deformation patterns occurred between the two acquisition dates(Ferretti et al., 2007). The phase fringes are a complete cycle which varies from - π to π, where a cycle represents the change in the elevation by half the wavelength of the sensor.

The more the closer the DInSAR fringes, the more intense the change or surface deformation. The result obtained from the DInSAR generation shows a pattern of fringes concentrated along NE to SW direction and at the central part of the study area. It could be related to the deformation.

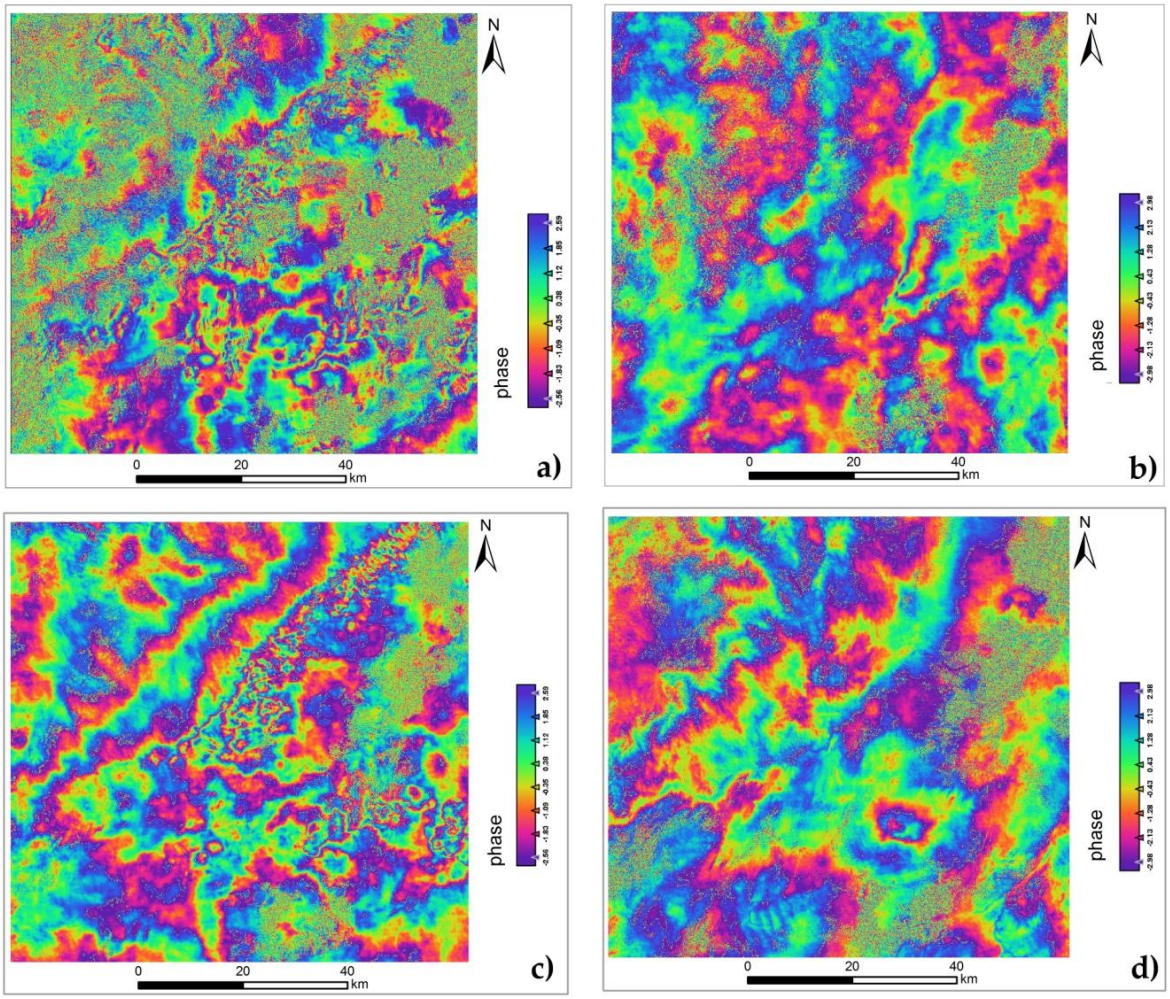

Fig 4. 5: DInSAR result: a) From 09 apr2015-180ct2015 b) 180ct2015- 10mar2016, c) 10mar2016-18Sep 2016 and d) 18 Sep 2016- 11mar2017

4.2.2 Coherence maps

The phase noise can be estimated from the interferometric SAR pair by means of the local coherence (Ferretti et al., 2007). The local coherence is the cross-correlation coefficient of the SAR image pair estimated over a small window (a few pixels in range and azimuth), once all the deterministic phase components (mainly due to the terrain elevation) are compensated for. The deterministic phase components in such a small window are, as a first approximation, linear both in azimuth and slant-range. Thus, they can be estimated from the interferogram itself by means of well-known methods of frequency detection of complex sinusoids in noise (e.g. 2-D Fast Fourier Transform (FFT)).

The coherence map of the scene is formed by a moving window that covers the whole SAR image. The coherence value ranges from 0 (the interferometric phase is just noise) to 1 (complete absence of phase noise).

Coherence map of this study is shown in (Fig 4.6). The map tells, low coherence area is occurred along the vegetation covered places, at water body and at mountain foots particularly north and North West of the study area. Since the coherence is directly related to the quality of the interferogram, it was used for masking out noise results obtained at the estimation of displacement.

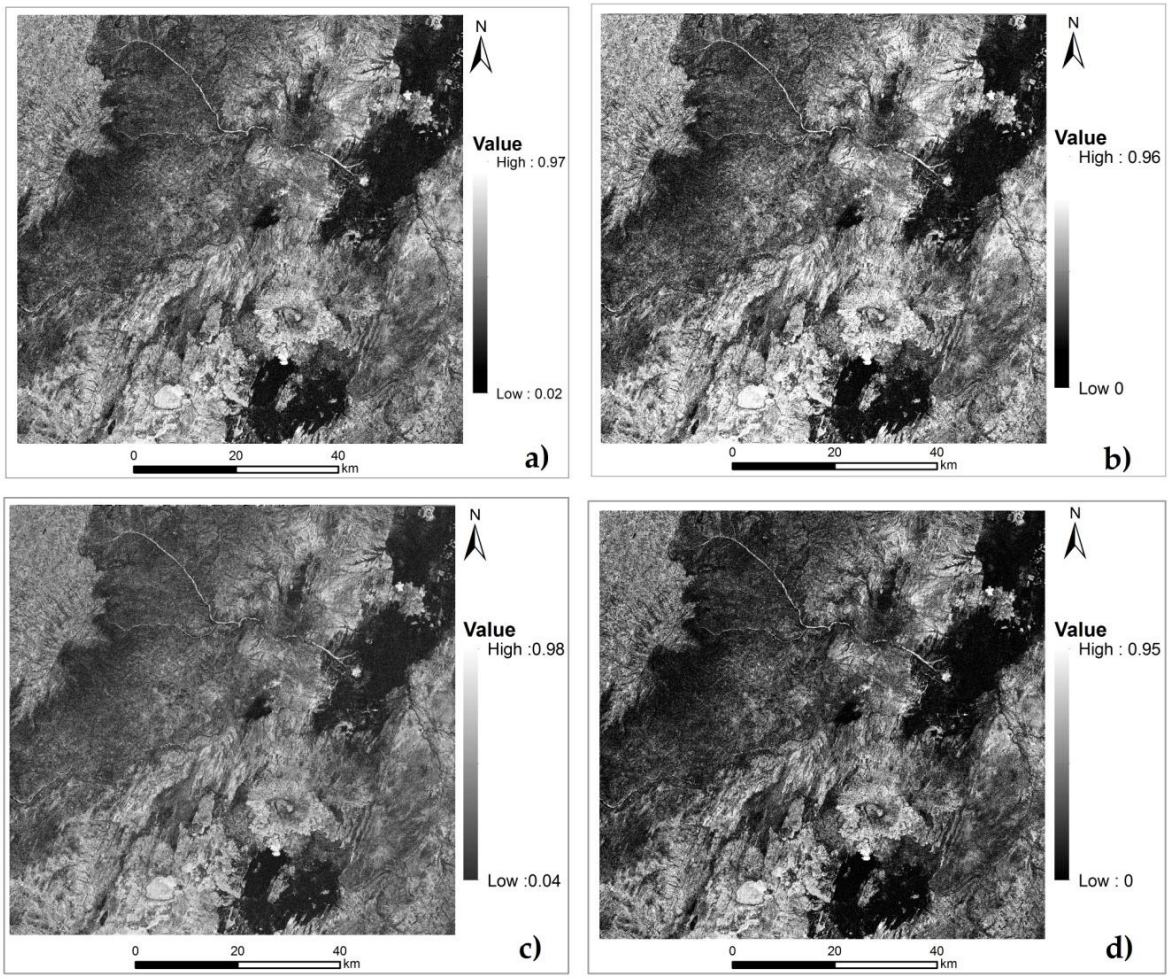

Fig4. 6: Coherence map: a) From 09 apr2015-180ct2015 b) 180ct2015- 10mar2016, c) 10mar2016-18Sep 2016 and d) 18 Sep 2016- 11mar2017

4.2.3 Displacement obtained from DInSAR

Fringes hold the wrapped phase information which varies from –π to π. The wrapped phase obtained in the fringes is converted to the unwrapped phase through phase unwrapping in snaphu-v1.4.2. The displacement map was obtained using band math's module in ESA SNAP platform using (Eq.7).

(Unwrapped phase*wavelength in mm)/(-4π*cos(rad(incidence angle))) (Eq.7)

Where: Wavelength ≈55.5 mm, obtained from sentinel -1A SAR information and incidence angle is found from metadata of the product.

The result of the displacement map (Fig 4.7) shows a pattern of deformation, where max deformation is -1.5mm subsidence and 0.6 uplift ranges. In addition, the low coherence area was masked out using 0.3 threshold value.

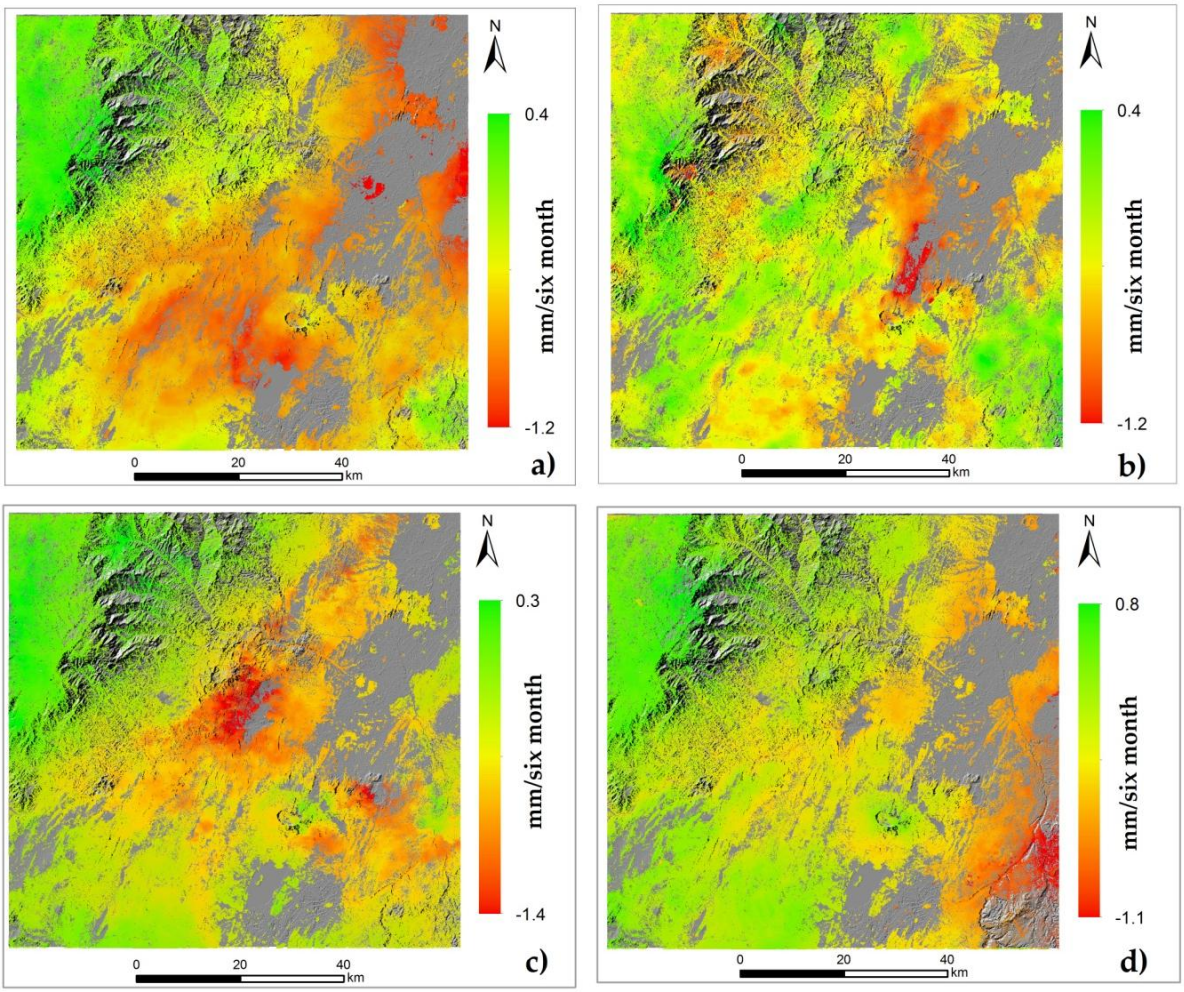

Fig 4. 7: Displacement map: a) From 09 apr2015-180ct2015 b) 180ct2015- 10mar2016, c) 10mar2016-18Sep 2016 and d) 18 Sep 2016- 11mar2017

In order to identify deformation spots the four displacement result obtained from the four DInSAR were modified. Displacement map obtained per six-month interval has been sum up and converted to year. Then an average of yearly displacements was computed using a raster calculator in Arc GIS. The result displacement map generated is depicted in (Fig 4.8). It shows max subsidence of 9.8 mm and uplift of 1.7mm. The result was used for cross-validation of the Geo-hazard susceptibility model generated from AHP method.

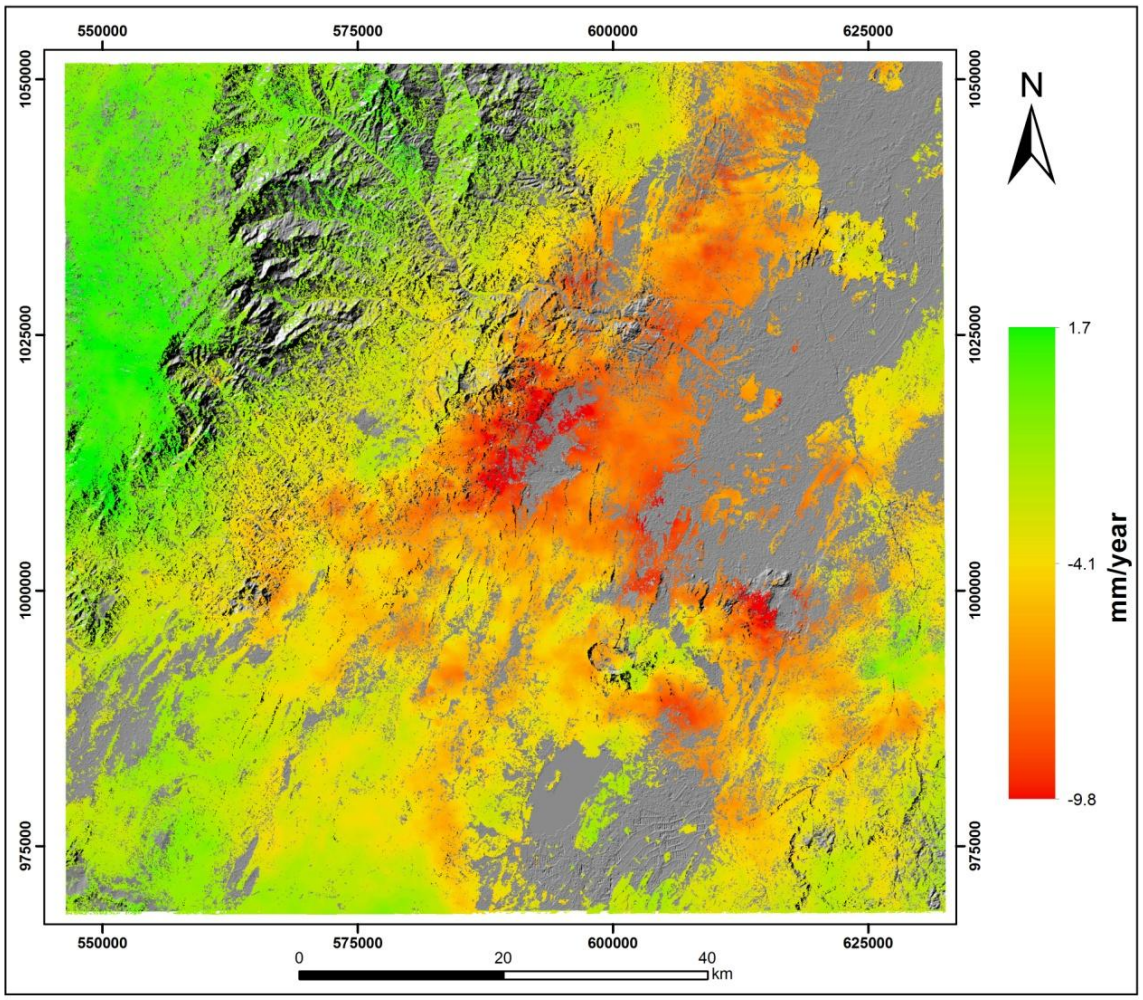

Fig 4. 8: Displacement map per year

4.2.4 Correlation of AHP model and SAR result

Total of 250 random points was generated and the pixel value of both AHP model and SAR result has been extracted using zonal statistics in Arc GIS. For the models, an index of susceptibility and for SAR result displacement map per year were used.

The correlation was done using Microsoft Excel 2013. Fig 4.9 shows a scatter plot of pixel values extracted from the resulting image. The y-axis is AHP model index in terms of susceptibility and the x-axis is the deformation index in terms of displacement (in cm). The scatter plot shows a positive linear regression between the two results. The R-squared value for each plot is displayed on the chart (Fig 4.9).

The R-Squared 0.3133 represents Landslide susceptibility, 0.44022 for Seismic hazard susceptibility , 0.3042 for volcanic hazard susceptibility model and 0.3904 for the combined three hazard susceptibility.

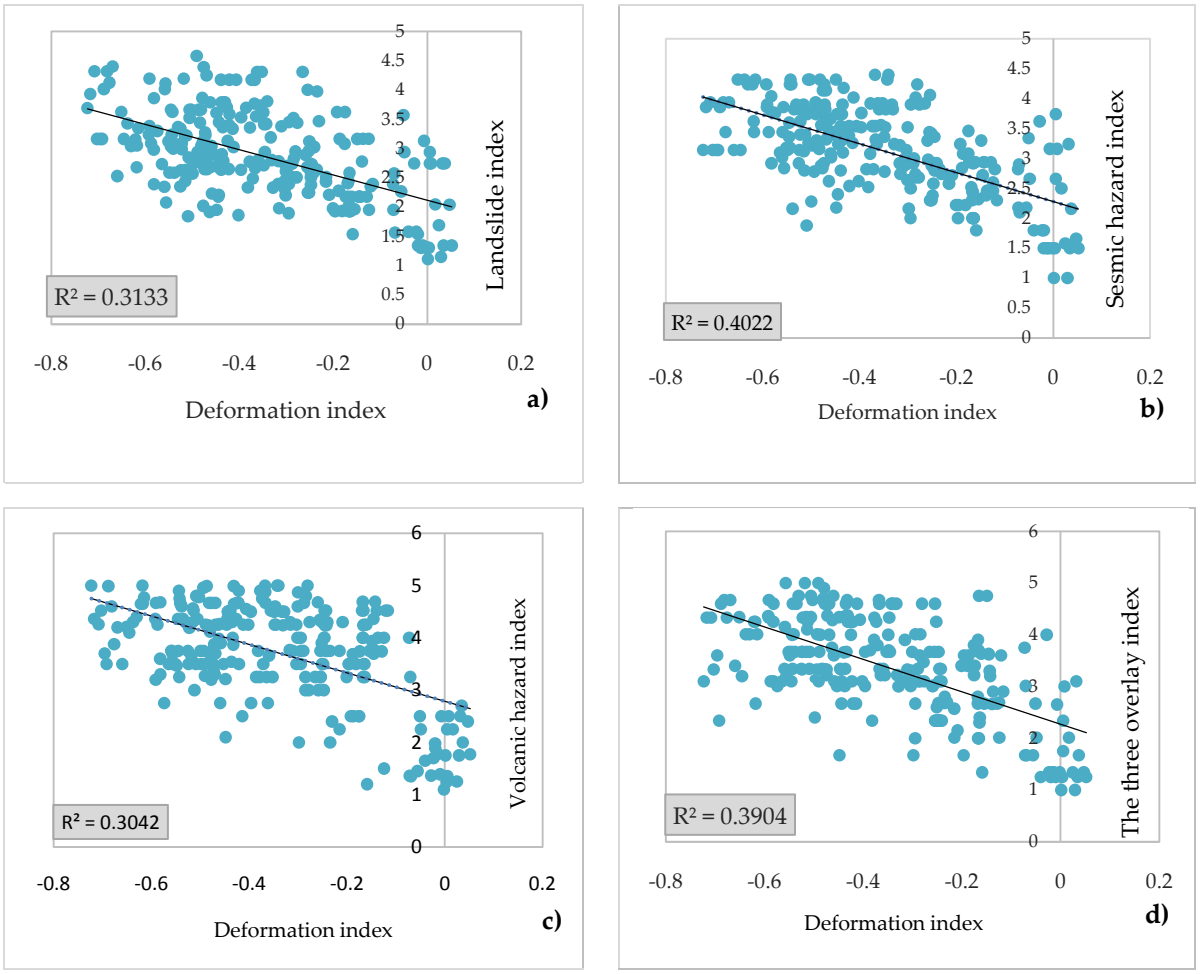

Fig 4. 9: Linear Correlation of AHP model and SAR result: a) Landslide susceptibility model, b) Seismic hazard susceptibility model, c) Volcanic hazard susceptibility model and d) the three hazard susceptibility model

4.2.5 Receiver operating characteristics (ROC)

The ROC curve is the plot of the probability of true positive (sensitivity) vs. the probability of false positive (1-specificity) as the cut of probability varies (Gorsevesky et al., 2000). ROC analysis is applied to assess the performance of spatial models that produce a probability map which presents the sequence in which the model selects the grid cells to determine the occurrence of a certain event. The best method has a curve with the largest AUC; the AUC varies from 0.5 to 1.0. If the model does not predict the occurrence of the event any better than chance, the AUC would equal 0.5. AUC stands for "Area under the ROC Curve." That is, AUC measures the entire two-dimensional area underneath the entire ROC curve (think integral calculus) from (0,0) to (1,1).

ROC curves were calculated for all four AHP model susceptibility maps. The vertical axis indicates the true positive rate, while the horizontal axis shows the false positive rate (Fig 4.10 and 4.11). True positive rates are the pixels that correctly referred to the model result, while the false positive rate is the pixels wrongly labeled to the model result.

To generate ROC curves, displacement map was computed from SAR image by slicing into 30 part and cone of larger displacement and zero displacement values were extracted as an inventory data set. The data was taken as exist and doesn't exist respectively. Using this data and an index of susceptibility map done in AHP method; a module in IDRISI software generates a result constituting the true positive % and false positive % values for each threshold that constitute the curve from which the ROC was calculated. The Results are reported in the module results box and saved to a file. Finally, the plot of true positive and false positive rate was executed in excels.

The area under the curve (AUC) is the measure that indicates the accuracy of the modeled susceptibility maps. The resulting AUCs indicate the probability that more pixels were correctly labeled than incorrectly labeled. The AUC values obtained from the ROC approach for Landslide, Seismic, Volcanism and the three associated susceptibility maps were 0.639, 0.706, 0.744 and 0.760, respectively. From this result, the performance of the model was acceptable.

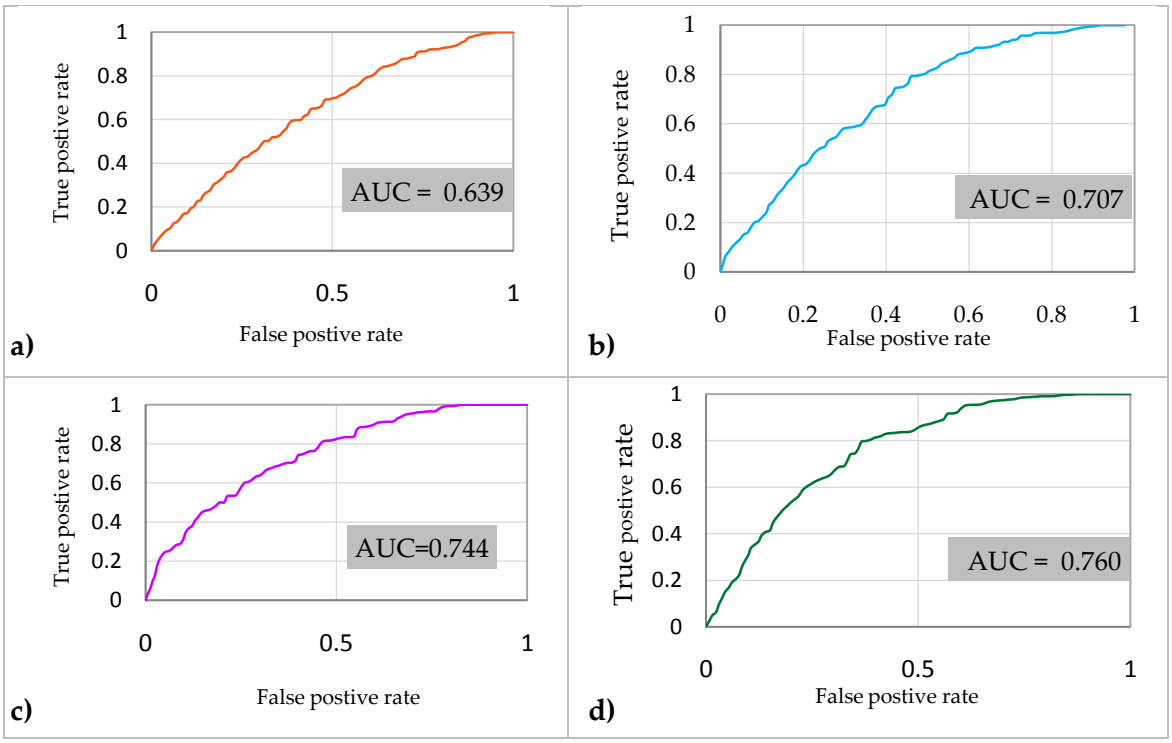

Fig 4. 10: Roc curve plot: a) Landslide susceptibility model, b) Seismic hazard susceptibility model, c) Volcanic hazard susceptibility model and d) the three hazard susceptibility model

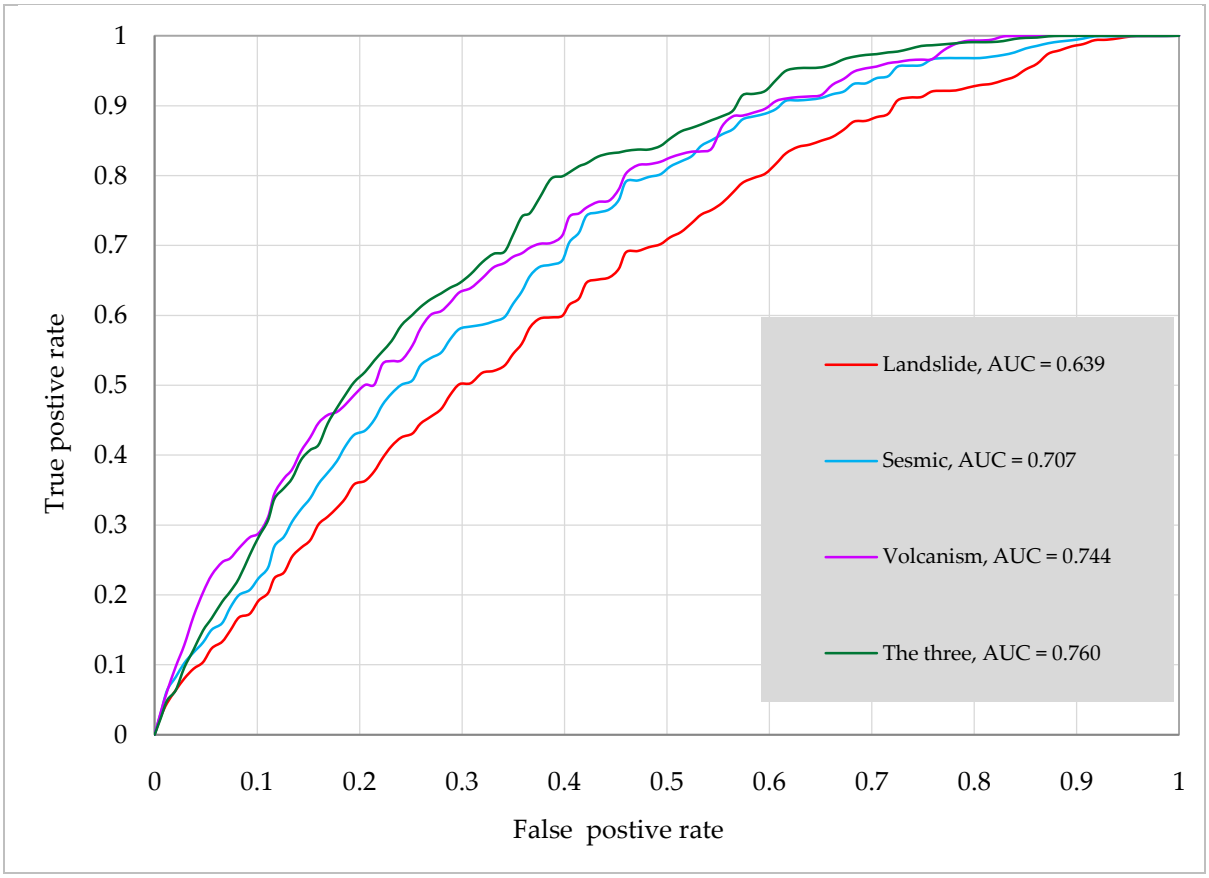

Fig 4. 11: Roc curve plot for all geo-hazard acceptability models

4.3 Model implementation

4.3.1 Assessing the spatial location of infrastructures with respect to the risk map

To assess the vulnerability of infrastructures and other property for the future or at the current situation, the geo-hazard susceptibility model includes the three associated hazards were used. All possible infrastructures, which are the subset of the study area, were prepared by its location from Google earth and satellite image. Built-ups including closer settlement and buildings, towns, road and railway, reservoir and natural lakes were used. Then after the spatial location of this infrastructure and property were overlain on the risk map (Fig 4.12).

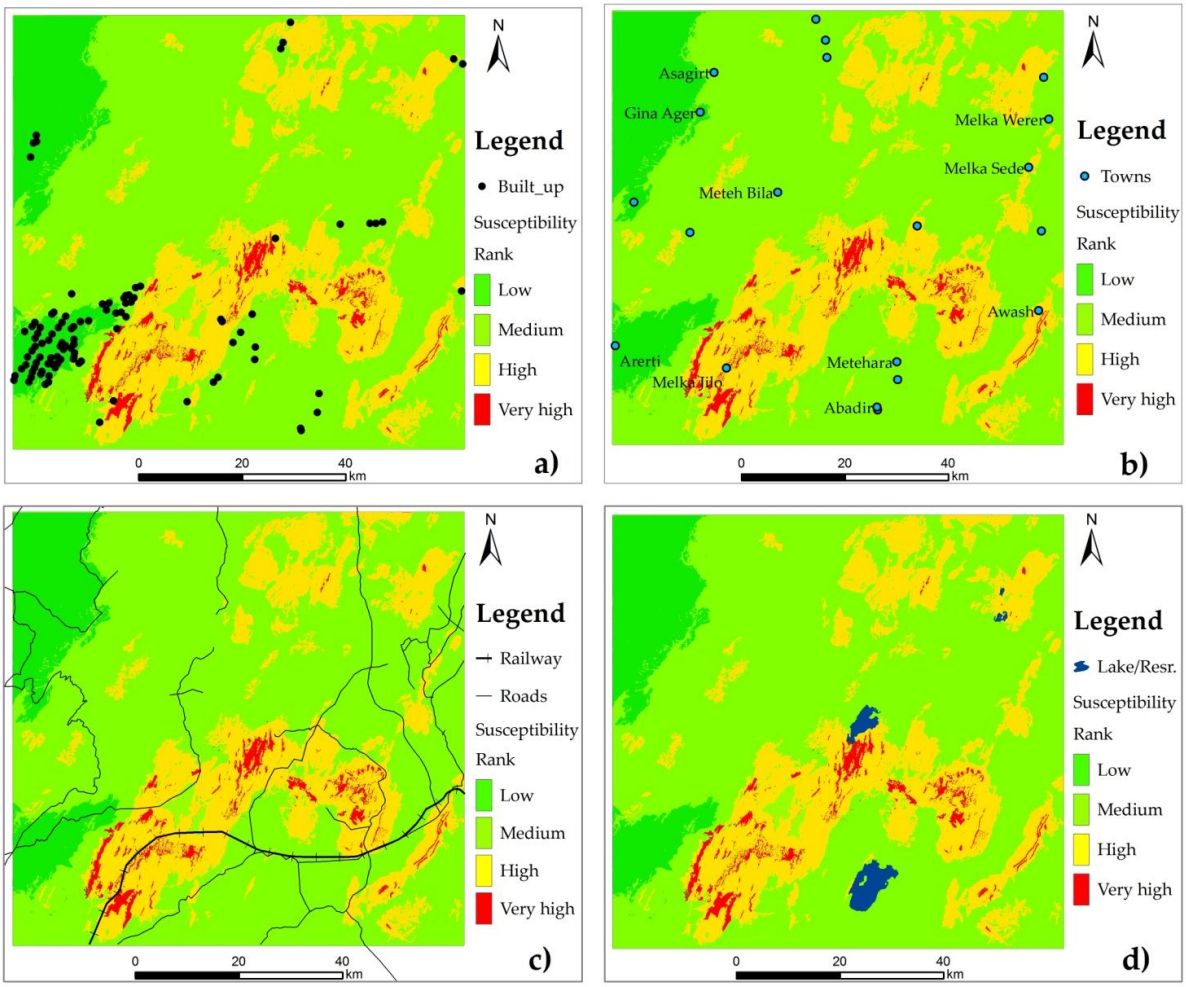

Fig 4. 12: Spatial location of infrastructures with respect to the risk map: a) built up areas, b) towns) road and railway and d) Lake and reservoir

The result shows some settlement and towns are a subset of high hazard susceptibility zone. Roads and a railway also cut across very high to high hazard susceptible zone. Reservoir called Kessem also found at a very close distance with the high hazard zone. In addition (Fig4.12) shows the spatial distance of all infrastructures with respect to the hazard risk map. For example settlements around Arerti town west of the study area lies under low hazard susceptible zone.

4.3.2 Inset map of selected infrastructure places

An inset map on the selected places was prepared using an image taken from Google earth with a resolution of CNES/Airbus satellite. The selected places are Kessem reservoir and Metehara town (Fig 4.13). The scale of the inset map was one to one hundred. Dark Blue rectangle highlights Kessem reservoir and light blue rectangle shows Metehara.

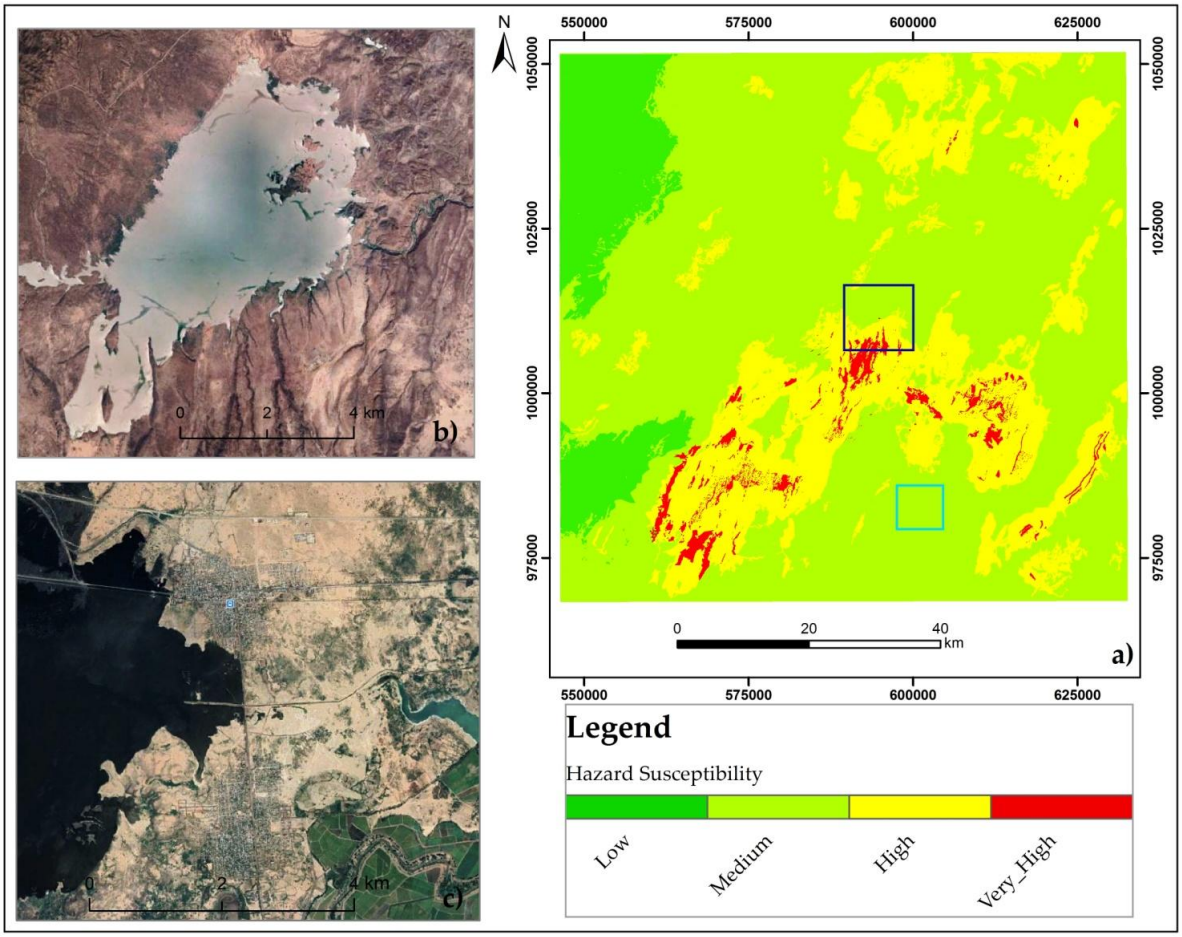

Fig 4. 13: Inset map of selected infrastructure places: a) hazard susceptibility, b) places around Kessem reservoir and c) place around Metehara and Abadir town

4.4 Discussion

Geo-hazards like Landslide, seismicity, and volcanism are one of the crucial environmental problems for the development of infrastructure and urbanization in Ethiopia, particularly in the Rift region (Bekele Abebe et al., 2010; Fubelli *et al*., 2015; Brown *et al*. 2015). The production of susceptibility maps /hazard zonation mapping/ is the first step in managing a sustainable risk mitigation program in any geo-hazard -prone area. In this research, landslide, seismic, volcanic and the three associated geo-hazard susceptibility maps for the entire study region were produced.

There are various methods for Geo-hazard susceptibility mapping. Atalye Ayeley, (2017) has used a Probabilistic seismic hazard analysis (PSHA) for Ethiopia and the neighboring region. The paper presents new probabilistic seismic hazard maps produced from a state-of-the-art PSHA study conducted using the classical Cornell McGuire approach. The hazard maps were produced for horizontal ground motion at bedrock level. The PGA values for 10% and 2%

probability of exceedance in 50 years in the spatial window of 0_N to 20_N latitude and 30_E to 50_E longitudes vary between 0 and 0.18 g and 0 to 0.35, respectively. The present study area lies with PGA value between 0.2 to 0.25 for 2% probability of exceedance within 50 years and 0.1 to 0.15 for 10% probability of exceedance within 50 years. Therefore this work enables to know, as the study area is more prone to seismic hazard.

Another study by Raghuvanshi et al., (2015) uses GIS-based Grid overlay method versus modeling approach in Meta Robi District of West Showa Zone in Ethiopia for landslide analysis. The paper uses six causative factors for landslide hazard zonation; slope material, slope, aspect, elevation, land use, and land cover and groundwater-surface traces. The validation of the result showed that 'GIS modeling' produced better compared to Grid overlay.

In this study, AHP technique was used to prepare the susceptibility maps in the study area and the model was validated using the DInSAR method. AHP method integrates different hazard contributing factors and finally depicts spots of geo-hazard prone areas. The DInSAR processing was aimed to show the general surface deformation (i.e instability) and correlated with the susceptibility map produced by AHP method. A work done by (Biggs et al., 2011) uses satellite-based interferometric synthetic aperture radar observations to demonstrate the significant deformation that has occurring at four volcanic edifices in the MER (Alutu, Corbetti, Bora, and Haledebi) from 1993 to 2010. This raises the number of volcanoes known to be deforming in East Africa. This study considers the well-known volcanoes like Kone, Fentale, and Dofan to look up their instability.

The susceptibility mapping obtained from AHP model shows that high landslide hazard susceptible classes cover the western rift margin part of the study area. This could relate to the steep slope topography of the place. However, the majority of the study area falls under low landslide prone including the rift floor and the top western plateau. In the case of seismic hazard, most of the study area occupies medium seismic hazard susceptibility zone. High susceptibility zone is the second large class and shown along the rift axial zone and along NNE margin of the study area, however low and very high seismic hazard covers a small area. They mostly follow the known rift structure that runs SW to NE direction. Whereas the model of volcanic hazard susceptibility shows most of the study area mainly the western highland are less susceptible, however, the rift axial zone is the more prone area. The high classes are concentrated at the recent active volcanic vents.

The correlation of the model result and DInSAR processing done using zonal statics and ROC curve analysis tells the performance of the susceptibility map were acceptable.

Linear regression analysis conducted using the index of hazard susceptibility and index of deformation has a positive correlation (Fig 4.9). However the correlation is not enough strong, this could be due to some outliers and errors in the pixel value.

The results of the AUC values obtained from the ROC approach for cross-validation of the four models done using AHP method and DInSAR result showed that the three associated hazard susceptibility map has greater accuracy, where AUC value is 0.760. While the AUC values obtained from the ROC approach for Landslide, Seismic, and Volcanism susceptibility maps were 0.639, 0.706, and 0.744 respectively. From this value, the correlation was an increase from landslide to seismic and volcanism. The result could be DInSAR process were detect deformations related to volcanism relative to landslide.

Finally, the hazard susceptibility map produced from this study could enable to assess the vulnerability of infrastructural which found at-risk zone. In addition, the spatial location of thus infrastructures with respect to the risk map can be an overlay and known their label of risk to the possible disaster that will pose. There are settlements, towns, roads railway reservoirs, which are found at-risk zone according to the prepared hazard susceptibility map. For instance, a reservoir called Kessem found closer to the high-risk zone.

CHAPTE- V CONCLUSION AND RECOMMENDATIONS

5.1 Conclusion

This study demonstrates the use of remote sensing and Geographic Information System (GIS) to assess geo-hazard prone areas. An attempt was made to map three geo-hazard susceptibilities using AHP and DInSAR method. Satellite data are found to be useful in mapping and quantitatively analyze natural disasters using different available software.

The production of susceptibility maps is the first step in managing a sustainable risk mitigation program in any geo-hazard -prone area. For the entire study, no previous attempts have been made to produce susceptibility maps using GIS and remote sensing approach. In this research, landslide, seismic, volcanic and the three associated geo-hazard susceptibility maps for the entire study region were done.

As the purpose of geo-hazard susceptibility map, to predict the probability of future geo-hazard occurrence in an area, identify the spatial location of very high geo-hazard prone area were targeted. For this purpose, eight geo-hazard contributing factors were generated and evaluated using AHP Technique. These spatial data sets are LULC, Faults and lineaments, active volcanic vent, slope, topography, soil texture and lithology. The Data were combined based on their significance, to map each geo-hazard susceptibility. To prepare landslide susceptible map, six major landslide causative factors were used; these factors are LULC, fault proximity, lineament density, lithology, soil, and slope. In the same approach to for seismic hazard susceptible ; five parameters such as fault proximity, lineament density, lithology, soil, and slope were taken. For volcanic hazard, structures (fault proximity plus lineament density), topography (elevation) and slope were combined. Finally, overlay analysis was done using the weighted value of each factor generated by the AHP method.

The result of the susceptibility mapping done for each hazard has been classified into four classes and their spatial area also calculated. For landslide 43%(3034.01km^2) of the study area occupies low, 26%(1870.89km^2) medium, 29% (2090.47km^2) High and 2% (142.82km^2) were very high hazard zones. For seismic hazard susceptibility, 8%(561.51km^2) of the study area occupies low, 53% (3801.99km^2) medium,35% (2526.04 km^2) High, and the rest 2% (142.82km^2) as very high hazard zone. In the Case of volcanic hazard 33% (2366.52km^2) of the study area falls under low, 34% (2447.60 km^2) medium, 25% (1810.08 km^2) high and 8% (614.69 km^2) very high hazard zones.

A combined hazard mapping was done using additive overlay of the three susceptibility map.

The result was also classified into four zones and the spatial area of the classes was calculated. It revealed that 10%(705.98 km^2) of the study area occupies low, 65% (4712.69km^2) medium, 23% (1636.31km^2) High hazard, and the rest 2% (150.25km^2) very high hazard zones.

To validate the geo-hazard susceptibility generated by AHP method, differential interferogram (DInSAR) methods were used. The method was done by using a two year six months temporal baseline master and slave image co-registration. Four DInSAR results have been generated and from it, four displacement maps were produced. Finally, the four displacement maps were added and averaged to produce one displacement map shows the yearly deformation per mm. The results was between -9.8 up to 1.7mm per year. Where the negative sign is down movement and the positive one is uplift.

In addation , two results (i.e AHP model and SAR result) were correlated using linear regression and ROC curve. To do correlation a total of 250 random points were generated and the pixel value of both AHP model and SAR result has been extracted using zonal statistics in Arc GIS. For the models, an index of susceptibility and for SAR result displacement map per year were used. From this, the two results show a positive correlation and validate the performance of the model.

In the case of ROC curve analysis displacement map computed from SAR image was slice into 30 part and cone of larger displacement and zero displacement values were extracted as an inventory data set. Using this data and an index of susceptibility map done in AHP method, ROC curve analysis was conducted. The AUC values obtained from the ROC approach for Landslide, Seismic, Volcanism and the three associated susceptibility maps were 0.639, 0.706, 0.744 and 0.760, respectively. From cross-validation the performance of the model was acceptable. Therefore the output maps can assist decision makers and planners to identify areas that are susceptible to future hazards. It will lead to the mitigation of future damage to infrastructure and human life.

Finally, as an implementation, the vulnerability of infrastructures and other property for the future or at the current situation were assessed by using the combine hazards succeptiblity map. For that, all possible infrastructures, which are the subset of the study area, were prepared by its location from Google earth, satellite image, and Ethio GIS shapefile. Built-ups including closer settlement and buildings, towns, road and railway, reservoir and natural lakes were extracted and overlay on the risk map. In addition, an inset map on the selected places was prepared using an image taken from Google earth with a resolution of CNES/Airbus satellite.

5.2 Recommendation

There is a need to plan for studying possible disaster that could pose a threat to human lives, settlement, infrastructure and agriculture lands, which found at a disaster prone area. Without any doubt, the study area is among the place in Ethiopia that will have Geo-hazard disaster. Understanding the nature of disasters, producing hazard susceptibility maps, assess the level of risks on the existing wealth, change monitoring and others are very crucial and possible measures which should be done.

Generally, remote sensing with repetitive and synoptic viewing capabilities, as well as multispectral capabilities, is a powerful tool for mapping, monitoring and assess disasters prone places. The use of remote sensing needs to be introduced for monitoring the activities developers and disaster management activity governers. This will help in reducing natural disasters that will occur due to inadequate monitoring and management activity.

- Generally, the following points can be recommended based on this work :
  - Using Remote sensing and GIS-based in Geo-hazard susceptibility mapping and risk assessment is recommendable.
  - RADAR technology can be recommended for surface change detection that occurs due to deformation and land instability.
  - The assessment and control of land instability for the design and location of stable infrastructures, settlements, and other development activities.
  - Perform monitoring activities at places, where development activities already running.
  - Understanding the level of risk of a particular place by preparing hazard susceptibility mapping

References

Abolghasem A., Noram I.B., and Ngien, K.(2016). Application of Public Domain Satellite-Based DEMs in Natural Hazard Modeling. *International Journal of Environmental Science and Development.***7**:140-143.

Acocella1, V. and Tesfaye Korme (2002). Holocene extension direction along the Main Ethiopian Rift, East Africa. *Terra Nova*. **14**:191- 197.

Acocella, V., Tesfaye Korme and Salvini, F. (2003). Formation of normal faults along the axial zone of the Ethiopian Rift. *Journal of Structural Geology*. **25**: 503- 513.

Acocella, V., Bekele Abebe, Tesfaye Korme, and Barberi, F. (2008). Structure of Tendaho graben and Manda Hararo rift: Implications for the evolution of the southern Red Sea propagator in Central Afar: *Tectonics*. **27**:40-16.

Antonio P. and Fabiana C. (2017). A Review of Interferometric Synthetic Aperture RADAR (InSAR) Multi-Track Approaches for the Retrieval of Earth's Surface Displacements. *Applied Science.* **7***:* 2-40.

Asfawossen Asrat, Berakhi, O., Branccaccio, L., Dramis, F. and Mohamed Umer (1997). Gravitational slope phenomena along the eastern escarpment of Wollo (Ethiopia). *International Conference on Geomorphology*. **3**: 59-72.

Asrat Worku, (2011). Recent developments in the definition of design earthquake ground motions calling for a revision of the current Ethiopian Seismic Code - EBCS 8: 1995. *Journal of Ethiopian Engineers and Architects*. 28:108 pp.

Atalye Ayele and Kulhánek, O. (2007). Spatial and temporal variations of seismicity in the Horn of Africa from 1960 to 1993. *Geophysical Journal International*. **130**: 805–810.

Atalye Ayele(2017).Probabilistic seismic hazard analysis (PSHA) for Ethiopia and the neighboring region. *Journal of African Earth Sciences*.**131**: 261-263.

Bahuguna, V., Joshi, S., Deshmukh, N.and Bhalchandra, P. (2013). Assessment the role of GIS for natural disaster management: a critical review. *International Journal of Innovative Research in Science*. **2**: 75–102.

Bartolini, S., Cappello, A., Martí, J., and Del Negro, C. (2013). QVAST: A New Quantum GIS Plugin for Estimating Volcanic Susceptibility. *Nat. Hazards Earth Syst Sci.* **13**: 3031–3042.

Bekele Abebe, Acocella, V., Tesfaye Korme and Derge Ayalew (2007). Quaternary faulting and volcanism in the Main Ethiopian Rift. *Journal of African Earth Science*. **48**: 115-124.

Bekele Abebe, Francesco, D., Fubelli, G., Mohamed Umer and Asfawossen Asrat(2010). Landslides in the Ethiopian highlands and the Rift margins. *Journal of African Earth*

Sciences **.56**:135-138.

Berhanu Temesgen, Mohamed Umer and Tesfaye Korme (2001). Natural hazard assessment using GIS and remote sensing methods, with particular reference to the landslides in the Wondogenet Area, Ethiopia. *Phys Chem Earth.* **26**:665–675.

Bisson, M., Sulpizio, R., Zanchetta, G., Demi, F., Santacroce, R.(2010). Rapid terrain-based mapping of some volcaniclastic flow hazard using GIS-based automated methods: a case study from southern Campania, Italy. *Natural Hazards*. **55**, 371–387.

Bisson, M., Zanchetta, G., Sulpizio, R., Demi, F. (2013). A map volcaniclastic debris flow hazards in Apennine areas surrounding the Vesuvius volcano (Italy). J. Maps. http://dx.doi.org/10.1080/17445647.2013.768948.

Biggs, J., Bastow, I.D., Keir, D. and Elias Lewi (2011). Pulses of deformation reveal frequently recurring shallow magmatic activity beneath the Main Ethiopian Rift. *Geochem. Geophys. Geosyst.***12**:2-9.

Boccaletti, M., Bonini, M., Mazzuoli, R., Bekele Abebe, Piccardi, L. and Tortorici, L.(1998). Quaternary oblique extensional tectonics in the Ethiopian Rift (Horn of Africa). T*ectonophysics*. **287**: 97-116.

Boccaletti, M., Mazzuoli, R., Bonini, M., Trua, T. and Bekele Abebe (1999). PlioQuaternary volcano-tectonic activity in the northern sector of the Main Ethiopian Rift: relationship with oblique rifting. *Journal of Africa Earth Science*. **29**:679-698.

Bonini, M., Souriot, T., Boccaletti, M. and Brun, J.P. (1997). Successive orthogonal and oblique extension episodes in a rift zone: laboratory experiments application to the Ethiopian Rift. *Tectonics*.**16**: 347-362.

Brown, S., Auker, M. and Sparks, R. (2015). Populations around Holocene volcanoes and development of a Population Exposure.Volcanic Hazards and Risk. Cambridge University Press, Cambridge. **31**: 223– 232.

Burgmann, R., Rosen P. and Fielding, E. (2000).Synthetic aperture radar interferometry to measure Earth's surface topography and its deformation. *Annu Rev Earth Planet Sci.* **28**:169–209.

Chinnery, M. (1961). The deformation of the ground around surface faults. *Bull Seismol Soc Am.* **51**:355–372.

Cevik, E. and Topal, T. (2003). GIS-based landslide susceptibility mapping for a problematic segment of the natural gas pipeline, Hendek (Turkey). *Environmental Geology*. **44**: 949–962.

Clerici, A., Perego, S., Tellini, C. and Vescovi, P. (2002). A procedure for landslide

susceptibility zonation by the conditional analysis method. *Geomorphology*. **48**: 349–364.

Dershaye Belay (2017). Environmental Impact Analysis of Infrastructures Development and Lake Beseka Expansion on the Integrity of Fentale-Metehara Blister Caves in the Main Ethiopian Rift. Unpublished Report, Addis Ababa, Ethiopia.

Daniel Meshesha, Dejene Haile Mariam and Abrham Mamo (2010). Geology of Debre Birhan Area,unpublished report.geoscience mapping core process,geological survey of Ethiopia(GSE).

Dai, F.C., Lee, C.F., Li, J. and Xu, Z.W. (2001). Assessment of landslide susceptibility on the natural terrain of Lantau Island, Hong Kong. *Environmental Geology*. **43**: 381–391.

Das, D.K.and Agarwal R.P. (2002). Physical properties of soil. Fundamentals of soil science. Indian Society of Soil Science, IARI: pp 75–77.

Das, D.K. (2007). Introductory soil science. Kalyani, New Delhi, pp 475–483

Eastman, J. R. (2006). IDRISI Andes Tutorial. Clark Labs Clark University, 950 Main Street Worcester, MA 01610-1477 USA. Manual Version 17.0

Ercanoglu, M. and Gokceoglu, C. (2004). Use of fuzzy relations to produce landslide susceptibility map of a landslide-prone area (West Black Sea Region, Turkey). *Engineering Geology*. **75**: 229–250.

Erden, T. and Karaman, H.(2012). Analysis of earthquake parameters to generate hazard maps by integrating AHP and GIS. *Nat. Hazards and Earth System Sci.* **12**: 475–483.

Faure, H. (1975) Neotectonics in the Afar (Ethiopia, T.F.A.I.). In: Suggate RP, Creswell MM (eds) Quaternary studies. Royal Society of New Zealand, Wellington. pp 121–126

Farrell, W. (1972). Deformation of the earth by surface loads. R*eview of Geophysics.* **10**:761–797.

Felpeto, A., Martí, J., and Ortiz, R. (2007). Automatic GIS-Based System for Volcanic Hazard Assessment. *Journal of Volcanol Geotherm Research*. **166**: 106–116.

Ferdaus A. and Chow, W.S. (2004). Landslide at Km 52, Tapah-Tanah rata road, Cameron Highlands, Malaysia. Malaysia-Japan Symposium on Geohazards and Geoenvironmental Engineering-Recent Advances, Geotechnical & Ecological Environment Management: Selangor, Malaysia. pp. 19-24.

Ferretti, A., Monti-Guarnieri, A., Prati, C.and Rocca, F.(2007). InSAR Principles: Guidelines for SAR Interferometry Processing and Interpretation. ESA Publications, Netherland.

Fikadu Kebede (1996). Seismic hazard assessment for the Horn of Africa. In Proceedings of the Ethiopian Association of Seismology and Earthquake Engineering (EASEE)—workshop on seismic hazard assessment and design of structures for earthquake resistance, Addis

Ababa, Ethiopia, pp 25–38.

Franceschetti ,G, Lanari ,R. (1999). Synthetic Aperture Radar Processing Techniques,CRC Press, Boca Raton.

Fubelli G., Vinci S., Bekele Abebe, Dramis F. (2008). Fubelli, G., Abebe, B., Dramis, F., Vinci, S., 2008. Geomorphological evolution and present-day processes in the Dessie Graben (Wollo, Ethiopia). Catena. **75**:28–37.

Fubelli G., Guida D., Cestari, A. and Dramis F. (2013). Landslide hazard and risk in the Dessie Town area (Ethiopia). *Landslide science and practice*. **6**: 357–361.

Fubelli G., Dramis F. (2015) Geo-hazard in Ethiopia. In: Billi P. (eds) Landscapes and Landforms of Ethiopia. World Geomorphological Landscapes.

Gabriel, A., Goldstein, R., Zebker, H.(1989). Mapping small elevation changes over large areas: differential interferometry. *Journal of Geophysical Research.* **94**:915–919.

Giday WoldeGabriel, Robert, C., Walter, J., Aronson, L. and William K. (1990). Geochronology and rift basin development in the central sector of the Main Ethiopian Rift. *Geol. Soc. of American Bulletin*. **102**: 439-458.

Gouin, P. (1976). Seismic zoning in Ethiopia. B Geophys Observ, Addis Ababa 7:1–46

Gouin, P. (1979). Earthquake history of Ethiopia and the Horn of Africa. International Development Research Center (IDRC), Ottawa.

Gorsevesky P.V., Gessler P. and Foltz R.B. (2000). Spatial prediction of landslide hazard using discriminant analysis and GIS. pp. 25-27. Denver, Colorado.

Habtamu Eshetu, Leta Alemayehu, Ezera Tadesse and Yewubinesh Bekele (2012). Engineering geological mapping of Nazareth map sheet. Geological Survey of Ethiopia.

Haile, Melaku(2004). Seismic micro-zonation for the city of Addis Ababa by using microtremors. Paper No. 2092 submitted to 13th World Conference on Earthquake Engineering, Vancouver, August 1-6.

Hencher, S.R. (1989).The implication of joints and structures for slope stability," In M. &. Anderson, Stability. *Geotechnical and Geomorphology*.**8**: 145-186.

https://learn.arcgis.com/en/related-concepts/digital-elevation-models.htm accessed on 17.03.2019.

https://en.wikipedia.org/wiki/Landslide accessed on 19.02.2019.

https://en.wikipedia.org/wiki/Earthquake) accessed on 19.02.2019.

https://www.emsccsem.org accessed on 18.02.2019.

https://owlcation.com/stem/Types-of-Volcanic-Vents accessed on 20.02.2019.

http://www.gis.com/content/what-gis accessed on 25.02.2019.

https://www.usgs.gov/faqs/fault accessed on 20.02.2019.

http://www.gis.com/content/what-gis accessed on 23 .02.2019.

Jensen, J. R. (1996). "Introductory Digital Image Processing", Prentice Hall Series in Geographic Information Science, New Jersey.

Kinde, Simachew (2002). Earthquake Risks in Addis Ababa and other Major Ethiopian Cities - Will the Country be Caught Off-guarded? MediaETHIOPIA

Koçal, A. (2004). A Methodology for Detection and Evaluation of Lineaments from Satellite Imagery. Ms. thesis, Middle East Technical University, 121 p.

Koike, K., Nagano, S. And Ohmi, M. (1995). Lineament Analysis of Satellite Images Using A Segment Tracing Algorithm (STA). *Computers and Geosciences*. **21**: 1091-1104.

Komac, M. (2006). A landslide susceptibility model using the Analytical Hierarchy Process method and multivariate statistics in perialpine Slovenia. *Geomorphology*.**74**: 17–28.

Krishnamoorthi, N.(2016). Role of Remote Sensing and GIS in NaturalDisaster Management Cycle. *Imperial journal of interdisciplinary research.***2**:145-152.

Lee, S., Choi, J. and Min, K.(2005). Probabilistic landslide hazard mapping using GIS and remote sensing data at Boun, Korea. *International Journal of Remote Sensing*. **25**: 2037–2052.

Lenhardt, N. and Oppenheimer, C. (2014). Volcanism in Africa: geological perspectives, hazards, and societal implications. *Geodesy and Geophysics*. **1**: 169–199.

Leprince S., Berthier E., Ayoub F., Delacourt C., and Avouac J. (2008). Monitoring Earth surface dynamics with optical imagery. EOS, *Transactions, American Geophysical Union.* **89**: 2-5.

Lillesand, T.M., Keifer, R.W. and Chipman J.W.(2004). "Remote Sensing and Image Interpretation", 5th Edition.

Lulseged Ayalew (1999). Causes and mechanisms of slope instability in Dessie town, Ethiopia. *Engineering Geology*. **58**: 9-19.

Lulseged Ayalew and Yamagishi, H. (2002). Landsliding and landscape development; the case in northern Ethiopia". *International Congress of INTERPRAEVENT 2002 in the Pacific Rim*. Matsumoto, Japan, pp. 595–606

Lulseged Ayalew and Yamagishi, H. (2005). The application of GIS-based logistic regression for landslide susceptibility mapping in the Kakuda–Yahiko Mountains, Central Japan. *Geomorphology*. **65**: 15–31.

Madani.Y., Kassie, T. H., and Hengsdijk , H. (2015). Climate variability and change in the

Central Rift Valley of Ethiopia: challenges for rainfed crop production. *Journal of agriculture science.***7**:104-111

Mansourian, A., Rajabifard, A. and Valadan Zoej, M.J. (2007).SDI Conceptual Modeling for Disaster Management. In Proceedings of the ISPRS Workshop on Service and Application of Spatial Data Infrastructure, Amsterdam.

Massonnet, D.and Feigl, K. (1998). Radar interferometry and its application to changes in the earth's surface. *Review of Geophysics*. **36**:441–500.

Mark, P., Tianqing C., Tim, D., Arthur, F.,Chris, W. and David S.(2004). Mapping fault rupture hazard for strike-slip earthquakes. 3rd World Conference on Earthquake Engineering.August 1-6, 2004: Paper No. 1094. Vancouver, B.C., Canada.

Martí. J., and Felpeto, A. (2010).Methodology for the Computation of Volcanic Susceptibility. An Example for Mafic and Felsic Eruptions on Tenerife (Canary Islands). *Journal of Volcanol Geotherm Research* .**195**: 69–77.

Mehdi M., Mohammad, H. and Zargham M.(2012). GIS-Based Landslide Susceptibility Mapping by AHP Method. *Journal of Basic and Applied Scientific Research.***2**: 6715-6723.

Mogi, K. (1958). Relations between the eruptions of various volcanoes and the deformations of the ground surfaces around them. *Bull Earthq Res Inst*. **36**:99–134.

Mohr , P.A. (1962) .The geology of Ethiopia. Addis Ababa University College Press, Addis Ababa.

Mohr, P. (1967). The Ethiopian rift system. Addis Ababa University College Press, Addis Ababa. **11**:1–65

Mohr, P. (1987). Patterns of faulting in the Ethiopian Rift Valley. *Tectonophysics.* **143**:169-179.

Nama, E.E. (2004). Lineament detection on Mount Cameroon during the 1999 volcanic eruptions using Landsat ETM. *International Journal of Remote Sensing*. **25**: 501-510.

Nestor Y., Pau P., Senior M., Ramon., B and Richard B.(2016).Interferometric Processing of Sentinel-1 TOPS Data. *IEEE transactions on geoscience and remote sensing*. **54**: 2221-2232.

Nielsen, T.H., Wright, R.h., Vlasic, T.C. and Spangle, W.E. (1979). Relative slope stability and land-use planning in the San Francisco Bay region, California. US Geological Survey Professional Paper., 944.

Olalekan Mumin Bello, Yusuf Adedoyin Aina, (2014). Satellite Remote Sensing as a Tool in Disaster Management and Sustainable Development: Towards a Synergistic Approach", Procedia – Social and Behavioural Sciences. **120**. 365-373

O'Leary, D. Friedman, J., Pohn, H.(1976).Lineament, linear, lineation: Some proposed new standards for old terms. *Geological Society America Bulletin*. **87**:1463-1469.

Okada, Y. (1985). Surface deformation due to shear and tensile faults in a half-space. *Bull Seismol Soc Am*. **75**:1135–1154.

Raghuvanshi, T. K., Jemal Ibrahim and Dereje Ayalew (2014). Slope stability susceptibility evaluation parameter (SSEP) rating scheme – An approach for landslide hazard zonation. *Journal of African Earth Sciences.* **99**: 595–612.

Raghuvanshi, T. K., Lensa Negassa and kala, P.(2015). GIS-based Grid overlay method versus modeling approach grid overlay method in Meta Robi District of West Showa Zone, Ethiopia. *The Egyptian Journal of Remote Sensing and Space Science.* **18**: 235-250.

Ramli, M.F., Yusof, N., Yusoff, M.K., Juahir, H., and Shafri, H. (2010).Lineament mapping and its application in landslide hazard assessment: a review. *Bulletin of Engineering Geology and Environment*. **69**: 215–233.

Rosen, P.A., Hensley, S., Zebker, H.A., Webb, F.H. and Fielding, E.(1996).Surface deformation and coherence measurements of Kilauea Volcano, Hawaii, from SIR-C radar J. Geophys. Res. Planets. **101**: 23109–23125.

Roslee, R., Tahir, S., Omang, A.K S. (2006).Engineering geology of the Kota Kinabalu area, Sabah, Malaysia. *Geological Society of Malaysia Bulletin*. **52**: 17- 25.

Saaty, T. (1977). A scaling method for priorities in hierarchical structures. *Journal of Mathematical Psychology*. **15**: 234–281.

Saaty, T. and Vargas, G.(2001). Models, Methods, Concepts, and Applications of the Analytic Hierarchy Process, Kluwer Academic Publisher, Boston.

Saaty, T.L. (2005). Theory and Applications of the Analytic Network Process, Pittsburgh, PA: RWS Publications.

Saaty, T. (2008).Decision making with the analytic hierarchy process. *International Journal of Services Sciences*. **1**:83–98.

Saha, A.K., Gupta, R.P., and Arora, M.K. (2002).GIS-based landslide hazard zonation in the Bhagirathi (Canga) Valley, Himalayas. *International Journal of Remote Sensing*.**2**: 357–369.

Sansosti, E., Manunta, M. Casu, F., Bonano.O., Marsella ,M.and Lanari, R.(2015). Radar remote sensing from space for surface deformation analysis: present and future opportunities from the new SAR sensor generation. *Geodesy and Geomatics to the edge.* **26**:76-81.

Siebert, L., Simkin, T. and Kimberly, P. (2010). Volcanoes of the World. 3rd edn. University of California Press, Berkeley.

Simons M., and Rosen, P.(2015). Interferometric Synthetic Aperture Radar Geodesy. In: Gerald Schubert (editor-in-chief) Treatise on Geophysics, 2nd edition. **3**: 339-385.

Scott, W., Iverson R., Schilling S. and Fischer, B. (2001). Volcano hazards in the Three Sisters Region, Oregon: U.S. Geological Survey OpenFile Report 99-437. Retrieved January 16, 2008, from: http://geopubs.wr.usgs.gov/open-file/of99-437/.

Skidmore, A.K. (2002). Taxonomy of environmental models in the spatial sciences.In: Environmental modeling with GIS and remote sensing. London: Taylor & Francis

Sparks, S., Aspinall, W., Auker, M., Crosweller, S., Hincks, T., Mahony, S., Nadim F., Pooley J. and Syre, E. (2012). Mapping and characterizing volcanic risk. In: Abstracts of the magmatic rifting and active volcanism conference, Addis Ababa, January 11–13.

Tenalem Ayenew (2004). Environmental implications of changes in the levels of lakes in the Ethiopian Rift Since 1970. *Regional Rural change.* **4**: 192-204.

Tenalem Ayenew & Barbieri, G. (2005). Inventory of landslides and susceptibility mapping in the Dessie area, Northern Ethiopia. *Engineering Geology*: **77**:1-15.

Van, Engelene W. and Dijkshoorn, J.A.(2012).Global and national soil and Terrain Databases(SOTER).Procedures manual version 2.0 , Draft for comments. ISRIC report 2012/04. ISRIC-World soil information. Wageningen, Netherland.

Van Westen, C. J. (2000), Remote Sensing For Natural Disaster Management, International Archives of Photogrammetry And Remote Sensing. Vol XXXVIII, part B7, Amsterdam.

Varnes, D.J. (1984).Landslide hazard zonation: a review of principles and practice, natural hazard 3, commission on landslides of the IAEG. UNESCO, Paris.

Wang, J., Howarth, K. and Philip J. (1990). Use of the Hough Transform in Automated Lineament Detection. *IEEE Transactions on Geoscience and Remote Sensing*.**28**:561-566.

Yalcin, A. (2008). GIS-based landslide susceptibility mapping using analytical hierarchy process and bivariate statistics in Ardesen (Turkey). *Catena*. **72**: 1–12.

Yao, X., Tham, L.G.and Dai, F.C. (2008). Landslide susceptibility mapping based on Support Vector Machine: A case study on natural slopes of Hong Kong, China. *Geomorphology*. **101**: 572–582.

Zvelebil,J.and Vilímek,V.(2010). Geo-risk management for developing countries—vulnerability to mass wasting in the Jemma River Basin, Ethiopia. *Landslides*. **7**:99–103.

Appendix

Appendix I: Accuracy assessments of land-cover classification

	Agriculture	Plantation	Water Body	Shrubland	Built Up	Bare land	Forest	Total	UA %
Agriculture	86	5	0	3	1	5	1	101	85
Plantation	2	10	0	1	0	0	1	14	71
Water Body	0	0	15	0	0	0	0	15	100
Shrubland	10	3	0	70	1	5	2	91	77
Built Up	1	0	0	1	5	1	0	8	63
Bareland	3	0	0	1	1	20	0	25	80
Forest	1	2	0	3	0	0	12	18	67
Total	103	20	15	79	8	31	16	272	
PA %	83	60	100	89	63	65	75		
PA = producer accuracy ; UA : User accuracy and All over accuracy=80.3, Kappa coefficient=0.78									

Appendix II : Average Densities for Common Igneous Rocks Source: Daly et al . ,1966)

Rock Type		*Range of Density(Mg/m^3)*	*Mean Density(Mg/m^3)*
Silicic			
	Rhyolitic pumice	0.500–1.500	1.000
	Rhyolitic tuff	1.000–1.800	1.400
	Rhyolitic welded tuff	1.800–2.400	2.100
	Rhyolitic obsidian	2.330–2.413	2.370
	Rhyolite		2.51
	Granite	2.516–2.809	2.667
Intermediate			
	Trachytic obsidian	2.435–2.467	2.450
	Trachyte		2.57
	Andesitic glass	2.40–2.537	2.474
	Andesite		2.65
	Syenite	2.630–2.899	2.757
	Granodiorite	2.668–2.785	2.716
	Quartz diorite	2.680–2.960	2.806
Mafic			
	Leucitic tephritic glass	2.52–2.58	2.55
	Basaltic glass	2.704–2.851	2.772
	Basalt		2.74
	Diorite	2.721–2.960	2.839

Appendix III: Pixel value extracted for correlation of hazards susceptibility model and DInSAR result

Deformation index	Landslide index	Seismic index	Volcanism index	The three index
-0.7230798900	3.6900999550	3.1400001049	5.0000000000	1.2500000000
-0.7169485090	3.9328999520	3.8599998951	4.3600000000	1.3400000330
-0.7080503550	4.3200998310	3.9400000572	4.2580000000	1.6699999570
-0.7028925420	3.1626000400	3.1400001049	4.5200000000	1.2500000000
-0.6955674290	3.1626000400	3.1400001049	3.7000000000	3.1000000000
-0.6918388610	3.1626000400	3.1400001049	3.5000000000	1.0000000000
-0.6881301850	4.0156002040	3.8599998951	4.9900000000	1.3400000330
-0.6813611840	4.3200998310	3.9400000572	4.6000000000	2.0099999900
-0.6764699520	4.1259999280	3.4400000572	3.8800000000	3.0000000000
-0.6693694000	4.4028000830	3.9400000572	4.2000000000	1.7500000000
-0.6595324720	2.5299000740	3.1400001049	3.5000000000	2.3399999140
-0.6511669610	3.6243000030	4.3200001717	4.2100000000	1.2500000000
-0.6454874580	3.1626000400	3.1400001049	4.1000000000	1.0000000000
-0.6377992030	3.4302001000	4.3200001717	4.3000000000	1.3400000330
-0.6304173920	3.0429999830	4.2399997711	4.4000000000	2.6500000000
-0.6212994460	3.1544001100	4.2399997711	4.6500000000	1.2500000000
-0.6184566390	2.6781001090	3.6199998856	5.0000000000	1.3400000330
-0.6179537250	3.0518000130	3.4400000572	4.6500000000	1.2500000000
-0.6151052190	3.3475000860	4.3200001717	4.7700000000	1.3400000330
-0.5923242870	3.2370998860	4.2399997711	4.3600000000	1.3400000330
-0.5912231650	4.1939001080	3.8599998951	3.2000000000	4.0000000000
-0.5909509580	3.3847000600	3.9000000954	4.6700000000	1.2500000000
-0.5875790490	3.0892000200	3.4400000572	4.2500000000	2.0099999900
-0.5820301920	2.9793000220	4.0399999619	3.6000000000	2.6700000760
-0.5818359180	2.3896999360	2.9200000763	4.6800000000	1.6699999570
-0.5817824970	3.8612000940	3.7799999714	3.3000000000	1.6699999570
-0.5740417170	3.3010001180	3.7599999905	2.7500000000	3.0099999900
-0.5645373460	2.7335999010	3.0999999046	3.5000000000	1.6699999570
-0.5594955760	2.3454999920	3.0199999809	3.7500000000	3.7500000000
-0.5586270240	4.0145998000	3.4400000572	3.7500000000	2.9000000000
-0.5570203810	4.1111998560	3.8599998951	3.6870000000	3.6000000000
-0.5555247520	2.0766999720	2.8399999142	3.5000000000	2.0099999900
-0.5508601670	3.1208000180	3.1800000668	3.5000000000	2.6900000000
-0.5485980210	2.5890998840	3.1400001049	3.4700000000	2.6700000760
-0.5456022550	3.6651999950	3.3599998951	4.3600000000	2.9000000000
-0.5451156200	3.0367000100	3.5999999046	3.7500000000	2.6600000000
-0.5438742790	3.2370998860	4.2399997711	4.9000000000	3.2000000000
-0.5431296300	3.1208000180	3.1800000668	3.2500000000	3.3000000000
-0.5425142120	3.6243000030	4.3200001717	4.7500000000	3.6200000000
-0.5408982930	2.9990000720	4.2399997711	4.6600000000	3.6300000000
-0.5382971840	2.5852000710	2.1600000858	4.6000000000	4.7500000000

-0.5350897460	3.0362000470	3.8199999332	4.3600000000	2.6700000760
-0.5307467280	3.3664999010	3.9000000954	4.3000000000	1.3400000330
-0.5253351850	2.3510000710	2.9200000763	3.7500000000	3.6300000000
-0.5249279740	3.3417000770	3.8199999332	4.2400000000	2.4000000000
-0.5239740760	2.6277999880	3.1400001049	3.5000000000	2.3000000000
-0.5224663760	2.9879000190	3.4000000954	4.2500000000	4.7500000000
-0.5224525180	3.0868000980	3.6199998856	4.1900000000	2.0000000000
-0.5181143430	4.1939001080	3.8599998951	3.6500000000	3.7000000000
-0.5158309640	3.2293000220	3.9000000954	4.3000000000	2.0000000000
-0.5149016160	2.4453001020	3.1199998856	4.5600000000	2.0000000000
-0.5137568710	2.6357998850	2.7999999523	4.5200000000	3.9000000000
-0.5121637510	3.2193000320	3.4000000954	3.0000000000	2.8000000000
-0.5092194300	1.8427000050	1.8799999952	3.5000000000	2.6700000760
-0.5082637070	2.8489000800	3.7400000095	4.8000000000	3.6800000000
-0.5058564250	3.6630001070	4.3200001717	4.8000000000	3.4000000000
-0.5056861790	3.5237998960	3.2599999905	4.3600000000	3.2200000000
-0.5024833980	3.6630001070	4.3200001717	4.7800000000	3.8000000000
-0.4995936900	2.5734000210	2.2799999714	3.7500000000	3.4000000000
-0.4981254040	2.7434999940	3.2200000286	3.5000000000	3.6000000000
-0.4937965800	2.8306000230	2.7799999714	4.9600000000	3.4000000000
-0.4934895780	2.8420999050	3.8199999332	3.7500000000	3.4500000000
-0.4907464240	4.5810999870	3.9400000572	3.2700000000	3.6000000000
-0.4903371630	2.7662000660	3.7400000095	3.5000000000	1.6699999570
-0.4887404290	2.9412999150	3.2999999523	4.2500000000	3.4000000000
-0.4867538060	3.6610000130	3.2599999905	4.9900000000	2.1500000000
-0.4833897200	3.4423000810	3.1600000858	4.2400000000	2.0099999900
-0.4818688710	3.6630001070	4.3200001717	4.6700000000	2.5700000000
-0.4804233460	3.0497000220	3.8199999332	4.1200000000	2.7000000000
-0.4796672240	2.9456000330	2.8800001144	3.2500000000	2.8000000000
-0.4789970070	3.8640999790	3.5599999428	3.6800000000	2.6800000670
-0.4775408660	3.1189000610	3.8199999332	3.2000000000	2.3399999140
-0.4768863690	2.0213000770	2.8399999142	4.6700000000	3.1000000000
-0.4757519810	4.3909001350	4.1399998665	3.7500000000	2.6800000670
-0.4743807390	2.6935000420	3.7400000095	3.5000000000	3.3399999140
-0.4739503560	2.6475000380	2.9200000763	3.5000000000	2.3399999140
-0.4728283730	3.2757999900	4.2399997711	3.3600000000	2.3399999140
-0.4719131440	3.2293000220	3.9000000954	3.8800000000	3.3399999140
-0.4703631250	2.9247999190	3.8199999332	3.3000000000	3.1000000000
-0.4695589100	4.2512998580	4.1399998665	4.6700000000	3.6700000760
-0.4690157620	2.8540000920	3.6199998856	3.7000000000	2.3500000000
-0.4687641190	2.6480000020	3.3199999332	4.2500000000	2.6800000670
-0.4633347690	1.9165999890	2.6199998856	4.2500000000	2.3399999140
-0.4621867090	3.7878999710	3.4600000381	3.9800000000	2.6000000000
-0.4602750390	2.6861000060	3.6600000858	4.2640000000	2.3399999140

-0.4595138130	3.0422000890	3.0799999237	2.7500000000	4.2500000000
-0.4584636910	2.2293999200	3.0199999809	3.9000000000	2.3399999140
-0.4529382660	2.8947000500	3.4000000954	3.5000000000	2.3399999140
-0.4485839980	3.6085000040	4.3200001717	3.2100000000	4.6000000000
-0.4481738810	1.9510999920	2.1800000668	2.1000000000	3.6700000760
-0.4464783150	2.6935000420	3.7400000095	4.2500000000	3.0099999900
-0.4448959980	2.1796000000	2.4000000954	4.3600000000	3.0099999900
-0.4438059030	2.2058999540	3.2400000095	4.5000000000	3.6700000760
-0.4433286940	3.4502000810	3.4800000191	4.5000000000	3.1000000000
-0.4389017450	4.1750998500	3.5399999619	4.3200000000	3.4700000000
-0.4387673740	2.6349000930	2.7999999523	4.5200000000	4.6000000000
-0.4378862310	3.7878999710	3.4600000381	4.3200000000	4.0100002290
-0.4372882840	2.9040999410	3.2999999523	4.3640000000	3.1000000000
-0.4362678160	2.6935000420	3.7400000095	3.5400000000	3.6000000000
-0.4351772000	3.3664999010	3.9000000954	4.3000000000	3.1000000000
-0.4339642450	2.7871999740	3.0999999046	4.0000000000	3.3399999140
-0.4326742140	3.7567000390	4.1799998283	3.8700000000	4.0100002290
-0.4316266250	3.7878999710	3.4600000381	4.9900000000	2.6700000760
-0.4308918120	3.7878999710	3.4600000381	4.6500000000	2.0000000000
-0.4267464950	3.7051999570	3.4600000381	4.3600000000	1.6699999570
-0.4246177150	3.1298999790	3.4000000954	4.6700000000	3.1000000000
-0.4226304960	2.6494998930	3.5199999809	4.6700000000	3.6700000760
-0.4218636080	3.4007000920	3.3800001144	4.6700000000	3.3000000000
-0.4213244470	4.1750998500	3.5399999619	4.9000000000	3.3000000000
-0.4210108520	3.5866000650	2.5399999619	3.5000000000	3.0099999900
-0.4141820970	3.3387999530	3.2599999905	2.5000000000	3.3299999240
-0.4123174030	3.0271999840	4.0199999809	4.2500000000	3.9000000000
-0.4064346850	4.1750998500	3.5399999619	4.5500000000	3.1000000000
-0.4018159580	1.8621000050	2.6199998856	4.2500000000	3.1000000000
-0.3963467110	2.6342999940	3.5199999809	4.5000000000	3.0000000000
-0.3961685300	3.5337998870	3.7599999905	2.7500000000	3.2200000000
-0.3856743870	3.6979999540	2.8199999332	3.2500000000	4.6000000000
-0.3817910700	2.3347001080	2.5199999809	3.7500000000	4.6000000000
-0.3780421240	2.7753999230	3.0799999237	3.2500000000	4.6000000000
-0.3774661940	3.3578999040	3.9200000763	4.9000000000	3.6700000760
-0.3735058010	4.1750998500	3.5399999619	4.7500000000	4.3299999240
-0.3712284940	2.4893000130	2.8199999332	3.5000000000	3.7000000000
-0.3679114580	3.7681999210	4.4000000954	5.0000000000	4.0000000000
-0.3672768180	4.1750998500	3.5399999619	4.8800000000	3.6700000760
-0.3666593880	2.6638000010	3.3199999332	4.6700000000	3.2200000000
-0.3643537310	3.5497999190	3.2400000095	3.2500000000	3.3399999140
-0.3619226810	4.3081998830	3.9200000763	2.7500000000	3.3299999240
-0.3595066440	2.8034000400	3.8199999332	3.6600000000	3.2200000000
-0.3557993470	3.7321999070	3.5599999428	4.5200000000	3.3399999140

-0.3523742410	4.3081998830	3.9200000763	3.2500000000	4.6000000000
-0.3491522370	3.6168999670	3.3599998951	4.5000000000	4.6700000760
-0.3482141350	2.7130000590	2.7799999714	4.2500000000	3.8000000000
-0.3471539910	3.4145998950	3.5199999809	4.6000000000	4.2500000000
-0.3456219660	2.9405999180	3.8199999332	4.2500000000	4.3299999240
-0.3426884490	3.4196999070	4.3200001717	5.0000000000	3.9000000000
-0.3404941780	3.8069000240	4.4000000954	5.0000000000	2.3399999140
-0.3329621630	3.1905999180	3.9000000954	4.5000000000	3.7000000000
-0.3309601920	2.8034000400	3.8199999332	4.2400000000	3.0099999900
-0.3283908590	2.3326001170	3.2400000095	4.5000000000	3.6700000760
-0.3173248470	2.3949999810	2.9200000763	3.7700000000	3.1000000000
-0.3164172170	2.7822000980	3.2200000286	4.3000000000	4.2900000000
-0.3154758740	1.9812999960	2.7400000095	4.2500000000	4.6000000000
-0.3104196860	3.3778998850	2.8599998951	3.7500000000	2.6700000760
-0.3037031930	2.4458000660	2.9000000954	3.5000000000	2.6700000760
-0.3035510890	2.3122999670	3.1400001049	4.2500000000	4.2500000000
-0.3013733590	2.2009000780	2.6400001049	4.0000000000	4.2500000000
-0.3006618660	2.6108000280	3.5199999809	4.6000000000	3.1000000000
-0.3002528290	2.6995000840	3.0000000000	4.8700000000	4.0000000000
-0.2983562830	2.5852000710	2.1600000858	2.0000000000	4.2500000000
-0.2947807130	1.8944000010	2.0000000000	3.5000000000	4.2500000000
-0.2944804360	2.3963999750	2.5000000000	4.0000000000	4.3700000000
-0.2942804060	3.4491999150	3.9000000954	3.7500000000	4.6700000760
-0.2889817770	2.4906001090	2.9200000763	3.7500000000	3.6700000760
-0.2878489720	2.7381999490	3.0000000000	4.6700000000	4.6000000000
-0.2854024620	2.5065000060	2.6800000668	3.0000000000	3.3399999140
-0.2849287540	3.5216000080	2.7400000095	3.2500000000	3.0099999900
-0.2842382340	2.8283998970	4.0199999809	4.8000000000	4.3500000000
-0.2807405960	2.9498000140	4.2399997711	5.0000000000	3.6600000860
-0.2778747680	2.5065000060	2.6800000668	3.0000000000	4.3500000000
-0.2764873390	3.4391999240	3.9000000954	4.3000000000	3.1000000000
-0.2653967780	4.3081998830	3.9200000763	3.2500000000	2.6700000760
-0.2597609350	2.8921000960	3.2999999523	4.6800000000	3.3299999240
-0.2586454530	2.8936998840	2.9800000191	3.0000000000	3.3399999140
-0.2555854800	2.6861000060	3.4400000572	4.3400000000	1.6699999570
-0.2545350230	4.0036997800	4.0599999428	3.7500000000	4.3400001530
-0.2541122960	2.2458000180	2.2999999523	3.2500000000	3.0099999900
-0.2537613730	2.2458000180	2.2999999523	3.2500000000	3.1000000000
-0.2518473010	2.9614999290	3.4200000763	3.9000000000	3.6000000000
-0.2512488890	2.2458000180	2.2999999523	3.5000000000	4.7500000000
-0.2510068940	3.1238999370	2.8800001144	4.3000000000	4.2800000000
-0.2489963550	2.6329998970	2.3800001144	3.5000000000	3.7500000000
-0.2476077150	2.5065000060	2.9000000954	3.0000000000	4.0000000000
-0.2475635150	2.3771998880	2.5799999237	4.3000000000	4.6000000000

-0.2472599040	2.5566000940	2.9200000763	4.0000000000	4.6700000760
-0.2460816500	2.7325000760	2.9200000763	4.0000000000	4.6700000760
-0.2455617110	2.6393001080	3.3599998951	4.5200000000	4.6000000000
-0.2452218910	2.6789000030	2.7999999523	4.2400000000	4.3700000000
-0.2432900670	2.6401999000	2.7999999523	3.7500000000	3.3299999240
-0.2427910450	2.5952999590	2.9200000763	4.5200000000	3.2200000000
-0.2419575300	3.0274000170	2.8800001144	4.2400000000	4.6700000760
-0.2409987340	2.5952999590	2.9200000763	3.7500000000	3.3299999240
-0.2404899150	3.0274000170	2.8800001144	4.3000000000	4.6000000000
-0.2348590640	2.6401999000	2.7999999523	3.7500000000	4.9000000000
-0.2345940840	3.9748001100	2.8199999332	2.0000000000	3.3299999240
-0.2305681070	3.4662001130	2.7400000095	2.4000000000	4.7000000000
-0.2156200070	2.4316999910	2.5799999237	3.7500000000	4.6700000760
-0.2152274180	2.5134999750	2.5799999237	2.2500000000	3.3399999140
-0.2089172420	2.2098999020	2.7200000286	4.3000000000	4.0000000000
-0.2006358280	1.9761999850	2.2200000286	3.2500000000	3.6700000760
-0.1965803280	1.9321999550	2.0000000000	3.5000000000	3.1000000000
-0.1955408420	1.9321999550	2.2200000286	3.5000000000	5.0000000000
-0.1920586820	3.6224999430	3.2400000095	2.5000000000	4.0100002290
-0.1884099470	2.2769999500	2.8399999142	3.6900000000	3.3299999240
-0.1862575490	3.1635999680	3.0799999237	2.5000000000	2.4000000000
-0.1814019870	1.9321999550	2.2200000286	3.5000000000	3.1500000000
-0.1755913350	3.0808999540	3.0799999237	2.5000000000	4.6700000760
-0.1752866990	3.6224999430	3.4600000381	2.5000000000	4.7500000000
-0.1737761870	2.1765000820	2.9400000572	3.7400000000	4.3400001530
-0.1693557020	2.4073998930	2.5199999809	4.5200000000	3.6700000760
-0.1678064470	2.1765000820	2.9400000572	4.6900000000	3.3400000330
-0.1676883180	2.4460999970	2.2999999523	4.0000000000	4.2500000000
-0.1670833860	2.0202000140	2.4400000572	4.0000000000	4.1000000000
-0.1670178400	1.9321999550	2.0000000000	3.2500000000	3.6700000760
-0.1666682030	1.9321999550	2.0000000000	4.2400000000	4.3400001530
-0.1660487800	2.0202000140	2.4400000572	4.5200000000	5.0000000000
-0.1655960640	1.9321999550	2.0000000000	3.5000000000	4.3299999240
-0.1653749870	2.5838000770	2.9200000763	4.2500000000	3.6700000760
-0.1644024810	1.9321999550	2.0000000000	3.5000000000	3.3299999240
-0.1637761480	1.9321999550	2.0000000000	3.2500000000	3.6700000760
-0.1606580060	2.1765000820	2.9400000572	4.2500000000	3.3399999140
-0.1589033190	1.5382000210	1.7999999523	1.2000000000	4.7500000000
-0.1545471600	1.9630000590	2.3199999332	3.7500000000	4.6000000000
-0.1489494740	3.1635999680	3.2999999523	3.9400000000	3.6699999570
-0.1459920970	2.1765000820	2.7200000286	4.3600000000	4.0100002290
-0.1454203860	2.1765000820	2.7200000286	3.6980000000	4.6000000000
-0.1436753570	2.1765000820	2.9400000572	3.7700000000	3.3399999140
-0.1427594670	2.1765000820	2.9400000572	4.6900000000	4.0000000000

-0.1391450780	2.7788000110	2.3800001144	4.5200000000	3.6700000760
-0.1366879700	3.1659998890	2.4600000381	4.0000000000	3.1000000000
-0.1287336460	2.1765000820	2.9400000572	3.7400000000	3.6000000000
-0.1245632770	3.1659998890	2.4600000381	4.0000000000	3.6700000760
-0.1242560710	1.9538999800	2.5999999046	1.5000000000	3.2000000000
-0.1207368450	2.3520998950	2.8199999332	4.5200000000	5.0000000000
-0.1162213740	2.3915998940	2.2999999523	4.5200000000	4.1500000000
-0.0728775790	2.3961000440	2.8199999332	4.0000000000	3.3399999140
-0.0718979120	1.9510999920	2.1800000668	1.3600000000	3.1000000000
-0.0707303170	2.5724999900	2.9000000954	3.2500000000	3.0099999900
-0.0691299790	1.5638999940	2.0999999046	1.3500000000	4.6000000000
-0.0557409370	2.2674999240	2.1800000668	1.4500000000	3.1000000000
-0.0507827480	3.5706000330	3.3399999142	2.5000000000	4.2500000000
-0.0487594310	2.9393999580	2.6600000858	2.2500000000	3.1000000000
-0.0400153500	1.5769000050	1.7999999523	1.6500000000	4.6700000760
-0.0280961670	2.7444000240	3.6199998856	1.3650000000	4.3299999240
-0.0231380020	1.5769000050	1.7999999523	1.7000000000	4.3600000000
-0.0197623830	1.3428000210	1.5000000000	1.9800000000	4.0100002290
-0.0196726220	1.5382000210	1.7999999523	1.8900000000	2.6700000760
-0.0133974690	1.3041000370	1.5000000000	1.7790000000	4.2500000000
-0.0096588460	1.3428000210	1.5000000000	1.3900000000	4.2500000000
-0.0070538200	3.1296999450	3.1600000858	2.5000000000	4.0100002290
-0.0019566270	1.3041000370	1.5000000000	1.1000000000	4.0100002290
0.0014070610	1.1090999840	1.0000000000	1.7500000000	3.2000000000
0.0033637500	1.3041000370	1.5000000000	1.2400000000	4.3400001530
0.0050929260	2.9393999580	2.6600000858	2.2500000000	3.4000000000
0.0051579600	2.7444000240	3.7400000095	1.3570000000	4.6700000760
0.0078069500	2.7444000240	3.1600000858	2.5000000000	4.3299999240
0.0167222180	2.0436000820	2.5000000000	2.2500000000	4.6700000760
0.0246870420	1.6913000350	1.5800000429	1.2500000000	4.6000000000
0.0292031210	1.1477999690	1.0000000000	1.7500000000	2.3399999140
0.0317259250	2.7444000240	3.2400000095	2.5000000000	3.6000000000
0.0344181920	1.3428000210	1.5000000000	2.7000000000	3.3299999240
0.0369932740	2.7444000240	2.1600000858	2.0000000000	4.3299999240
0.0471097370	2.0397999290	1.6599999666	2.4000000000	4.3299999240
0.0519484840	1.3418999910	1.5000000000	1.7700000000	3.1000000000

Appendix IV: False positive and true positive rate value report used to produce Roc curve analysis

Landslide		Seismic		Volcanism		The Three	
False Posi. Rate	True Posi. Rate	False Posi. Rate	True Posi. Rate	False Posi. Rate	True Posi. Rate	False Posi. Rate	True Posi Rate
0	0	0	0	0	0	0	0
0.007216	0.026358	0.006161	0.031693	0.006017	0.032981	0.007477	0.024506
0.015659	0.045505	0.012263	0.063722	0.012656	0.062368	0.014911	0.049254
0.024258	0.063737	0.020686	0.082632	0.018267	0.097688	0.024102	0.063904
0.033134	0.080344	0.028954	0.102421	0.024713	0.128195	0.030273	0.095911
0.042446	0.094386	0.038011	0.117752	0.029314	0.16934	0.037549	0.121569
0.052549	0.103776	0.047255	0.13202	0.035131	0.203472	0.044502	0.149088
0.060865	0.123671	0.055785	0.15033	0.042491	0.228707	0.053154	0.166836
0.070979	0.133003	0.065907	0.159639	0.051095	0.246758	0.060832	0.190182
0.07997	0.14893	0.073772	0.181708	0.061847	0.252421	0.070039	0.204739
0.088449	0.167867	0.082333	0.19984	0.071076	0.266866	0.078486	0.223666
0.099297	0.172886	0.092814	0.20712	0.080122	0.282371	0.084446	0.256892
0.107754	0.191954	0.101572	0.224138	0.090827	0.288307	0.091639	0.283022
0.117645	0.202593	0.110714	0.238988	0.098586	0.311236	0.099252	0.306743
0.125662	0.224246	0.117041	0.269744	0.104416	0.34529	0.105599	0.337743
0.135985	0.232344	0.126373	0.283516	0.112426	0.366771	0.114696	0.352935
0.14383	0.255009	0.134339	0.305011	0.121901	0.379798	0.124	0.366935
0.153402	0.267524	0.142976	0.322713	0.129133	0.405768	0.131173	0.393189
0.16325	0.278413	0.151969	0.338406	0.13746	0.425421	0.140434	0.407433
0.1711	0.301048	0.16007	0.359135	0.145602	0.446141	0.150887	0.414829
0.18094	0.311988	0.169036	0.374979	0.155374	0.457454	0.157296	0.445472
0.190514	0.324487	0.177911	0.391338	0.166355	0.461797	0.165223	0.467388
0.199938	0.337874	0.185996	0.412158	0.176349	0.471831	0.173767	0.485754
0.208181	0.358198	0.194774	0.429061	0.18565	0.48586	0.182264	0.504397
0.219025	0.363239	0.205461	0.435178	0.194858	0.500433	0.191447	0.519093
0.22838	0.377026	0.214481	0.450718	0.206522	0.500833	0.200348	0.535407
0.236915	0.395633	0.222472	0.472069	0.21312	0.530462	0.209809	0.548509
0.24566	0.413012	0.231384	0.488221	0.224127	0.53465	0.218959	0.563397
0.255249	0.425423	0.240945	0.5007	0.235655	0.535833	0.22681	0.585746
0.266033	0.430818	0.251622	0.506876	0.243776	0.556675	0.235961	0.600627
0.275298	0.445136	0.259575	0.528443	0.251276	0.581096	0.245734	0.611932
0.285321	0.455004	0.269496	0.538891	0.259616	0.600674	0.25555	0.622989
0.295118	0.466196	0.279845	0.546916	0.270403	0.606135	0.265802	0.631539
0.303479	0.485824	0.288351	0.565358	0.280095	0.617913	0.27618	0.639366
0.312528	0.501413	0.29745	0.580449	0.289244	0.632822	0.286783	0.645902
0.323962	0.502984	0.308588	0.58402	0.299898	0.63905	0.296244	0.659002
0.33314	0.517816	0.319906	0.586574	0.30917	0.653245	0.30502	0.676036
0.344384	0.520506	0.330854	0.591214	0.318237	0.668628	0.314683	0.687975
0.35481	0.528006	0.341525	0.597424	0.328883	0.674904	0.325891	0.691032
0.363648	0.544831	0.349926	0.616456	0.339079	0.683773	0.33342	0.715232
0.372847	0.559538	0.358543	0.634277	0.349933	0.688847	0.34065	0.741154
0.380612	0.58267	0.366426	0.65624	0.360272	0.696888	0.351505	0.746243

0.390164	0.595304	0.375882	0.669313	0.371057	0.702363	0.359423	0.76821
0.401567	0.59706	0.387091	0.672478	0.382573	0.703614	0.366431	0.795407
0.412919	0.599112	0.397832	0.678291	0.392525	0.71389	0.377582	0.798793
0.421867	0.615297	0.404943	0.704617	0.399536	0.741138	0.388312	0.804597
0.432088	0.623999	0.414279	0.718372	0.410453	0.745847	0.39854	0.813285
0.439895	0.646883	0.421734	0.742755	0.420718	0.754318	0.409543	0.817521
0.450876	0.65112	0.432727	0.747139	0.431079	0.762233	0.41964	0.826959
0.46205	0.654218	0.443731	0.751469	0.442495	0.764062	0.430591	0.831496
0.471653	0.666551	0.453104	0.765012	0.451417	0.780286	0.442082	0.832928
0.479312	0.690306	0.460195	0.791452	0.45921	0.803016	0.453413	0.835273
0.490716	0.692055	0.4717	0.792943	0.468902	0.814792	0.464825	0.837156
0.501489	0.697514	0.482565	0.798057	0.480393	0.816191	0.47655	0.837239
0.51248	0.701694	0.493689	0.801707	0.49153	0.819635	0.487417	0.842255
0.522464	0.711787	0.503458	0.813013	0.502191	0.825821	0.497273	0.853086
0.532897	0.719246	0.513938	0.820296	0.513083	0.830675	0.507255	0.863187
0.54241	0.732108	0.52439	0.827744	0.524212	0.834161	0.518118	0.86823
0.552066	0.744124	0.533551	0.842486	0.535874	0.834569	0.52901	0.873103
0.562612	0.750916	0.543878	0.850634	0.546885	0.838737	0.539685	0.87922
0.572598	0.761004	0.554151	0.859092	0.553068	0.87076	0.550428	0.884949
0.58175	0.775981	0.56463	0.866385	0.56238	0.884728	0.560773	0.892968
0.591131	0.789619	0.57394	0.880288	0.573949	0.885678	0.568695	0.91491
0.601634	0.796663	0.584938	0.884644	0.584905	0.89016	0.580096	0.916857
0.612315	0.802661	0.596033	0.888457	0.595704	0.895554	0.591108	0.921043
0.621591	0.816918	0.606614	0.895179	0.60553	0.906554	0.600139	0.936612
0.630765	0.831772	0.616295	0.906978	0.616644	0.910127	0.609574	0.94986
0.640917	0.840876	0.627984	0.907432	0.62802	0.912189	0.620662	0.953603
0.652044	0.844253	0.639529	0.908703	0.639584	0.913166	0.632348	0.953913
0.662787	0.84989	0.65089	0.911011	0.650952	0.915277	0.64394	0.954761
0.673569	0.855297	0.661718	0.916334	0.660153	0.929887	0.654909	0.959191
0.683499	0.865707	0.672797	0.920235	0.670427	0.938306	0.665401	0.966363
0.693248	0.87718	0.68263	0.931179	0.680359	0.948699	0.676517	0.969948
0.704775	0.878209	0.694271	0.931907	0.691275	0.953412	0.687806	0.972538
0.715562	0.883586	0.70473	0.939311	0.702577	0.955898	0.699346	0.97369
0.726486	0.888156	0.716015	0.94205	0.713468	0.960759	0.71066	0.976136
0.734889	0.907541	0.725336	0.955887	0.724928	0.96234	0.722186	0.977361
0.745909	0.91155	0.736887	0.957124	0.736183	0.965096	0.733259	0.981197
0.757477	0.912333	0.748513	0.957931	0.747793	0.965809	0.74427	0.985384
0.767828	0.92027	0.758809	0.966261	0.759419	0.966425	0.755844	0.986333
0.77937	0.921214	0.77028	0.967949	0.76893	0.97925	0.767348	0.987691
0.790988	0.921703	0.78204	0.968	0.779071	0.988433	0.778832	0.98916
0.801996	0.925785	0.793803	0.968038	0.790046	0.992809	0.790307	0.990679
0.81309	0.929355	0.805573	0.968039	0.801724	0.993133	0.802031	0.990771
0.82447	0.931248	0.816995	0.970001	0.813257	0.994288	0.813736	0.990973
0.835331	0.936187	0.828334	0.972438	0.824187	0.99892	0.825239	0.992333
0.846157	0.941335	0.839456	0.976095	0.835813	0.99954	0.836438	0.995437

0.856098	0.951683	0.850222	0.981763	0.847546	0.99954	0.847912	0.996965
0.866407	0.959866	0.86134	0.985446	0.859265	0.999623	0.859577	0.997397
0.875659	0.974262	0.872429	0.989295	0.870953	0.999887	0.871014	0.999137
0.886522	0.979188	0.883764	0.991751	0.882676	0.999948	0.882644	0.999768
0.897264	0.984828	0.89522	0.993521	0.894409	0.99995	0.894371	0.999837
0.908417	0.988058	0.906559	0.995957	0.906134	0.999997	0.906099	0.999908
0.919172	0.993618	0.917766	0.999137	0.917867	0.999998	0.917824	0.999988
0.930764	0.994267	0.929521	0.999221	0.9296	0.999998	0.929564	0.999988
0.942099	0.996423	0.94129	0.999221	0.941333	0.999999	0.941304	0.999988
0.953358	0.999025	0.95303	0.99939	0.953067	0.999999	0.953043	0.999993
0.96499	0.999439	0.964774	0.999535	0.9648	0.999999	0.964782	0.999993
0.976684	0.999485	0.976543	0.999535	0.976534	0.999999	0.976522	0.999993
0.988369	0.999584	0.988312	0.999539	0.988267	1	0.988262	0.999994
1	1	1	1	1	1	1	1

Appendix V: Histogram shows the textural class of soils produced from SAGA GIS (2.3.2)

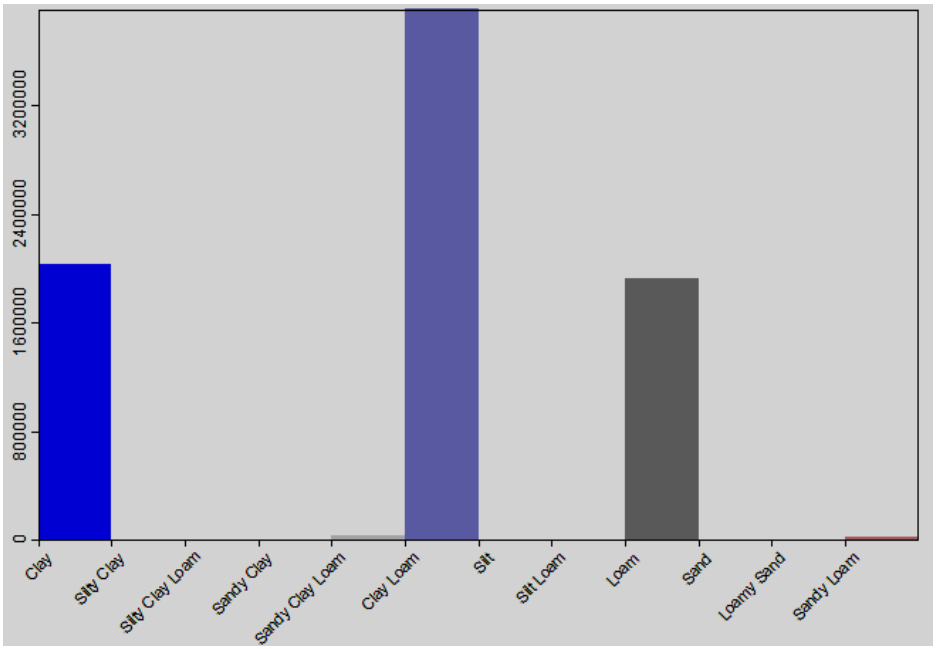

1.Clay
2. Silt _Clay
3.Silt_Clay_ Loam
4.Sandy_ Clay
5.Sandy Clay Loam
6. Clay_ Loam
7. Slit
8.Silt_ Loam
9.Loam
10.Sand
11. Loamy Sand
12.Sandy Loam